12-2003

"Design of Molecular Mechanics Modeling Techniques For Exploring Molecular Recognition Using Cyclodextrins.

Shannon Bradley Fox
University of Tennessee - Knoxville

To the Graduate Council:

I am submitting herewith a dissertation written by Shannon Bradley Fox entitled ""Design of Molecular Mechanics Modeling Techniques For Exploring Molecular Recognition Using Cyclodextrins.." I have examined the final electronic copy of this dissertation for form and content and recommend that it be accepted in partial fulfillment of the requirements for the degree of Doctor of Philosophy, with a major in Chemistry.

M. J. Sepaniak, Major Professor

We have read this dissertation and recommend its acceptance:

Elizabeth Howell, S. D. Gilman, Z. Xue

Accepted for the Council:

Carolyn R. Hodges

Vice Provost and Dean of the Graduate School

(Original signatures are on file with official student records.)

To the Graduate Council:

I am submitting herewith a dissertation written by Shannon Bradley Fox entitled "Design of Molecular Mechanics Modeling Techniques For Exploring Molecular Recognition Using Cyclodextrins." I have examined the final electronic copy of this dissertation for form and content and recommend that it be accepted in partial fulfillment of the requirements for the degree of Doctor of Philosophy, with a major in Chemistry.

M. J. Sepaniak

_____

Major Professor

We have read this dissertation
and recommend its acceptance:

Elizabeth Howell

_____

S. D. Gilman

_____

Z. Xue

_____

Accepted for the Council:

Anne Mayhew

_____

Vice Provost and Dean of
Graduate Studies

(Original signatures are on file with official student records.)

DESIGN OF MOLECULAR MECHANICS MODELING TECHNIQUES FOR EXPLORING MOLECULAR RECOGNITION USING CYCLODEXTRINS

A Dissertation
Presented for the
Doctor of Philosophy Degree
The University of Tennessee, Knoxville

Shannon Fox
December 2003

DEDICATION

This dissertation is dedicated to
my mother, Martha Fox
and my father, Steve Fox
and my sister, Elise Fox
and Mohsena Purkaystha
for their love, support, and encouragement.

ACKNOWLEDGEMENTS

There are many people who have helped me during my time in graduate school, and I don't think I could have made it to the finish line without their assistance. First I would like to thank Dr. Mike Sepaniak for his continued patience, guidance, and support during my time as a graduate student.

I would like to thank the many colleagues with whom I have had the privilege to work. Special thanks to fellow research group members Chris Tipple, Lance Riddle, Marco DeJesus, Mustafa Culha, and Jim Schaeper for their friendship during my time at UT.

I would also like to express my appreciation to Dr. R. J. Hinde for his assistance with writing unix scripts for molecular modeling experiments, and to Dr. S. Douglass Gilman for his help and patience in maintaining the departmental website, and for being on my committee. Also thanks to Dr. Ben Xue and Dr. Elizabeth Howell for being committee members.

Thanks to the many departmental support staff who have provided help and friendship over the years. Thanks to Bill Gurley and Johnny Jones for their tireless help with departmental network, and for teaching me many things during my time working with the Electronics Shop.

Thanks to Trevor and Lenore Smith, John Edward, and Jeff Givens for their friendship, and for helping me enjoy my time here in Knoxville.

Finally, I would like to thank my family for always being there for me. Their love, encouragement, and steadfast support has helped me more than they can know.

ABSTRACT

Molecular mechanics modeling techniques have been developed to study the behavior of cyclodextrins (CDs) in capillary electrophoresis (CE) separations. Using the commercial computational package, Sybyl, the mechanisms of molecular recognition between organic analytes and CDs are investigated.

Cyclodextrin-modified capillary electrochromatography (CDCE) experiments were conducted to separate neutral derivitized naphthalene solutes using carboxymethyl-beta-cyclodextrin (CM-β-CD). Grid conformation-searching programs were developed to explore the interaction space between CD and solute and to calculate their interaction energies using molecular mechanics. The interaction energies correlated remarkably well with the separation behavior. It was found that extensive minimization (more than 3000 iterations) was required at each of the docking positions to achieve the best agreement between computational and experimental distribution coefficients (K_d).

Molecular modeling techniques were also used to guide the development of a new charged cyclodextrin resolving agent, heptakis (6-O-carboxymethyl-2,3-dimethyl)-β-cyclodextrin (HDMCM-β-CD). Molecular computer aided design (MolCAD) analysis and docking techniques revealed that HDMCM-β-CD would be superior to commercially available CDs for forming inclusion complexes with the target naphthalene derivative analytes. Molecular modeling studies also showed that significant intermolecular CD-CD interactions can occur under certain conditions, explaining some anomalous experimental findings. Additionally, the grid conformation-searching modeling technique was applied to chiral CDCE separations of dansyl amino acids (AAs) to

explain separation behavior and to investigate different CD-CD interactions.

TABLE OF CONTENTS

LIST OF TABLES

LIST OF FIGURES

LIST OF ABBREVIATIONS

ASP	Aspartic Acid
CD	Cyclodextrin
CDCE	Cyclodextrin Distribution Capillary Electrochromatography
CE	Capillary Electrophoresis
CM-β-CD	Carboxymethyl Beta Cyclodextrin (degree of substitution = 1)
CMC	Critical Micelle Concentration
DHN	Dihydroxynaphthalene
DMN	Dimethylnaphthalene
DNN	Dinitronaphthalene
DNS	Dansyl
EFF	Empirical Force Field
EOF	Electroosmotic Flow
EXPT	Experimental
GC	Gas Chromatography
GLU	Glutamic Acid
HCM-β-CD	Heptakis(2,3-O-dimethyl-6-O-carboxymethyl)-β-CD
HDAS-β-CD	Heptakis(2,3-O-diacetyl-6-O-sulfato)-β-CD
HDMS-β-CD	Heptakis(2,3-O-dimethyl-6-O-sulfato)-β-CD
HLPC	High Performance Liquid Chromatography
I.D.	Inner Diameter
LEU	Leucine
MEKC	Micellar Electrokinetic Chromatography
MD	Molecular Dynamics
MM	Molecular Mechanics
MOLCAD	Molecular Computer Aided Design
O.D.	Outer Diameter
RAM	Random Access Memory
SDS	Sodium Dodecyl Sulfate
SER	Serine
VAL	Valine

CHAPTER 1

INTRODUCTION TO MOLECULAR RECOGNITION AND THE SUPRAMOLECULAR CHEMISTRY OF MACROCYCLIC COMPOUNDS

Introduction and History

Supramolecular chemistry is the area of chemistry that deals with all the intermolecular forces present between molecules that are not covalent bonds. Jean-Marie Lehn, who was awarded the Nobel Prize in 1987 along with Pedersen and Cram for their work in "host-guest chemistry" eloquently describes supramolecular chemistry in his book:[1]

> "Molecular chemistry rules the covalent bond. Supramolecular chemistry is 'chemistry beyond the molecule', whose goal is to gain control over the intermolecular non-covalent bond. It is concerned with the entities of higher complexity than molecules themselves - supramolecular species and assemblies held together and organized by means of intermolecular, binding interactions. It is a highly interdisciplinary field of science and technology, bridging chemistry with biology and physics."

While covalent bonds are typically characterized by bond energies around 50 -100 kcal/mol, non-bonded interactions are much smaller. These include electrostatic forces which can be between 1-10 kcal/mol, hydrogen bonding (1-20 kcal/mol), and van der Waals forces, dipole-dipole interactions, $\pi-\pi$ stacking, and hydrophobic effects (less than 1 kcal/mol).[2-7] None of these forces individually reach the strength of a covalent bond. However, during certain structural alignments of two molecules, multiple instances of these forces can be additive, and they may achieve a stability which is commensurate with covalent bonding. The magnitude and nature of the forces that come into play in this manner are generally structurally dependant, leading to very specific interactions

between the receptor (host) and the substrate (guest). This is known as molecular recognition.

It can be said that all life is possible because of molecular recognition. The selective binding and reactivity of such biological molecules as enzymes and antibodies is key to the function of an organism. The macrocyclic hemoglobin molecule selectively binds oxygen in our lungs and carries it to the rest of the body. The recognition of the enzyme is so specific for its substrate that it led Emil Fischer to describe it with his lock and key image over 100 years ago, representing an important landmark in supramolecular chemistry. Since then, chemists have been on a continuing quest to master the science of intermolecular chemistry. Indeed biochemical phenomenon have motivated chemists in much of the current research in chemical recognition. The field of supramolecular chemistry is vast and integrated into all the subdisciplines of chemistry; a comprehensive review would be beyond the scope of this writing. This chapter will, however, concern itself mainly with an overview of some of the most common and interesting macrocyclic compounds and their host-guest chemistry properties.

Inclusion Complexes

Since supramolecular complexes are held together by forces weaker than the covalent bond, they maintain an equilibrium between the host (H) and substrate (S) and the complex (HS). (see Equation 1.1). The equilibrium characteristics of the supramolecular entity depend on the rate of the complex formation and decomposition, and the difference in free energy (ΔG) between the free species and the complex. In a bimolecular complex, the equilibria can represented by the following equations.[8,9]

For a 1:1 complex:

$$\mathbf{H + S \leftrightharpoons HS} \qquad (1.1)$$

For a 1:2 complex:

$$\mathbf{HS + S \leftrightharpoons HS} \qquad (1.2)$$

And for a 2:1 complex (host to guest):

$$\mathbf{H + HS \leftrightharpoons H_2S} \qquad (1.3)$$

The binding constants (also called association constant K_a, formation constant K_f, or stability constant K_s) are then as follows:

$$\mathbf{K_{11} = [HS] / ([H][S]),} \qquad (1.4)$$

$$\mathbf{K_{12} = [HS] / ([HS][S]),} \qquad (1.5)$$

$$\mathbf{K_{21} = [H_2S] / ([H][HS]),} \qquad (1.6)$$

The brackets represent molar concentrations, and the K constants represent concentration quotients, not thermodynamic values. However, considering the accuracy of most experimental measurements the difference in these values is usually disregarded, and it is common for ΔG^o (free energy change) to be calculated from these constants.

The enthalpy and entropy changes (ΔH and ΔS, respectively) can be determined by measuring how the equilibrium constant changes with temperature or by performing calorimeter experiments. In solution, the stability constant (K) is dependant on both the temperature and the difference in free energy:[10,11]

$$\mathbf{K = e^{(-\Delta G / kT)}} \qquad (1.7)$$

where (k) is the Boltzmann constant. The Gibbs-Helmholtz states:

$$\Delta G = \Delta H - T\Delta S \qquad (1.8)$$

where ΔH and TΔS denote the enthalpy and entropy change upon complexation, respectively. It therefore follows that:

$$RT \ln K = -\Delta H + T\Delta S \qquad (1.9)$$

During complexation, there is usually somewhat a simultaneous structural adaptations between guest and host called 'induced fit'. The two species will together arrange their geometries to optimize energy considerations and maximize host-guest attraction. This process can be very complex, such as in the case of an enzyme folding around a substrate molecule and making a uniquely selective structure. In contrast, more rigid molecules like many macrocyclic species may only experience minimal induced fit phenomenon to accommodate a guest.

Crown Ethers and Cryptands

One of the pioneering landmarks in the evolution of supramolecular chemistry came with the discovery of crown ethers in 1967 by Charles J. Pedersen at du Pont.[12] He discovered that certain salts could be dissolved in nonpolar solvents by the metal cation forming a complex with cyclic polyethers. Pedersen called these new compounds "crown ethers", and their discovery and use is sometimes considered the beginning of molecular recognition studies in chemistry.

Pedersen continued his work in throughout the 1960s, synthesizing over 50 crown ethers. He discovered that the size of the cavity in the crown ethers dictated which metal cations would be preferentially bound.[13,14] Cram et al. later explored this area by

derivatizing many crown ethers and determining the characteristics that lead to strong complexation and selectivity.[15]

The primary building block in a crown ether is the ethyleneoxy (-CH_2CH_2O-) unit. Molecules with three or more of these units are considered crown ethers, with 1,4-7-trioxacyclononane being the first member of this group (dioxane and ethylene oxide are considered as cyclic ethers). Very large crowns have been synthesized, some possessing more than 20 repeating units, yielding ring sizes of 60 or greater. Crown ethers are named as "x-crown-y" where the total number of atoms in the cyclic backbone is given by x, and the number of oxygen atoms given by y. Crowns where the oxygen atoms have been replaced by nitrogen atoms are called cryptands. The cryptands are named as "[x.y.z]-cryptand" where x, y, and z are the numbers of oxygen donor atoms in each of the three chains spanning the nitrogen atoms.[16] Figure 1.1 shows examples of some crown ethers and cryptands.

The ethylene units are separated from each other by oxygen atoms. Since the oxygen atoms in the ring structure have no sterically hindering hydrogens associated with them, they are able to allow the crown ether to form symmetrical binding conformations, such as the D_{3d} configuration of 18-crown-6. As shown by the example in Figure 1.2, when potassium ion binds with 18-crown-6, the complex is symmetrical, while the free host orients its methylene groups inward in the uncomplexed form.

Crown ethers and cryptands form cation complexes in two different ways. Crown ethers bind their guest in an essentially two dimensional ring of donor groups. Cryptands however have an additional half-ring of donor groups spanning the nitrogen atoms, giving them a three-dimensional binding arrangement with cations.

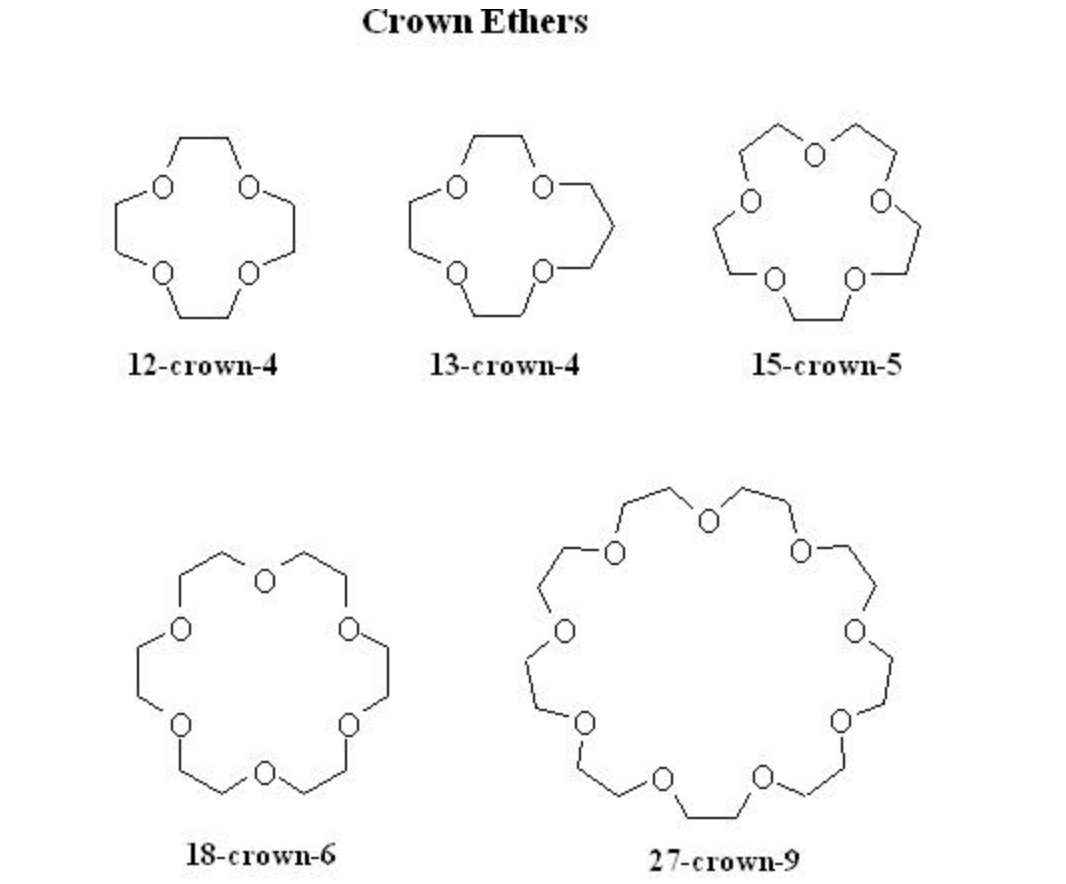

Figure 1.1. Some basic crown ethers and cryptands are shown.

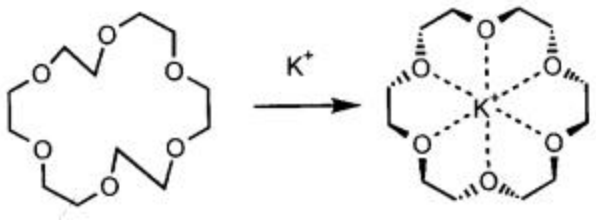

Figure 1.2. 18-crown-6 assumes a symmetrical structure upon complexation with the potassium ion.

Crown ethers have also been reported to bind molecular species as well. Pedersen first noted this when he observed thiourea complexing with various hosts.[17] He also found in the early 1970s that complexes could be formed between 18-crown-6, and many other molecular complexes have since been found.[18-20]

Modification of the crown ethers has led to many other classes of host molecules. Thousands of derivatives have been synthesized since crown ethers were first discovered. Azacrown ethers, thiacrown ethers, and crown ether diesters have all been prepared and shown be selective for a large number of ions and molecules.[21,22] Larger ring systems have been created by introducing aromatic rings into crown ethers. These endeavors eventually led to the creation of cyclic polyphenols, a new class of host molecules called calixarenes.

Calixarenes

Adolf von Bayer may have been the first to synthesize calixarenes in the 1800s when he reacted formaldehyde with p-substituted phenols and found that it produced a viscous mixture of unknown products.[23] Alois Zenke later discovered and reported that these products have a cyclic tetrameric structure.[24] However, the modern age of the study of calixarenes was initiated when Gutsche determined that the products were oligomeric, and called them "calixarenes". [25]

In 1979, Andreetti, et al. conducted X-ray analyses of calix[4]arene and determined that in the solid state a molecule of toluene could be found strongly attached inside the cavity, demonstrating the guest binding ability of calixarenes for the first time.[26] In later research, this group also reported that calixarenes in solution were found have ion binding abilities.[27]

The synthesis of calixarenes is relatively simple, as demonstrated in Figure 1.3. Formaldehyde is used to treat phenol or resorcinol to yield the cyclic oligomers. Calixarenes are named by the number of aromatic units in the structure, with the number being expressed in brackets, as shown in Figure 1.4. The most common and widely used calixarenes are the ones with 4, 6, and 8 aryl residues; species with odd numbers of residues or larger than 8 units are difficult to produce and isolate.[28]

There are many comparisons between calixarenes and cyclodextrins (see section below). Structurally they are very similar, but they differ greatly in their conformational flexibility. Cyclodextrins are rigid, cage-like molecules that can undergo slight structural changes to accommodate guests. In contrast, calixarenes are highly flexible molecules capable of rearranging its structure during an "induced fit" complexation, and can even experience complete ring inversions.

Cornforth was the first to understand the different conformational possibilities of calix[4]arene, which can have its aryl groups oriented in the upward ('u') or downward ('d') positions, relative to the ring plane formed by the methylene groups.[29,30] The four conformations are called 'cone' (u,u,u,u), 'partial cone' (u,u,u,d), '1,2-alternate' (u,u,d,d), and '1-3-alternate (u,d,u,d) (see Figure 1.5).

The cone conformation is most prevalent in solution at room temperature. This is attributed to the fact that it has strong intramolecular hydrogen bonding between the 4 hydroxyl groups. However, fast interconversion between the conformers occurs at room temperature. As the calixarenes increase in size, the number of possible conformations multiplies. For example, calix[6]arene can exist in 8 conformations, while calix[8]arene can have 16 different arrangements. This makes graphical representations of the

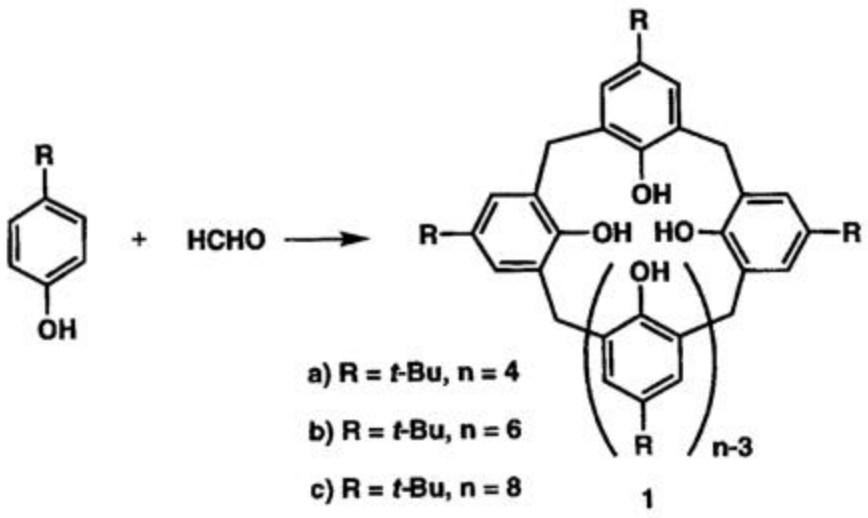

Figure 1.3. Calixarenes are synthesized by the reaction of either phenol or resorcinol with formaldehyde.

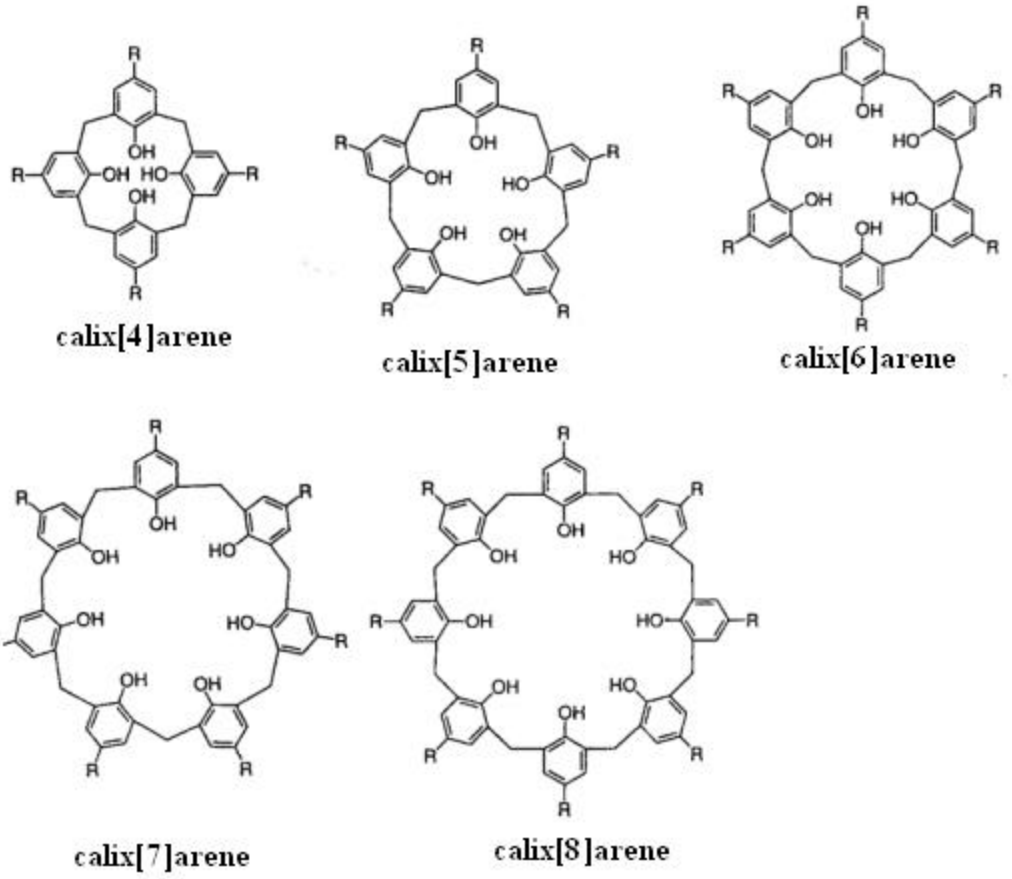

Figure 1.4. Several basic calixarenes are shown.

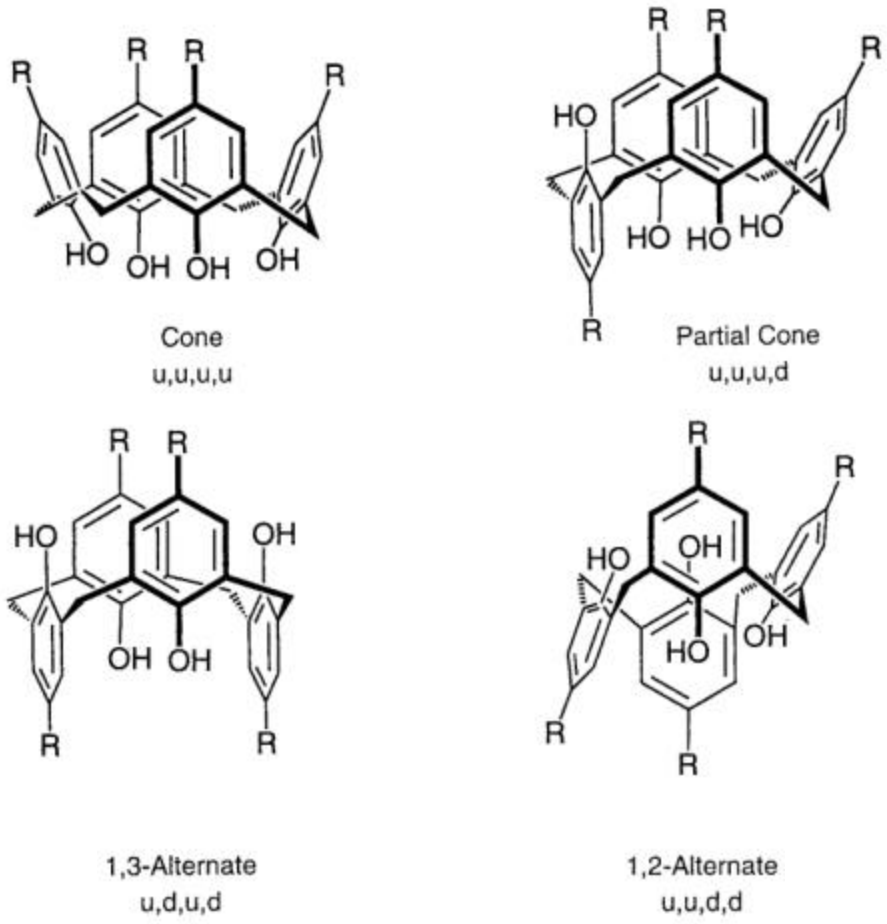

Figure 1.5. The different possible conformations of calix[4]arene are shown.

calixarenes difficult, and introduces complications in attempts to model the structures and complexes.

Like other macrocyclic host compounds, calixarene-guest complexes usually are a result of hydrogen bonding, electrostatic attraction, $\pi-\pi$ stacking, van der Waals forces, and charge-transfer interactions. Calixarenes are able to form metal ion complexes with many species.[31-34] In a striking example of molecular recognition and selectivity, Shinkai et al. reported that calix[5]arene and calix[6]arene p-sulfonates were exceptional hosts for UO_2^{2+}, even in the presence of other ions, such as Mg^{2+}, Ni^{2+}, and Cu^{2+}.[35] These materials have been used to generate resins that can selectively absorb over 100 μg of uranium from sea water for every 0.1 g of resin used. This feat is even more noteworthy when one considers the extraordinarily low concentration of uranium in sea water.

It has been shown that cavity size and shape both play a significant role in the strength of the calixarene-guest interaction. In revealing work by Sun and Sepaniak, it was shown that calix[4]arene is too small to achieve appreciable complexation with polyaromatic hydrocarbon (PAH) solutes. Conversely, calix[8]arene was found to be too large to form the necessary "snug fit" between it and the guest. However, calix[5]arene and calix[7]arene were found to be appropriately sized to form the best complexes with the PAHs. Interestingly, it was noted that calix[6]arene poorly complexed the PAHs, despite its seemingly ideal size. Molecular modeling of the structure, however, revealed that in its minimized energy state, the calix[6]arene assumes a more flat configuration, essentially losing its accommodating shape and cavity.

Calixarenes have proven their ability to include neutral organic molecules as well.[37-39] In 1992, Williams and Verhoeven found that a large calix[8]arene derivative

could even complex with C60.[40] Among a myriad of other uses, calixarenes have been used as catalysts,[41] in ion separations,[42] and molecular separations.[43]

Cyclodextrins

Several unique aspects of cyclodextrins afford them a distinguished position in host-guest chemistry. First, CDs are easy and very inexpensive to produce, being synthesized from abundant natural starch by a simple enzymic conversion. Second, they are produced industrially on large scale (metric tons per year) without producing toxic bi-products. Third, they are non-toxic and can be extensively used by people in food, medicine, and cosmetics. [44]

Villiers was the first to publish about a CD in 1891 when he reported that digesting starch with the bacteria Bacillus Amylobacter produced a crystalline substance.[45] After recrystallizing he noted two distinct species were formed (which were most likely α- and β-CD). Schardinger, who also worked with bacterial digestion of starch helped to develop the fundamentals of CD chemistry with his efforts.[46] Later in the 1930s, Pringsheim significantly advanced the progress of CD research when he discovered that organic compounds have a strong propensity to form complexes with crystalline CDs. [47,48]

Further developments occurred in the 1930s and 1940s when Freundenberg discovered CDs are comprised of maltose units, linked only by alpha 1-4-glycosidic linkages.[49,50] He is also credited with establishing that the CD structure was cyclic in nature.[51] Another milestone in CD chemistry was reached in 1948 when γ-CD was discovered.[52]

CDs are made up of a ring of D(+) glucopyranose units bound together by α-(1,4)- linkages (Figure 1.6). CDs with 6, 7, and 8 ring units are the most common, and they are called α, β, and γ-CD, respectively. Secondary hydroxyl groups align the rim of the CD on one side, primary hydroxyl groups are found on the other. The shape resembles that of a bowl, or a torus, with one opening of the cavity being wider than the other. The CDs cavities are wider where the secondary hydroxyl groups reside, at the C2 and C3 positions, while it is more constricted on the side with the primary hydroxyl groups.

Intramolecular interactions occur as the secondary hydroxyl groups at C2 and C3 can form hydrogen bonds. This restricts free movement of their relative positions, but the primary hydroxyl groups are free to move around.[53-55] C2 – C3 attractions are strongest in β-CD where the secondary hydroxyl groups form a rigid belt around the top of the structure characterized by 6 hydrogen bonds. This intramolecular attraction is the reason the natural cyclodextrins are able to maintain their rigid structure and basket-like cavities. α-CD, with one less ring unit, has one of the –OH groups in a distorted position so that only 4 hydrogen bonds can be formed. The γ-CD is a more flexible coplanar structure which can deviate from the bowl-like shape, allows it to be the most soluble of these 3 CDs.

In the past decade, several larger CDs have been isolated and studied. CDs with greater than 8 glucopyrnose rings are frequently found to have mostly collapsed structures resulting in real cavities that are smaller in volume than that of γ-CD.[56] (See Figure 1.7) Therefore use of these larger structures as inclusion hosts will most likely

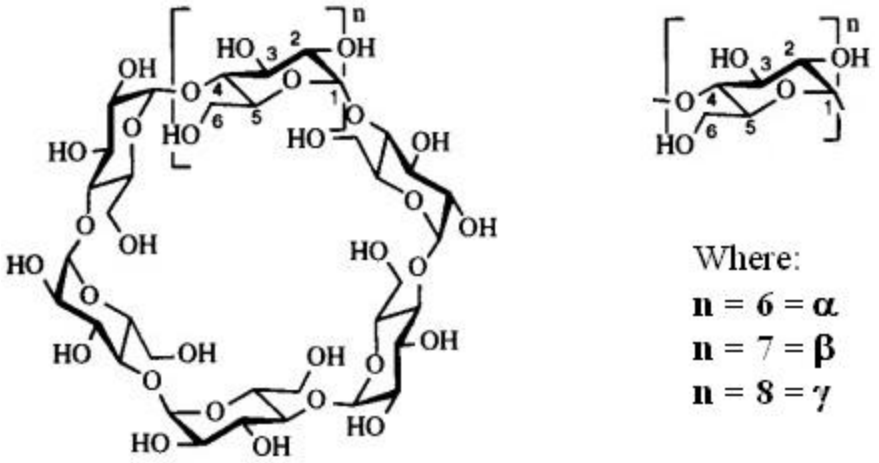

Figure 1.6. The structure of α, β, and γ-CD is shown.

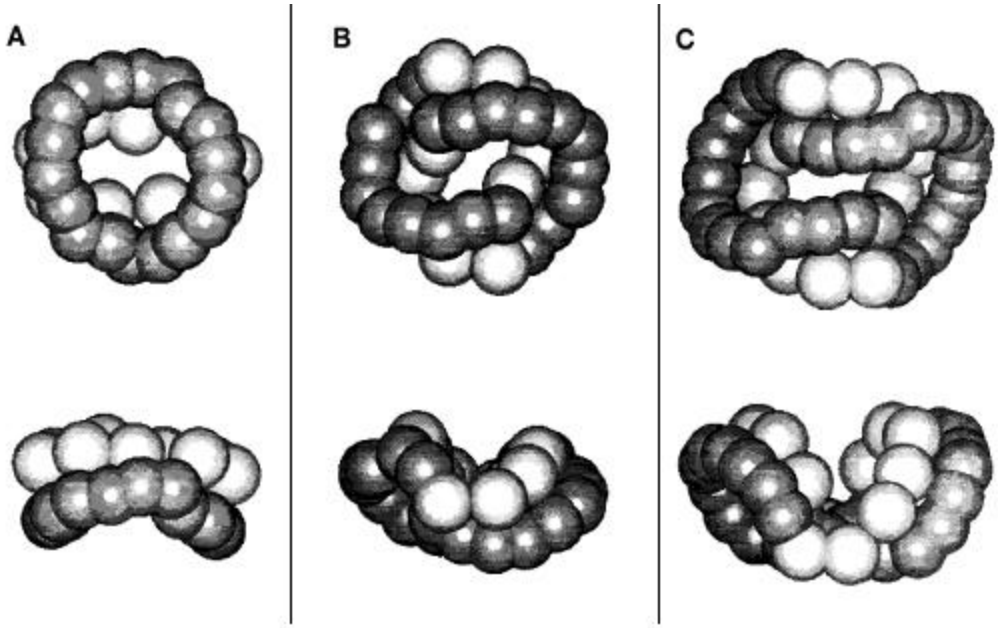

Figure 1.7. Cyclodextrins with 9 ring units (A : δ-CD), 10 ring units (B : ε-CD), and 14 ring units (C : ι-CD) are shown. For clarity, only O2,O3 (dark) and C6 (light) atoms are shown.[57]

remain limited. The dimensions of the three basic CDs are shown in Figure 1.8.

The cavity of the cyclodextrin is moderately hydrophobic, making it amenable to a wide variety of organic guests. Van der Waals and hydrophobic considerations are believed to be the main factors involved in complexation. [58-65] However, steric effects and hydrogen bonding play a role as well.[66,67] The size of the cavity and the CD ring structure is decisively important. A tight spacial fit of the guest is necessary so that multiple instances of the weak forces can add up from various attractions and functional groups to allow complexation. Selectivity is determined by the size, structure, and physiochemical properties of both the guest and CD. There are several books[68] and journals[69] have extensively reviewed CD host-guest chemistry.

This phenomenon of the CD being able to include guests into its cavity is very useful in chromatographic applications. Non-polar analytes have an affinity for the hydrophobic cavity, which allows for an increase in their solubility in an aqueous environment. This is advantageous for those solutes that suffer from problems with detectability. Additionally, some CDs have the ability to experience enantioselective interactions with chiral guests through interactions with the secondary hydroxyl carbons. CDs have been extensively used in electrophoretic separations of a variety of analytes.[70-76] They are especially well suited for capillary electrophoretic (CE) based separations (as discussed in Chapter 2) because they are fairly soluble in aqueous buffers.[77] They are also optically transparent in the UV spectral region, enabling common UV detection methods to still be employed.

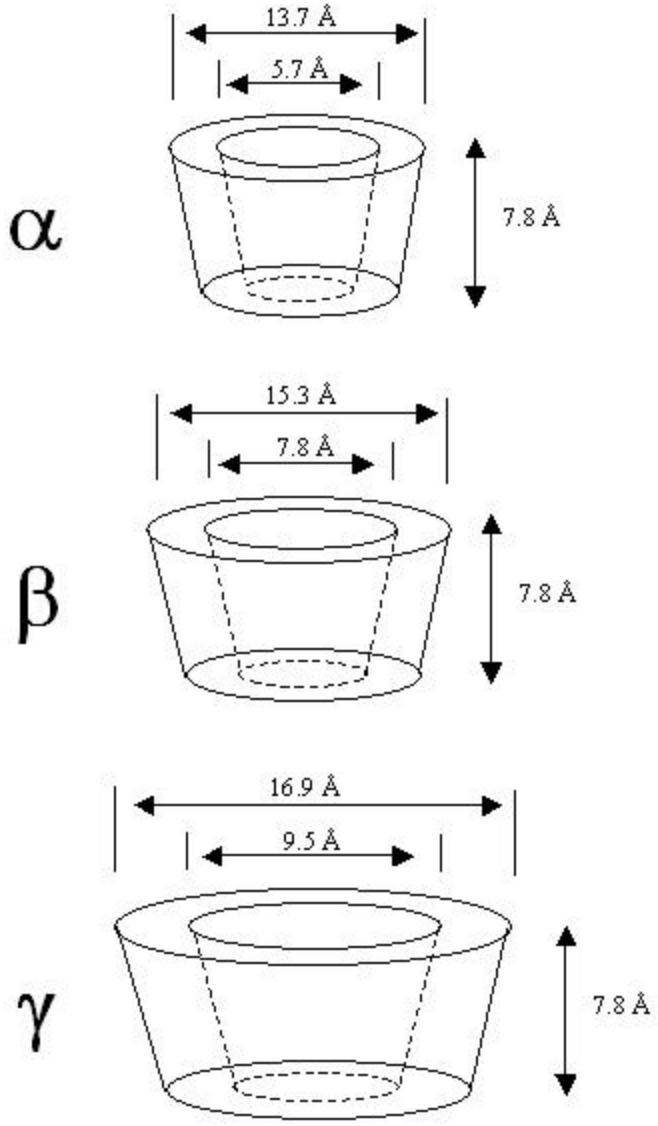

Figure 1.8. The dimensions of α, β, and γ-CD are shown.

CHAPTER 2

INTRODUCTION TO CAPILLARY ELECTROPHORESIS

Introduction and History

Capillary Electrophoresis (CE) is an analytical separation technique where solutes migrate with band velocities (V_b) based on an applied electric field (E) across a capillary and the electroosmotic (μ_{eo}) and electrophoretic mobilities (μ_e).

$$V_b = E \left(m_{EOF} + m_e \right) \qquad (2.1)$$

The roots of CE can first be traced back to Hittorf, Helmholtz, and Kohlrauch who, in the mid 1800s, conducted research into the electrophoresis of small inorganic ions. In 1930, Tiselius performed electrophoresis experiments on proteins, which along with some of his other pioneering work in that area, won him the Nobel Prize in 1948.[78]

The electrical heating of the free solution electrophoresis system, known as joule heating, causes significant band broadening problems. Aware of this issue, Tiselius attempted to remedy it by cooling his cells with circulating water. Other earlier efforts to alleviate joule heating, which are still useful today, included the use of support media such as starch or paper to restrict band diffusion. In 1967 Hjerten found that conducting electrophoresis experiments in small diameter tubes (300μm) significantly reduced the thermal problems.[79] Later in 1979 Verheggen, Mikkers, and Everaerts used a 200μm teflon capillary to further reduce band broadening.

The modern era of CE began in 1981 when Jorgenson and Lukas performed separations in narrow bore glass capillaries less than 100μm in diameter.[80] The

diminutive sizes of these capillaries resulted in efficient dissipation the of electrophoretic heat, thereby permitting the application of large fields without thermal dispersion. The explosion of activity that ensued is evidenced by the enormous number of citations in recent reviews[81,82] and monographs[83-86] on the topic of CE. Advantages relative to high performance liquid chromatography (HPLC) include higher efficiency, speed of analysis, lower solvent and sample consumption, and the ease with which the running buffer can be altered with a wide variety of reagents to change separation selectivity.

Theory

In an applied electric field, ions will migrate toward the oppositely biased electrode in a process called electrophoresis. The electrophoretic mobility of the ion is defined as the ratio of its velocity to the applied electric field (E):

$$\mu_e = \frac{V_b}{E} \qquad (2.2)$$

The magnitude of the ion's mobility is governed by the ratio of the electrical force (F_E) propelling it to the frictional force (F_F) that retards its movement through the given media. These two forces are equal and opposite at equilibrium and relate to the μ_e according to Equation (2.3):

$$\mu_e \propto \frac{F_E}{F_F} \qquad (2.3)$$

The electrical force is simply the product of the electric field and the charge on the ion (q), while the frictional force is governed by the radius (r) of the ion, the viscosity (η), and the ion's velocity (V):

$$F_E = qE \quad (2.4) \qquad F_F = -6\pi\eta rV \quad (2.5)$$

These two forces will be equal and opposite at equilibrium, and therefore can be related to each other according to Stoke's law:

$$qE = 6\pi\eta rV \quad (2.7)$$

Solving for (V) and substituting into Equation (2.2) gives:

$$\mu_e = \frac{q}{6\pi\eta rV} \quad (2.8)$$

This equation reveals all the parameters that affect the mobility of the ion: charge, size and velocity of the ion, and the viscosity of the solution.

Electroosmotic Flow

Electroosmotic flow (EOF) is another important mechanism in CE by which solutes are transported through the capillary to the detector. Capillaries are most often made of fused silica, which is a highly crosslinked polymer of silicon dioxide. The inner surface of the capillary is dominated by terminal silanol groups, which become deprotonated at higher pH. It attracts a tightly bound layer of cations from the buffer solution forming an electrical double-layer (Figure 2.1). Next to this layer is a loosely associated region that is also generally rich in cations. The shear plane (or slipping plane) is an imaginary surface separating the thin layer of buffer bound to the capillary wall. It shows elastic behavior in contrast to the rest of the buffer that exhibits normal viscous behavior. An electric potential exists at the shear plane called the zeta potential (ζ).

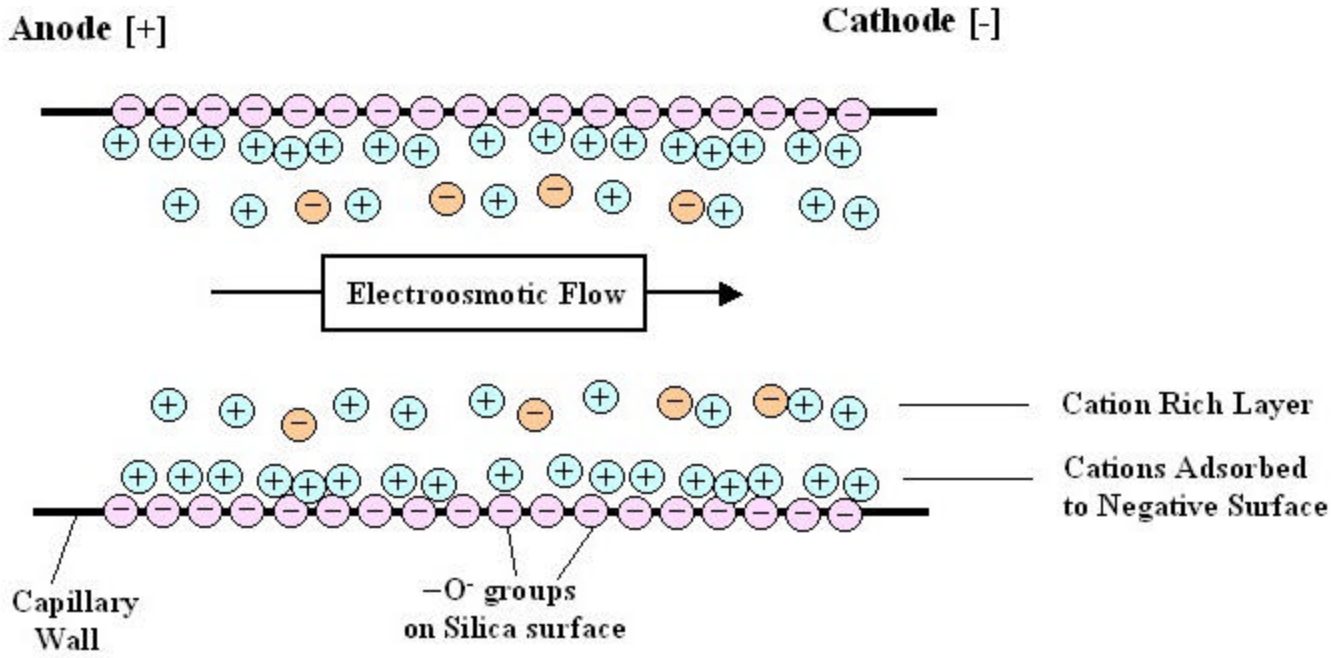

Figure 2.1. Electroosmotic flow occurs as a result of the cation rich layer near the walls migrating toward the cathode.

As the potential is applied across the capillary, the solvated cations near the walls begin to migrate toward the negatively biased cathode. This mass migration induces flow (EOF) and sweeps the entire solution down the capillary, including any neutral and charged species present. The magnitude of the EOF is measured in velocity (V_{EOF}) or mobility (μ_{EOF}):

$$V_{EOF} = \frac{\varepsilon\zeta}{\eta} E \qquad (2.9)$$

or

$$\mu_{EOF} = \frac{\varepsilon\zeta}{\eta} \qquad (2.10)$$

The EOF increases with pH due to more of the silanol groups becoming deprotonated and increasing the zeta potential. At pH values of 4 or less, the EOF is almost nonexistent, whereas a pH of 9 or greater results in a completely ionized surface and strong flow. An increase in ionic strength will cause a decrease in EOF. This is because the zeta potential is affected by the buffer concentration as described by the expression in Equation (2.11), where (δ) is the double-layer thickness or Debye ionic radius, (e) is the total excess charge in solution per unit area, and (ε) is the dielectric constant:

$$\zeta = \frac{4\pi\delta e}{\varepsilon} \qquad (2.11) \qquad\qquad \delta = (3x10^{7})\,(Z)\,(C^{1/2}) \qquad (2.12)$$

In the Debye radius expression, (Z) is the total number of valence electrons and (C) is the buffer concentration. As can be seen from these equations, the EOF decreases with the square root of the buffer concentration. Additionally higher ionic strength will

increase the current across the capillary and exacerbate joule heating and band broadening. Therefore, buffer component concentrations are typically kept around the 10-20 mM range in CE.

Observed Mobility

As stated in Equation (2.1), the observed velocity of a band is governed by the applied electrical potential, the EOF, and the solute's own electrophoretic mobility in the applied field:

$$V_b = E\ (\ m_{EOF} + m_e) \qquad (2.1)$$

The observed mobility (μ_{obs}) of a solute is a function of its electrophoretic mobility and the EOF:

$$m_{obs} = m_{EOF} + m_e \qquad (2.13)$$

A depiction of the different effective mobilities for charged and neutral species is shown in Figure 2.2. Neutral species will move at the same speed as EOF because they do not experience any electrophoretic mobility. However, the cations will migrate toward the negatively biased cathode, making their μ_{obs} higher than EOF. Since the μ_e is determined by the charge to mass ratio, smaller cations will experience greater observed mobility than equally charged more massive cations. Similarly, the smallest anions will electromigrate fastest toward the anode, essentially "swimming upstream" against the EOF.

The migration time (t) of a given solute band can be determined by Equation (2.14), where (L) is the total length of the capillary, (l) is the effective length of the capillary from inlet to the detection site, and (V) is the velocity of the band.

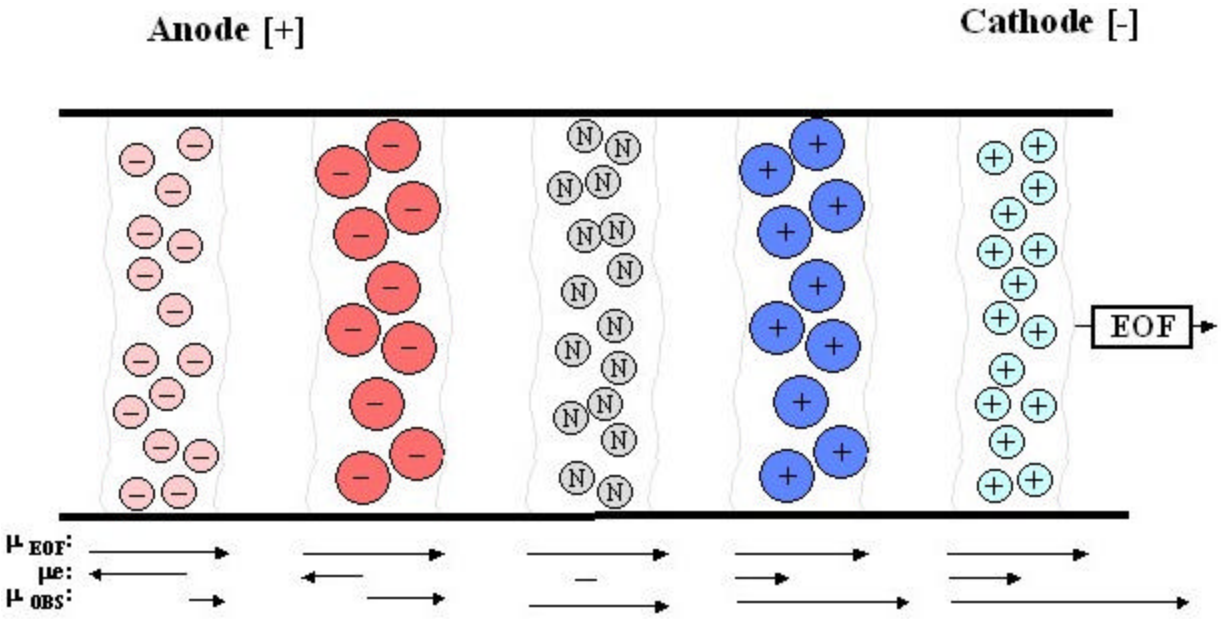

Figure 2.2. Neutral and charged species of different sizes separate as a result of their different effective mobilities, μ_{obs}.

$$t = \frac{l}{\mu_{obs} E} = \frac{l L}{\mu_{obs} V} \qquad (2.14)$$

Efficiency and Resolution

Efficiency and band broadening are primarily dependant upon diffusion in CE, because flow profile does not introduce a large amount dispersion like it does in some pressure driven separation techniques. The EOF exhibits a flow profile that is plug-like in nature. This is the principal phenomenon in CE that is responsible for the extraordinarily high separation efficiencies that can be achieved. Unlike the parabolic flow that arises from hydrodynamic pressures in techniques such as HPLC, the plug-like flow characteristic greatly reduces band broadening (Figure 2.3). With parabolic flow, hydrodynamic pressure forces the solution in the middle of the column to move faster than the solution near the walls. This results in band broadening as the parabola shaped band diffuses laterally, making a wider band. There is substantially less band broadening with the plug-like flow, resulting in significantly more narrow bands.

The width of a peak at its baseline (w_b) is equal to 4 times the standard deviation of the peak (σ):

$$w_b = 4\sigma \qquad (2.15)$$

Efficiency (N) is the number of theoretical plates and can be defined by σ :

$$N = \left[\frac{l}{\sigma}\right]^2 \qquad (2.16)$$

The variance (σ^2) in CE is diffusion dependant and can be given by the equation:

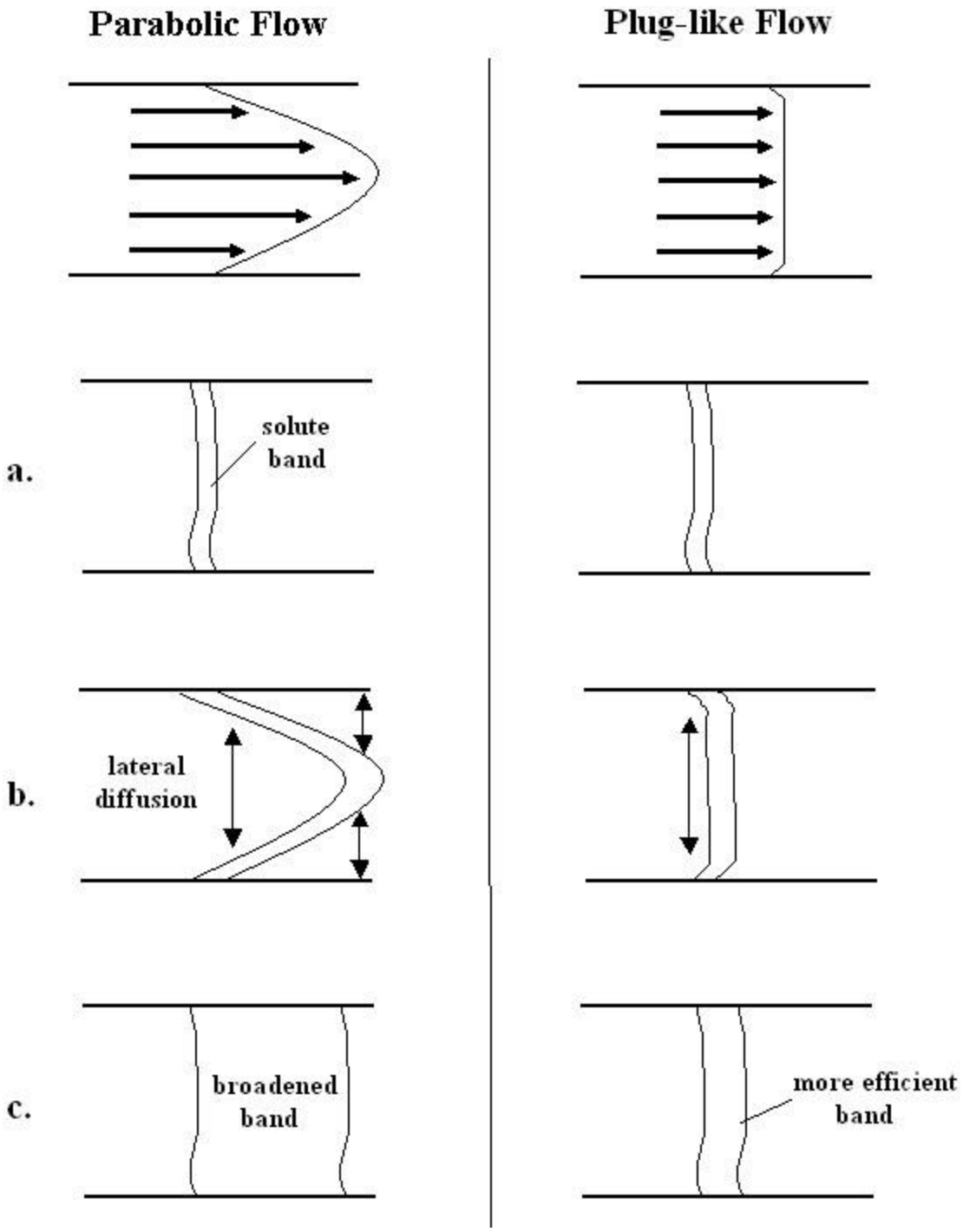

Figure 2.3. The effect of parabolic flow vs. plug-like flow on a solute band (a) is shown in (b). Plug-like flow results in more efficient bands (c).

$$\sigma^2 = 2Dt = \frac{2Dt\, l\, L}{\mu_e V} \qquad (2.17)$$

Where (D) is the diffusion coefficient. Relating this to (N), the fundamental equation for efficiency in CE is obtained:

$$N = \frac{\mu_e V l}{2DL} = \frac{\mu_e E l}{2D} \qquad (2.18)$$

Although the dominant factor contributing to band broadening in CE is diffusion, other phenomenon do have a measurable effect. The total variance of the system (σ^2_T) is the sum of all of these factors and includes contributions from diffusion (dif), injection (inj), temperature (tem), adsorption (ads), electrodispersion (eld), detector (det), and any additional contributing factor (misc):

$$S^2_T = S^2_{dif} + S^2_{inj} + S^2_{tem} + S^2_{ads} + S^2_{eld} + S^2_{det} + S^2_{misc} \qquad (2.19)$$

The resolution (R_s) can be calculated from the electropherogram itself using the width of the two peaks at baseline (W_1, W_2) and the difference in migration time between them (Δt):

$$R_s = \frac{\Delta t}{W_1 + W_2} \qquad (2.20)$$

Resolution is based on efficiency, and can also be described using the difference in electrophoretic mobility ($\Delta\mu$) and the average mobility of the two peaks (μ_{avg}):

$$R_s = \frac{N^{1/2}\, \Delta\mu}{4\, \mu_{avg}} \qquad (2.21)$$

Instrumentation

One of the main advantages of CE is the simple instrumentation. A schematic diagram of the components is shown in Figure 2.4. These basic components are easily put together in a homemade system. A power supply that can generate up to 30 kV is used to apply the electrical potential across the capillary. The capillary is generally 20 to 70 cm long, with inner diameters between 10 and 75 µm and the terminal ends are placed into vials containing the buffer solution. A window in the capillary is prepared by removing the protective polyamide coating on the capillary so that an optical detection method can be used. Fluorescence, laser-induced fluorescence, and UV/Vis detection are common. The sample can be introduced by electrokinetic injection or pressure injection. For pressure injection, positive pressure is applied to the capillary for a given amount of time to introduce the sample. Alternatively, negative pressure can be used to suck in the sample. With electrokinetic injection, the sample is introduced into the capillary by electrophoresis by applying an electric field for a given period of time. Commercial instruments often apply a pressure to a sealed sample vial to introduce the sample into the capillary. used to apply the electrical potential across the capillary.

The capillary is generally 20 to 70 cm long, with inner diameters between 10 and 75 µm and the terminal ends are placed into vials containing the buffer solution. A window in the capillary is prepared by removing the protective polyamide coating on the capillary so that an optical detection method can be used. Fluorescence, laser-induced fluorescence, and UV/Vis detection are common. The sample can be introduced by electrokinetic injection or pressure injection. For pressure injection, positive pressure is applied to the capillary for a given amount of time to introduce the sample.

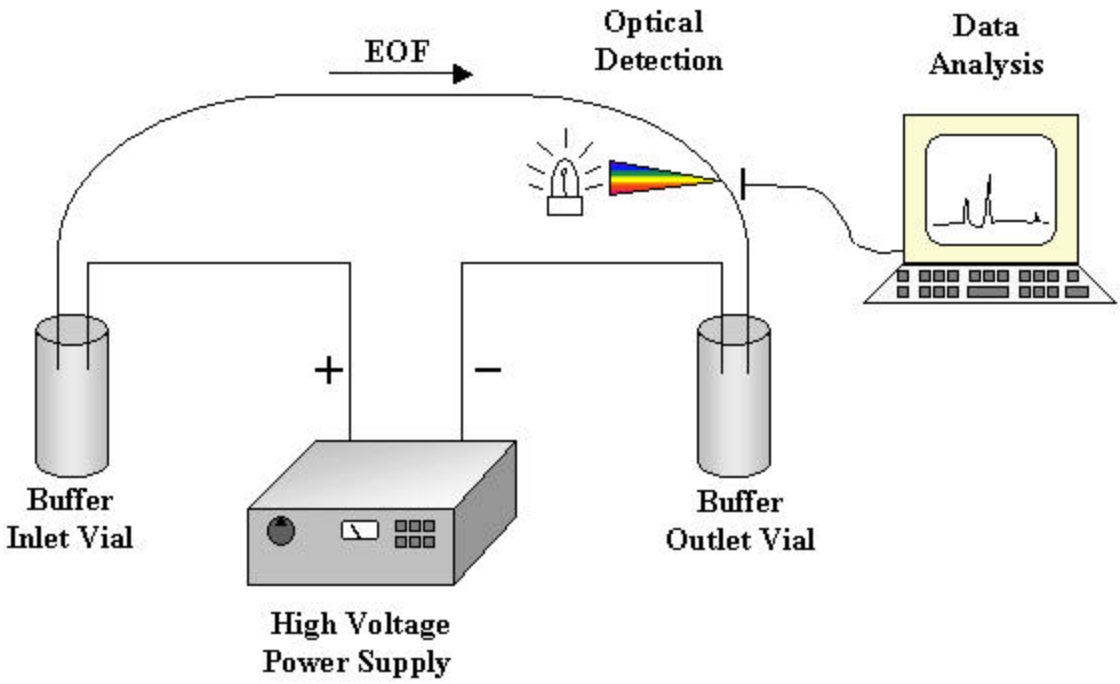

Figure 2.4. A schematic diagram of a CE system.

Alternatively, negative pressure can be used to suck in the sample. With electrokinetic injection, the sample is introduced into the capillary by electrophoresis by applying an electric field for a given period of time. Commercial instruments often apply a pressure to a sealed sample vial to introduce the sample into the capillary.

Buffer Additives

The purpose of the buffer in CE is to provide precise control of the pH and maintain a steady EOF. A wide variety of buffers are possible, and phosphate or borate buffers are most common. Concentrations generally range between 10 and 100 mM.

Many different types of reagents are commonly added to the running buffer in CE to achieve functions other than maintaining the pH. Organic solvents can be added to change the hydrophobicity and increase solubility of non-polar compounds. Reagents such as polyamines, linear polymers, and cationic surfactants are sometimes included to reduce the problems of solutes sticking to the walls, or to modify EOF.

The use of some additives can extend the utility of CE well beyond the simple separation of charged species based on their size to charge ratio. By the use of compounds for which solutes have an affinity, a differential partitioning between the additive and the buffer can occur, essentially forming a "pseudophase" within the capillary. There are a wide variety of additives of this nature, including surfactants, cyclodextrins,[87] dendrimers,[88] macrocyclic antibiotics,[89] crown ethers,[90] polymeric ion-exchangers,[91,92] and polymeric surfactants.[93]

Micellar Electrokinetic Chromatography

The technique of adding a surfactant to the buffer to modify the mobility of the solutes is called micellar electrokinetic chromatography (MEKC). This advance was first

reported by Terabe, et al. in 1984 and 1985.[94,95] When a surfactant such as sodium dodecylsulfate (SDS) is present above a certain concentration known as the critical micelle concentration (CMC), aggregates called micelles spontaneously form. Other examples of molecular aggregates used as a "pseudophase" include microemulsions,[96-98] liposomes,[99] and vesicles.[100]

In solution, the long hydrophobic portion of surfactant molecules collect together to minimize the surface exposed to the aqueous environment. The polar ends orient themselves on the outside of this collection and a charged micelle is formed (Figure 2.5). The overall negative charge of the micelle imparts upon it a mobility that is opposite of the EOF. As solutes partition between the micelle and the running buffer, the observed mobility of the solute is modified as illustrated in Figure 2.6. Neutral solutes can be separated with MEKC in this manner based on their differential affinity for the micelles. Charged solutes also experience this partitioning and are simultaneously separated both electrophoretically and by the interaction with the micelles.[101]

In general, solutes elute within a window bound by the void time of the system (t_o) and the effective retention time of the charged micelles (t_{mc}). The velocity of a neutral solute band in MEKC is given by Eq. 2.22,

$$\mathbf{V_b = E\ (\ f_{mic} \cdot m_{mic} + f_{rb} \cdot m_{eo})} \qquad (2.22)$$

where f_{mic} and f_{rb} are the fractional amount of the solute in the micellar and running buffer phases, respectively, and μ_{mic} is the net mobility of the micelles. In general, the elution characteristics of MEKC resemble that of reversed phase HPLC; i.e., retention scales as the lipophibicity of the analyte. The fundamental equation for the capacity factor (k') in MEKC is:

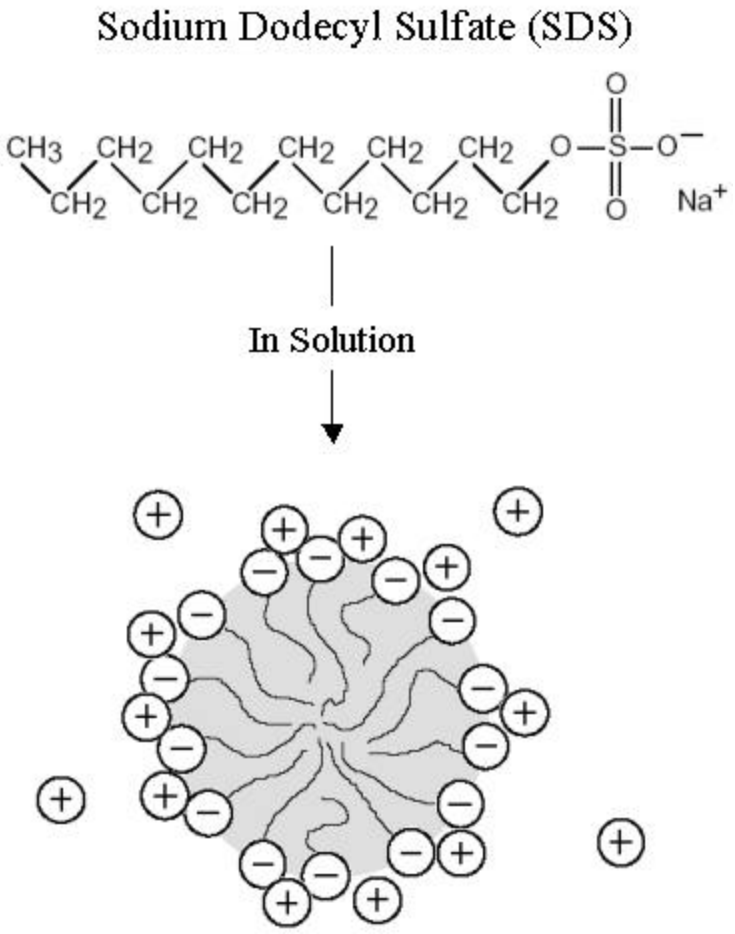

Figure 2.5. The surfactant sodium dodecyl sulfate aggregates into a micelle at conditions above the critical micelle concentration.

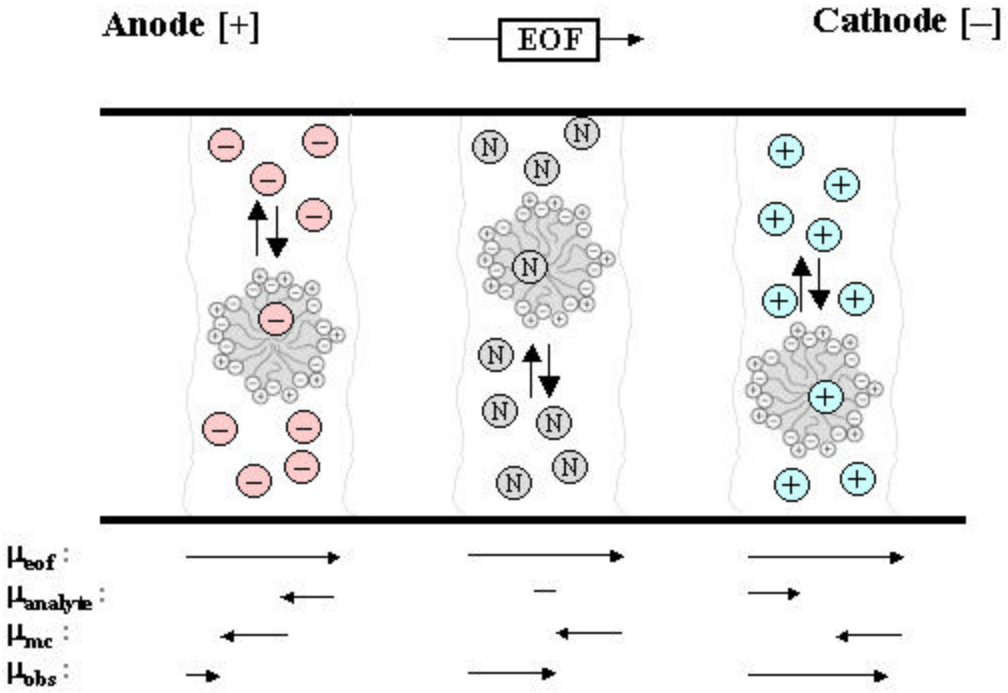

Figure 2.6. Neutral and charged solutes partition between the buffer and micelles in a MEKC separation. The observed mobility (μ_{obs}) of the analyte is dependant upon the electrophoretic mobility of the analyte ($\mu_{analyte}$), the electroosmotic flow (μ_{eof}), and the mobility of the analyte in the micelle (μ_{mc}).

$$k' = \frac{t_R - t_o}{t_o\,(1 - t_R/t_{mc})} \qquad (2.23)$$

where t_R is the retention time of the solute. As the velocity of the micelles approach zero, they essentially do effectively become a stationary phase. When (t_{mc}) approaches infinity, Equation (2.23) becomes the general chromatographic equation for (k').

Resolution for two solutes in MEKC is given by Equation (2.24). The separation factor (α) = $[A]_{mc}[B]_{rb} / [A]_{rb}[B]_{mc}$, where the concentrations of solute [A] and [B] in both the running buffer (rb) and micelles (mc) are given.

$$R_s = \frac{N^{1/2}}{4}\left[\frac{\alpha - 1}{\alpha}\right]\left[\frac{k'_2}{1 + k'_2}\right]\left[\frac{1 - t_o/t_{mc}}{1 + (t_o/t_{mc})\,k'_1}\right] \qquad (2.24)$$

Again, it can be seen that as the t_{mc} approaches infinity, the equation reduces to the classical chromatographic expression for resolution.

Cyclodextrin Modified MEKC and Cyclodextrin Distribution Electrochromatography

Natural and synthetic macrocyclic compounds have demonstrated utility for chemical separations. Macrocycle reagents have a higher order of selectivity than is generally possible with micellar systems. Moreover, the molecular architecture of many macrocycles may be computationally modeled and synthetically adjusted to probe analyte recognition. Also, combinations of the macrocycles may be employed with predictable effects. Surfactant mixtures cannot be used in the same manner because of the formation of structurally complicated and dynamic mixed micelles.

The macrocycles that have received the greatest attention are the CDs. Native CDs are neutral, cylindrical-shaped, macrocyclic sugar molecules that posses a hydrophobic cavity and a hydrophilic exterior, as described in Chapter 1. CDs have the distinct advantage that they are transparent in the UV-Vis spectrum, which is very commonly used in CE. This allows analytes with absorbance in the UV-Vis spectral region to be detected without interference from the CDs.

A popular technique is to combine cyclodextrins into the running buffer of a MEKC separation, known as cyclodextrin modified MEKC. One difficulty in MEKC is that the affinity of many hydrophobic solutes for the micelles is so high that they sometimes all co-elute with each other at (t_{mc}). When cyclodextrins are added to the mixture they compete with the micelles for the solutes, which can have selective associations with the CDs. This secondary pseudophase selectively forces the solutes to have the mobility of the EOF when associated with the neutral CDs

If equilibrium constants for this complex formation differ between solutes, separation is achieved. Because the separation mechanism is different for CDs (complex formation) and micelles (surface interaction), the combination of the two can be a very useful technique when dealing with hydrophobic solutes, such as polycyclic aromatic hydrocarbons,[102,103] polychlorinated biphenyls,[104] or nitroaromatic compounds.[105] Terabe and coworkers have separated positional isomers of dimethylnaphthalenes and optical isomers of dansylated amino acids using and SDS buffer modified with γ-CD.[106]

Another application involving CDs is called Cyclodextrin Distribution Capillary Electrochromatography (CDCE).[107] In this technique charged CDs are employed in the running buffer, sometimes mixed with another neutral CD or multiple CDs. The charged

cyclodextrin will selectively modify the mobility of the solute while it is complexed, providing the basis for separation. The neutral CDs compete for the analytes. The velocity of the solute band (V_b) will be dependant on the fraction of time (f) the solute spends in the CDs and the running buffer:

$$\mathbf{V_b = f_{CD1}V_{CD1} + f_{CD2}V_{CD2} + f_{CD3}V_{CD3} + \ldots + f_{rb}V_{EOF}} \qquad (2.25)$$

Chiral Recognition

In the area of chiral recognition, CE has established itself as being a versatile technique, and distinctly superior to LC in terms of cost, speed, and resolution. Gassmann, et al. were the first to demonstrate chiral recognition in CE by adding cupric ion and $_L$-histidine to the running buffer and separating dansyl amino acids.[108] Chiral surfactants and mixed micelles have been used as well.[109,110]

Today, the reagents used most for chiral CE separations are cyclodextrins. Since 1989 when Fanali first used CDs for a chiral separation of optical isomers,[111] hundreds of published works in this area have appeared. Because CDs lend themselves easily to derivatization, CD buffer additives beyond the traditional α-, β-, and γ-CD appeared soon afterwards.[112-114] Later, in 1994 the first charged CDs were used, which migrate opposite the EOF and further enhance separation.[115] The charged Carboxymethyl β-CD (degree of substitution 3.6 and 6.0) and succinylated β-CD (degree of substitution 3.5) were in enantiomeric separations by Schmitt and Engelhardt.[114]

Vigh and coworkers developed the next generation of CDs by synthesizing and using highly charged, single isomer CDs for chiral separations.[116,117] This not only alleviates the problems of multiple isomers with charged CDs, but also allows for the enantiomeric separations to have the advantage of very large elution window (the time

between the elution of the charged CD and t_o). Also, the additional charge on the CD enables even more electrostatic interaction between the solutes and CD, significantly influencing the enantiomeric separation. Work using Vigh's highly charged cyclodextrin and others used for chiral separations of dansylated amino acids is presented in Chapter 5.

CHAPTER 3

INTRODUCTION TO COMPUTATIONAL MOLECULAR MODELING

Introduction

Chemists have been attempting to create increasingly realistic and useful models of atoms and molecules for centuries. In the early 1800s Dalton's model first described atoms as tiny, indivisible, indestructible particles that have a certain mass, size, and chemical behavior. Building on a model proposed by Kelvin in 1902, Thompson developed a "plum pudding" model of the atom where atoms were composed of spheres of evenly distributed positive and negative charges.

Rutherford, Bohr, Schrodinger, and others expanded and improved upon previous models to give us our current working model of the atom. The noteworthy point is that *models change* and *improve* over time. The pattern of improvement has generally been characterized by "quantum leaps" in understanding, which open the flood-gates of advancement as scientist utilize their new knowledge.

Today we have a wide array of models and systems designed to simulate and help understand the processes and interactions that occur at the molecular level. Scientists today are now armed with computers, which allow previously unattainable levels of calculations to be performed, new data analysis techniques to be used, and enable visualization methods that are drastically improving our understanding of the chemical world. This chapter will take a broad look at molecular modeling and discuss how

different models are designed and function, and explore how some of these modeling techniques are optimally utilized.

Molecular Mechanics

Molecular mechanics (MM) is a non-quantum mechanical computational method of determining the energy and structure of a molecule. In the simplest sense, MM predicts the most energetically favorable conformations of a molecule. This is done by considering the molecule as a collection of atomic nuclei held together by elastic bonds having differing force constants. The forces that hold the atoms together are described by potential energy functions of bond lengths, bond angles, and non-covalent bonding interactions. The potential energy functions are calculated with respect to an "ideal" structure of the molecule in question (they are relative). The sum of these energies is the energy of the molecule in a given configuration. The geometry of the nuclei in the molecule can be altered (configuration changed) and the energy recalculated in pursuit of energetically favorable conformers. MM is generally much faster than quantum mechanical calculations, because EFFs deal with electrons in a more direct and simple manner.[118]

Force Fields

There have been many force fields developed over the past few decades. A discussion of the general approaches of all force fields is presented here rather than an attempt to review all such efforts. A list and description of well known and often used force fields can be found in Appendix A.1.

Force fields describe chemical bonds by stretching, bending, and torsional potentials. Ab initio data at the Hartree-Fock level is used to determine the parameters

for the bonded interaction. Electrostatic interactions are addressed by calculating and assigning partial charges to the atoms.

The energy, E, of a molecule derived from a force field is given by a sum of energy contributions. The earliest MM models used force fields that added only three energy terms: the contribution from the energy in a bond (E_{bonds}), the contribution from each bonding angle (E_{angles}), and the energy of van der Waals forces (E_{vdw}).[119-121] However, later it was determined that a term for the torsion angles, $E_{torsion}$, was important. Energy contributions from charge interactions, E_{charge}, were also found to be necessary for the force field to function properly for molecules with electronegative groups.

Most force fields use these energy terms, and follow the general pattern shown in the expression below (Equation 3.1.) Force fields are often individualized by additional terms as well (E_{misc}).

$$\mathbf{E_{MM} = E_{bonds} + E_{angleS} + E_{vdw} + E_{torsion} + E_{charge} + E_{misc}} \qquad (3.1)$$

A review of different force field approaches was published as early as 1956,[122] in which Hendrickson accurately predicted that "machine computation" would be the future of molecular mechanics calculations.[123]

E_{bonds} is the first term in the force field expressions, dealing with the bond stretching energy. As described in Figure 3.1, the bond is treated as a spring. The energy can be described by Hooke's law approximation, which gives a harmonic energy curve. The energy, E_{bonds}, is the square of the displacement of the two atoms ($l - l_o$), multiplied by the "spring constant" (k):

$$\mathbf{E_{bonds} = k_1 (l - l_o)^2} \qquad (3.2)$$

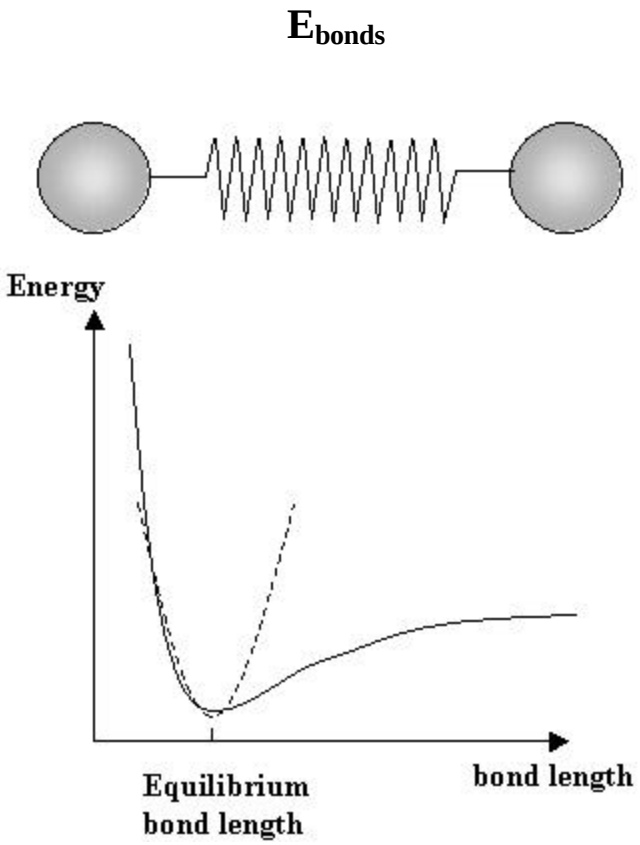

Figure 3.1. A chemical bond is treated as a spring. The plot below shows change of energy with bond length, and Hooke's Law approximation (dashed).

As can be seen from the Equation 3.2, the energy increases during both compression and stretching of the bond. Hooke's Law approximation (Figure 3.1, dashed line) would dictate that the energy continually increase as the bond stretching is increased. However, in real bonds the attraction between atoms will eventually deviate from the "spring constant" value, k, and the bond will be broken. A distance dependant k value is therefore sometimes implemented for E_{bonds} calculations, with the values being determined by X-ray diffraction and infra-red spectroscopy. There are large databases of such information, from which force fields can obtain their parameters.[118]

The bending of a bond angle between two atoms (E_{angles}), can be described by Equation 3.3, where the energy is dependant on the square of the displacement from equilibrium (see Figure 3.2 a):

$$\mathbf{E_{angles}} = \mathbf{k}_q (q - q_o)^2 \qquad (3.3)$$

The torsional angle energy ($E_{torsion}$) is also shown represented in Figure 3.2 b. Energy barriers to rotation occur as molecules rotate along single bonds. This energy can be calculated by a partial Fourier series:

$$\mathbf{E_{torsion} = V_1/2\ (1 + \cos}\ q\mathbf{)} + \mathbf{V_2/2\ (1 - \cos}\ 2q\mathbf{)} + \mathbf{V_1/2\ (1 + \cos}\ 3q\mathbf{)} \qquad (3.4)$$

where (θ) is the torsion angle between the four atoms involved. These rotation barrier parameters are found in databases of experimental data from microwave spectroscopy and NMR measurements.

Atoms behave as though they have a definite size, and the van der Waals radius is a measure of this. As atoms approach each other at very close ranges, the energy goes up very quickly (see Hooke's Law approximation, Figure 3.2). The van der Waals radius is

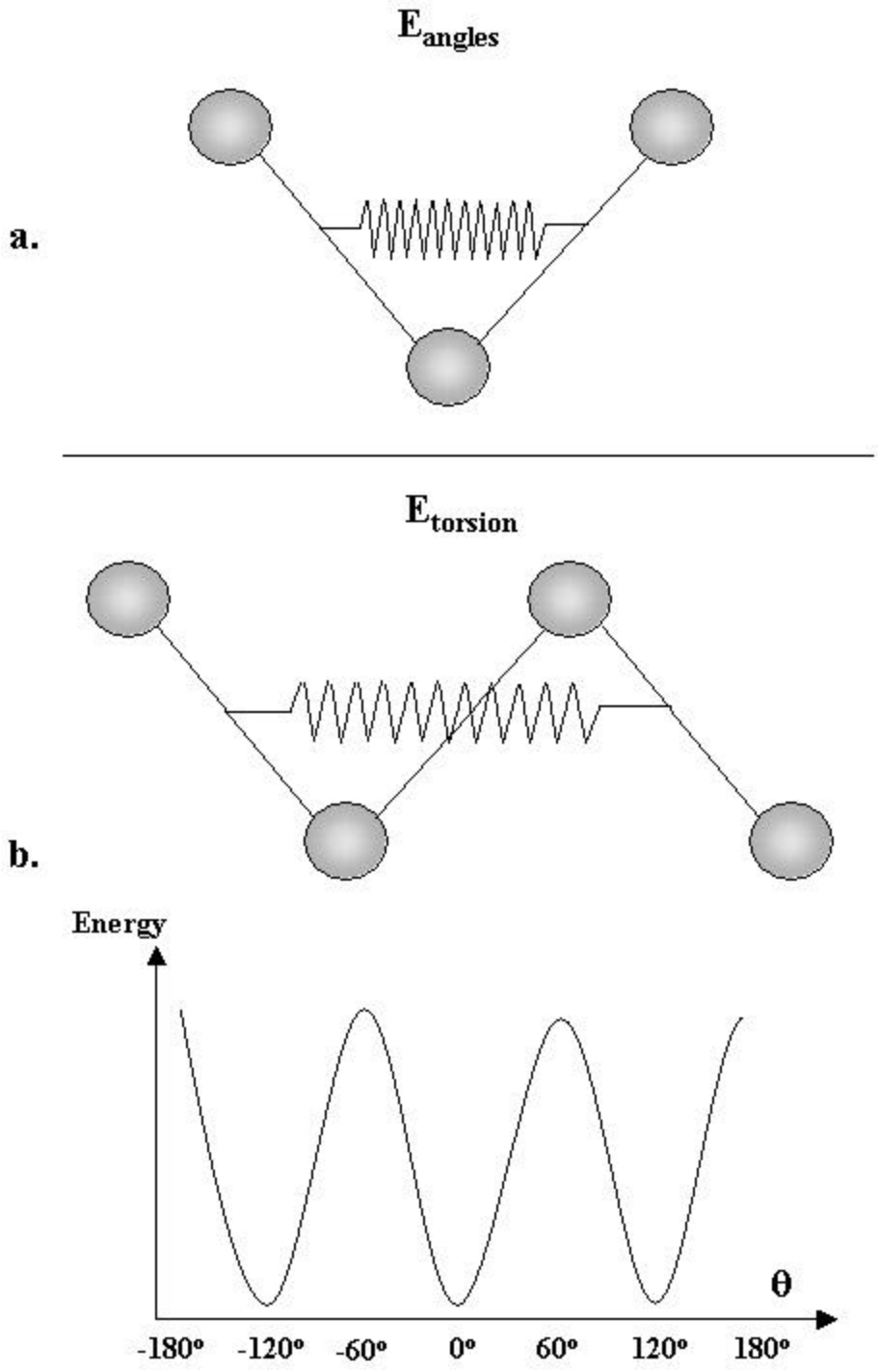

Figure 3.2. Angle bending of atoms (a) is shown. The constraining of a torsion angle (b) creates a barrier to rotation, as shown in a typical plot of energy vs. rotational angle, θ.

usually estimated from X-ray diffraction experiments. The kinetic theory of gases also allows for cross-sectional areas to be calculated.[124] The energy of van der Waals interactions (E_{vdw}) is a measure of the interaction between atoms that are separated by three or more bonds. This is because the E_{angle} and $E_{torsion}$ already deal with the closer interactions. The Lennard-Jones potential uses a $1/r^{12}$ term, and various force fields use this in expressions for E_{vdw} and give similar results. The expression for E_{vdw} and other energy terms can be found in Appendix A.2.

Coulomb's Law is used to calculate the energy of electrostatic attractions and repulsions (Equation 3.5). Charge-charge interactions are determined via a partial charge assigned to every atom.

$$E_{charge} = \frac{1}{4\pi\varepsilon} \frac{q_1 q_2}{r} \qquad (3.5)$$

The partial charges from the two atoms are included in Equation 3.5 as q_1 and q_2. The attractive or repulsive force between the two charged particles has a $1/r^2$ dependance, and the energy has a 1/r dependance. ε is the dielectric constant. Calculation of the partial charges is frequently accomplished by considering their electronegativity, as used in a technique developed by Gasteiger et al.[125]

The number of calculations needed to determine E_{charge} rises exponentially with the number of atoms to address. E_{charge} must be calculated by adding up the resulting energies for all pairs of atoms. For a molecule with N atoms, there are N^2 interactions to consider. A common approach is to specify a cut-off distance, where atoms separated by this distance or more are considered to have no interaction.

Most force fields also apply additional energy consideration terms to the calculation of E_{MM}. For example, the stretching of a bond may also affect the bending of that bond. These effects are usually added into the E_{misc} term to improve force field results.

Energy Calculation

The thermodynamic value that is most interesting for many experiments is the free energy (G). However, since this value is dependant on the entropy of the molecule, free energy can be difficult to calculate directly from modeling results. Molecular mechanics calculations will yield the E_{MM} energy (as described in Equation 3.1) by summing up all the various interactions between atoms. This value is not the free energy, but it does relate to it.

E_{MM} is most closely comparable to the internal energy (U) of a molecule. Because absolute values of E_{MM} are generally not based on a zero point, differences in energy are used to relate it to the change in internal energy (ΔE_{MM} and ΔU). This has the additional advantage that errors in certain calculations may cancel.

The internal energy can be related to the other thermodynamic quantities using standard equations. The enthalpy is given by:

$$\mathbf{H = U + PV} \qquad (3.6)$$

and

$$\mathbf{\Delta H = \Delta U + P\Delta V} \qquad (3.7)$$

where V is the volume and P is the pressure. If there is no external pressure to consider, such as in a molecular mechanics calculation, the enthalpy can be related to the calculated energy:

$$\Delta H \tilde{} \Delta U \tilde{} E_{MM} \qquad (3.8)$$

The fundamental equation for free energy change (ΔG) shows its relation to enthalpy:

$$\Delta G = \Delta H - T\Delta S \qquad (3.9)$$

where ΔS is the change in entropy and T is the temperature. Under certain circumstance the change in entropy can be considered to be small, and the molecular mechanics energy can be considered a reasonable approximation of ΔG.

Conformation Searching

Single low energy conformations usually do not adequately describe most molecules. The lowest energy conformation (global minimum) is generally useful information, but many structures near the global minimum are also very important. Conformation searching can be used to find these structures, and can be conducted in different ways.

Systematic Search

A systematic search is a type of conformation searching that assumes the various possible conformations of a molecule are only different in their torsion angles. Every possible combination of torsion angles is explored by systematically creating and minimizing each one. In principle, all possible minima are addressed, including the global minimum. The time to interrogate the angles is usually very long, unless the possible torsion angles are restricted to large rotational increments.. This approach is

rather comprehensive in its intent, but necessitates an extraordinary amount of computation, even for small molecules.

Monte Carlo Searching

Monte Carlo (MC) searching is another method to find molecular conformations that is generally faster than the exhaustive systematic technique. MC searching is also called semi-random searching, and is based on the idea that most structurally important low energy configurations will have many features in common. Once a low energy conformation has been identified, then small changes are made to it by moving one or two atoms or twisting angles slightly.[126-128]

MC starts by considering all the atoms as particles and determines the initial energy (E1) of this system. Then a second configuration is generated by randomly moving some of the particles in the system, and the energy (E2) is calculated. The second configuration is determined to be important if E2<E1 with some probability:

$$\mathbf{p = exp[(E2 - E1)/kt]} \qquad (3.10)$$

Large numbers of these energetically important conformations are created which are then analyzed or averaged. MC searching has been commonly used to study the arrangements of solvent molecules around solutes.[118]

The utility of MC methods that use the Metropolis criteria[129] have been demonstrated as being competitive with molecular dynamics simulations for studies involving liquid simulations, and in rigid systems with small numbers of variable torsion angles.[130-134] Larger systems are more efficiently studied with molecular dynamics (MD)

to simulate complex molecules[135] when using Cartesian coordinates of the atoms as the natural variables of motion.

Molecular Dynamics

Molecular dynamics (MD) is a molecular modeling method used to simulate molecules in motion. The molecule is set in motion by giving kinetic energy to each atom in the structure. As the molecule then moves around, the Newtonian equations of motion can be used to describe its behavior:

$$\mathbf{F_i(t) = m_i a_i = m_i d^2 r_i(t)/dt^2} \qquad (3.11)$$

where $F_i(t)$, $a_i(t)$ and $r_i(t)$ are the force, acceleration and position of an atom i at the time t, respectively. A force field (like those used in molecular mechanics) is selected to determine the potential function for each atom in this calculation. The equations of motion are used with the calculated velocities and positions to create a history of the system's motion. Small time steps are needed in this technique, necessarily small in comparison with the highest frequency motion in the molecule (usually hydrogen bond stretching).[136] With time steps in the region of 1 femtosecond to picosecond, only very fast molecular phenomenon can be studied.

Molecular dynamics simulations are most useful in large systems, where the amount of computation is beyond the scope of systematic searching, i.e. protein or other macromolecular conformations. MD has been successfully employed to study large biomolecules in many cases,[137-142] and been used to simulate peptides,[143,144] proteins[145] and non-peptide biopolymers.[146,147]

MD is also frequently used in a process called simulated annealing.[148] This process works by making random changes to the structure and evaluating whether the new or old structure is more energetically favorable, using the Metropolis criterion.[129] Simulated annealing was designed as a technique to accomplish both a computational model of experimental annealing techiniques, and to use temperature as a mechanism with which to overcome torsional barriers in structures.

Simulated annealing is similar to experimental annealing, where the compound is heated and cooled slowly so that the resulting structure is more thermodynamically favorable rather than kinetically favored. In the computational version, the temperature is systematically increased and decreased for a structure with initially random velocities and configurations for each atom. As the temperature is cycled, the motion of the molecule is traced. Simulated Annealing has a higher chance of finding the global minimum the slower the energy is removed. The computing time, however, increases proportionally with the degree to which the cooling is slowed down.[149]

Molecular Graphics

With the very large amounts of data that are generated by molecular mechanics, molecular dynamics, and Monte Carlo simulations, methods to manage and analyze the information are very important. Molecular graphics and visualization techniques can present the vast collections of data in understandable, manageable formats. Different rendering options like ball-and-stick, line, and space-filled are useful for viewing molecular structures. Three dimensional views are another frequently used molecular graphic, made additionally useful by images that emphasize interesting structural, chemical, or reactivity features of the molecule. Dynamic processes can be simulated

and viewed as movies. Molecular graphics allow the user to stand back from the theories and equations and conceptualize the "big picture" of the many processes occurring at the molecular level.

One exceptionally useful molecular graphics tool is known as MolCAD (Molecular Computer Aided Design), and is part of the Sybyl software from Tripos.[150] MolCAD can generate a visual representation of a molecule's surface using different methods. Connolly surfaces and electron density surfaces are methods generally used for all molecules. Ribbon representations are useful for large macromolecular systems, like proteins, where other visualizations are not adequate. The protein is usually shown as a ribbon, and it can be colored based on atomic flexibility, residue flexibility, packing density, or residue lipophilicity.

The Connolly surface is constructed by calculating the solvent accessible surface of a molecule using the coordinates of all the atoms in the molecule.[151,152] The electron density surface is similar, but the procedure is based on a program from Gopinathan et al.[153] A three dimensional grid is set up, and the electron density is evaluated at each grid point using the sum of all the densities that can contribute to that point. Once a surface is generated, MolCAD is capable of color coding the surface by mapping chemical properties onto it, including the electrostatic potential, hydrogen bonding properties, and lipophillic potential. The electric field can also be displayed on the surfaces; it is defined as the gradient of the electrostatic potential.

Minimization

Minimization is the process by which the energy of a molecule is reduced using some algorithm in an attempt to move toward the lowest energy structure. Large

numbers of variables (Cartesian coordinates) are optimized during the minimization process. There are 3xN number of variables to optimize, where N is the number of atoms in the system. There are different optimization algorithms that can be used, and they fall into two categories. Methods that decide on the minimization direction using the slope of the potential energy surface are called derivative methods, while methods that do not are called non-derivative methods.[149]

The simplex method is the most widely used non-derivative process.[154] It is used on an atom by atom basis until the force on any atom is below a designated value. The minimization process is best described in two dimensions. It begins with three points being chosen to form a triangle. The energy is calculated at each point, and the one with the highest value is identified. The triangle is reflected from that point through the line made by the other two point, creating a new triangle. This process continues and results in the triangle repeatedly reflecting downhill toward lower energy configurations. Additional functionality beyond this simple scheme is usually incorporated into the simplex method. For example, if the minimization is proceeding progressively downhill in a constant direction, larger steps can be triggered. At some point the simplex will zero in on a minimum energy using smaller and smaller steps until the step increment is so small that no differences in energy between the points is observed. The three dimensional simplex process can be achieved by the use of an initial *four* points, generating a tetrahedron. This is then treated in a manner analogous to the two dimensional process, where the shape is reflected through the plane of the three points with the lowest energy. Simplex is most useful for dealing with highly distorted

structures, where derivative methods cannot work because of discontinuous potential energy surfaces.[149]

In derivative methods, the atomic coordinates of all the atoms are simultaneously altered based on the first derivative of the energy equation with respect to the degrees of freedom. Derivative methods are divided into four different classes:

(a) Steepest Descents
(b) Newton Raphson
(c) Conjugate Gradients
(d) Variable Metrics

The most basic approach is taken by steepest descents, which simply finds the direction of the steepest slope and goes downhill in that direction. The Newton Raphon method, which works better than steepest descents for large molecules, determines the minimization direction by accounting for the both potential energy gradient and its curvature.

Conjugate gradient and variable metrics methods employ an algorithm that takes information from multiple line searches and uses it to decide the direction to proceed for the rest of the minimization.[155] A line search works by selecting a direction from the current position in the n-dimensional space. Steps are taken in that direction, and a quadratic interpolation is performed once a minimum is bracketed to pinpoint the minimum. The search continues until the change between the current minimum and the previously found minima is within a specified value. A Wolfe line search is a more advanced form of the conventional line search in that it is three times faster and is more tolerant to inexact line searches. The Powell method is a very popular form of conjugate

gradient minimization[156] which uses more advanced rules than the general conjugate gradient method and utilizes the Wolfe line search.

Minimization of the atomic coordinates of the structure proceeds in steps until a minimum of energy is reached. It generally fails to produce the global minimum; a local minimum close to the starting coordinates is almost always the result. One approach to determining the global minimum, is to systematically use different sets of starting coordinates. This form of conformational searching is used in the work described in later chapters.

CHAPTER 4

DEVELOPMENT OF A GRID CONFORMATION-SEARCHING MODELING TECHNIQUE

Introduction

The development of this grid conformation-searching modeling technique was performed using cyclodextrin-modified CE. The choice of CE as the mode of separation was based on its exceptional separation efficiency and the fact that the reagents used to selectively modify analyte migration rates are fluid components in the CE running buffer. The latter point renders the modeling of macrocyclic host-analyte interactions more manageable than in conventional chromatographic techniques. Insights into molecular recognition for conventional reversed phase HPLC have been pursued with differing levels of success.[157] However, when the phases responsible for recognition are immobilized on solid supports as in HPLC, analytes experience heterogeneous environments and unpredictable orientation factors. These complications are greatly relaxed with the CE approach. Moreover, the CE reagent phases can be rapidly changed and/or mixed without changing columns or instrumental configurations.

The system that was chosen to investigate selectivity and molecular recognition was the separation of naphthalene derivates using the single isomer carboxymethyl-β-CD (CM-β-CD), with the degree of substitution equal to 1. The analytes that were selected (Figure 4.1) were 1,5-dinitronaphthalene (1,5DNN), 1,8-dinitronaphthalene (1,8DNN), 2,7-dinitronaphthalene (2,7DNN), 1,5-dimethylnaphthalene (1,5DMN), and 1,5-dihydroxynaphthalene (1,5DHN), and were obtained from Aldrich Chemical Co.

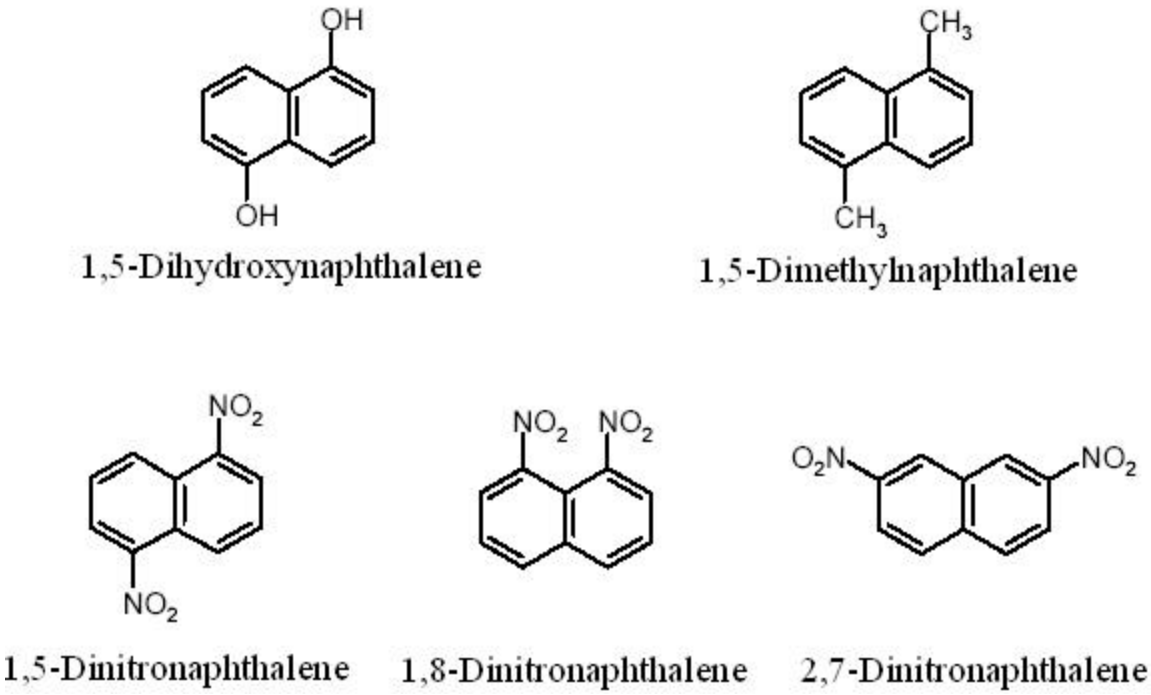

Figure 4.1. The naphthalene derivatives used as solutes are shown.

(Milwaukee, WI).

The DNNs (1,5-, 1,8, and 2,7-DNN) were chosen to study if different substitutional isomers could be effectively modeled while the DXNs (1,5-DNN, -DMN, and -DHN) were chosen to probe the selectivity the CD exhibits toward different functional groups. These solutes were also a good choice because their size and hydrophobic nature make them well suited to form complexes in the hydrophobic cavity of the CD. Additionally they all exhibit similar symmetry, reducing the need to model CD-solute inclusion in certain configurations that would be redundant.

CM-β-CD was selected for several reasons as well. First, because this buffer additive has a -1 charge, it is able to impart an electrophoretic mobility to the neutral species in the CDCE separation (Figure 4.2). Second, CM-β-CD is a single isomer unlike multiply charged CDs, which would necessitate modeling every analyte with each of the possible isomers. Given the time and computing intensive nature of the modeling experiments, this would simply not have been feasible at the time of this work. Third, the dimensions of the CM-β-CD cavity are such that it can accommodate each solute only lengthwise, thereby limiting the orientations to consider. Additionally it is commercially available and is readily soluble in common CE running buffer systems, making it amenable to being used as an additive.

Separations

Separations were performed using a Hewlett Packard automated Capillary Electrophoresis system ($HP^{3D}CE$) with a diode array detector interfaced to a Pentium I personal computer. Fused silica capillaries were obtained from Polymicro Technologies

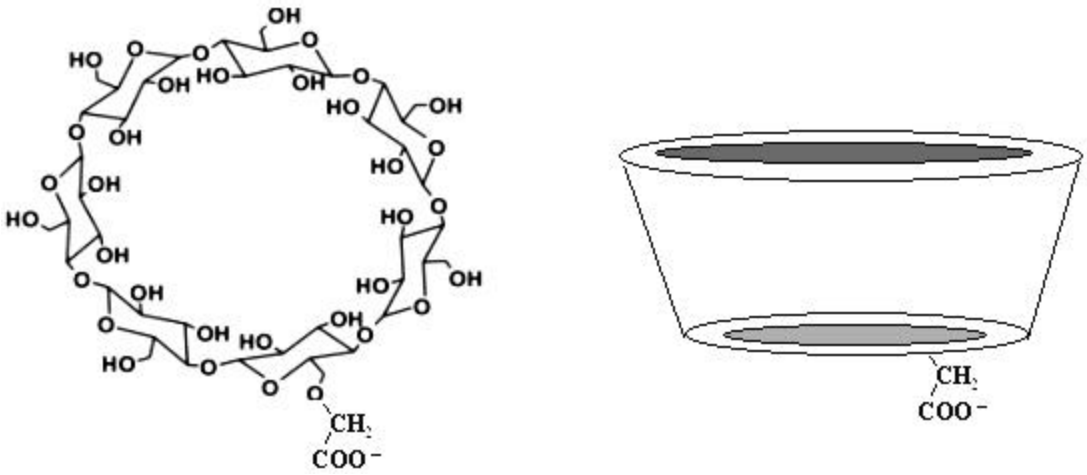

Figure 4.2. The negatively charged CM-β-CD is shown.

Inc. (Phoenix, AZ) and were 50 μm inner diameter (i.d.) and 360 μm outer diameter (o.d.).

The running buffer used was a 10 mM CM-β-CD and 25 mM phosphate solution, adjusted to a pH of 5.0 with an Orion Model SA 520 pH meter. Gasses were removed from buffer solutions to prevent disruptions in detection and electroosmotic flow reproducibility. This was accomplished by first placing the buffer in an ultrasonic bath for 15 minutes. Next the solution was passed through a 0.22 micrometer filter before being placed under vacuum conditions for 10 minutes. The buffer was prepared immediately before each experiment because it was found that the microorganism growth within the solutions would generally render them unusable after 24 hours. It was discovered that they could be stored for up to 36 hours if placed in the refrigerator. Adding antimicrobial agents such as sodium azide successfully countered the growth but altered separation conditions so it was not used.

The samples were prepared by diluting 10^{-4} M methanol stock solutions with running buffer or a buffer-methanol mixture (20% v/v). Many of the hydrophobic analytes were near their solubility limit in the stock solution, so methanol was added to the samples to improve solubility. There was no methanol added to the running buffer, and it was found that the small amount of methanol present in the sample during injection was insignificant with respect to the separation results.

The fused silica capillaries were cut to a length of 48 cm with the coating removed at 39.5 cm for detection. A special preconditioning and washing sequence was performed on each capillary used to ensure more reproducible separation conditions. This was done because it was found that the charged CDs were sticking to the walls of

the capillary and changing the EOF between separations. The procedure involved first flushing the capillary with 0.1 M sodium hydroxide for 5 minutes. Then a solution of 5% (w/w) sodium dodecylsulfate (SDS) and 0.1 M sodium hydroxide was run through for 15 minutes, followed by rinsing with distilled water for 2 minutes. The capillary was then filled with buffer and ready for use.

Injection of the sample was accomplished with 10 mbar of pressure to the inlet vial for 6 seconds. A 15 kV potential was applied for separations, and UV detection was achieved by a diode array detector with signals collected at 254 and 205 nm. The separation was conducted at a constant temperature 24 ± 1 ^{o}C since distribution coefficients are temperature dependent.

The resulting electropherogram from this CDCE experiment is shown in Figure 4.3. The t_{ch} is the mark indicating the elution time of the charged CD. It is evident that the functionalized 1,5-DMN and 1,5-DHN solutes elute later due to stronger interaction with the charged CD, while the dinitronaphthalene compounds are less retained due to poorer inclusion. The inclusion constants (K_d) for each of the solutes is shown in Table 4.1 and were calculated using additional separation experiments described elsewhere.[158]

Modeling Experiments

The modeling experiments were performed using the Sybyl 6.6 molecular modeling software[150] and run on a Silicon Graphics Octane workstation with dual 270 MHz MIPS processors and 768 MB RAM. The solute molecules were constructed with the SKETCH feature in Sybyl. The CM-ß-CD molecule was built by using SKETCH to modify a ß-CD structure obtained from the Cambridge Crystallographic Data Center's

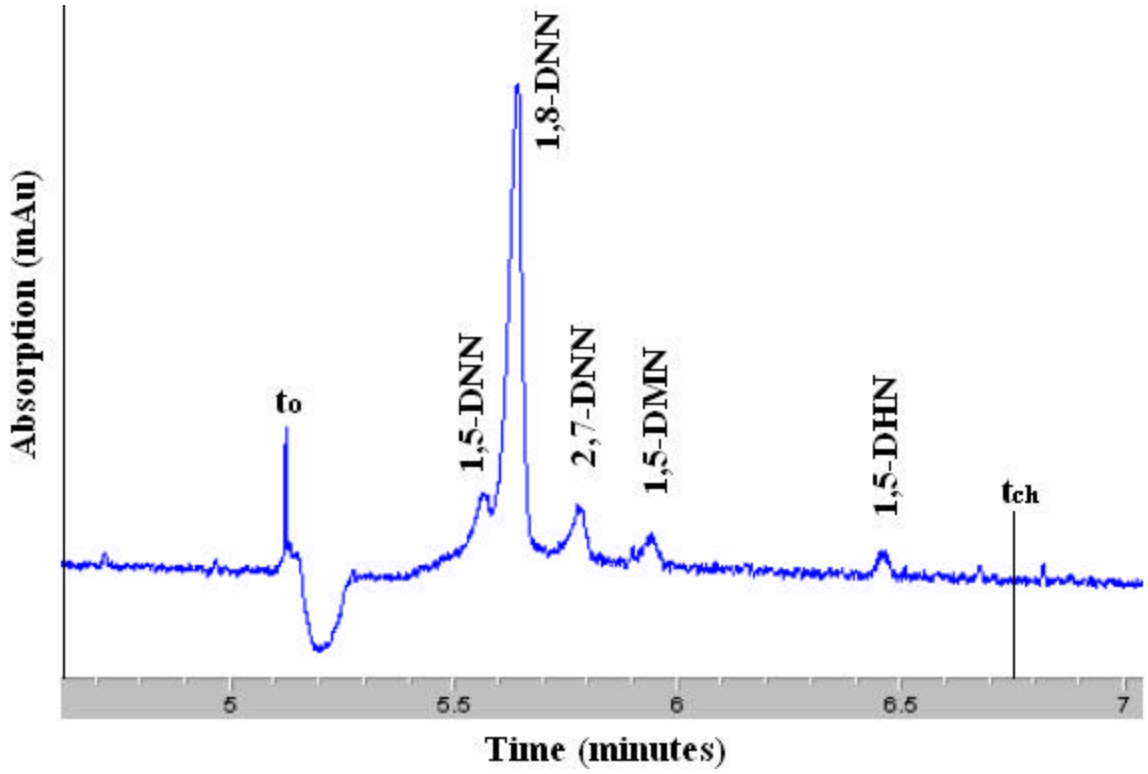

Figure 4.3. The electropherogram from the separation of the naphthalene derivative solutes is shown.

Table 4.1: Experimental inclusion constants (K_d) calculated from the separation.

Solute	Experimental K_d
1,5-DNN	47
1,8-DNN	65
2,7-DNN	96
1,5-DMN	130
1,5-DHN	490

structural database. The molecules were then each minimized in a water environment using the Sybyl MAXIMIN2 function with the Tripos force field and the Geistiger-Hückel charge calculation method. This was so that the structures of the molecules used in these calculations more accurately matched their configurations in the aqueous separation environment. After minimization in the solvent environment, each of the water molecules was removed and the remaining structure was stored on the computer's hard drive.

There are several force fields available with the Sybyl software, including the Kollman and Amber force fields, MM2 (77), MM2 (91) and MM3 (94), Tripos force field, and MMFF94. The Tripos force field was selected for use in all the modeling experiments. It was designed and optimized for treating small organic molecules and biomolecules,[150] which makes it appropriate for this work. A list of many of the most commonly used force fields is presented in Appendix A.1. The energy terms involved with the use of the Tripos Force Field are listed in Appendix A.2.

Macro programs were written in Sybyl Programming Language to achieve the grid search docking for each solute with the CM-ß-CD. These programs systematically translated and rotated the solute into the cavity of the CD as shown in Figure 4.4.

The centers of mass were used to help visually align the solute and CD prior to docking. The solute was then translated from -5.0 Å out of the CD cavity to 0 Å (centered deep inside the cavity) in increments of 0.1 Å. At each of these translational positions, the solute was rotated 360 degrees, in increments of 5 degrees. The energy of the solute-CD complex was minimized with 100 iterations at each step and recorded to an output file along with the translational and rotational coordinates.

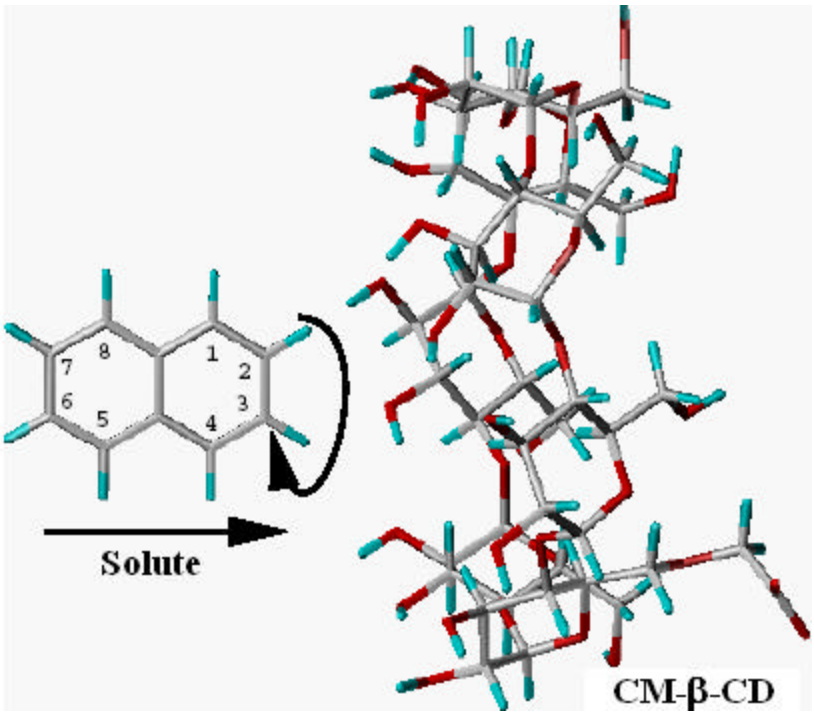

Figure 4.4. Depiction of the translation and rotation of the solute during the docking sequence. The solute is translated toward the CD at 0.1 angstrom steps and rotated with increments of 5 degrees at each step.

The output files were imported into the Sigma Plot software[159], and 3-dimensional plots of all of the minimized energies vs. translational and rotational position were created for analysis. Figure 4.5 shows an example of one of these plots. These energy profiles of the explored interaction space between solute and CD revealed several interesting features.

It is very evident that there are certain rotational angle "valleys" that result in very favorable interaction energies. These favorable areas are separated by "ridges" of energetically unfavorable CD-solute conformations. These features in the 3-dimensional plots were exhibited by all of the solutes in the experiment. This can be attributed to the fact that when the structure of the CD was minimized, it did not have a perfectly circular cavity but was instead elliptical. The solutes are mostly planar due to their common naphthalene structures and fit more easily (or poorly) into the cavity with a 180 degree repetition.

It can also be seen from the energy map that the optimal distance for inclusion of the solute into CD was unexpectedly found to be about 2 to 5 Angstroms away from the center of the cavity. This was characteristic of each of the solutes. In order to further investigate this phenomenon, individual points at both favorable (2-5 Å) and unfavorable (0-1 Å) distances were selected and visually observed in the Sybyl program. It was observed that the favorable location away from the center enables the –OH groups on rim of the cavity to experience significant electrostatic interactions with the naphthalene π-system of the solutes. Additionally, hydrogen bonding was observed to occur at these locations between the –OH groups of the CD and the functional groups on the solutes. However when the solutes were deep within the cavity of the CD, it was evident that no

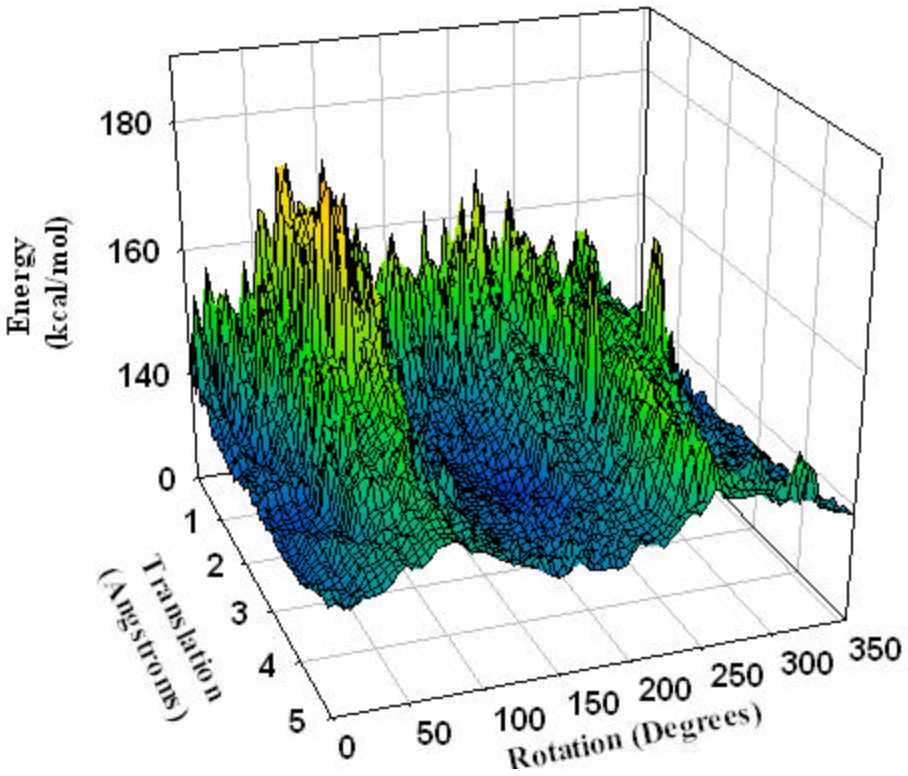

Figure 4.5. Three dimensional plot of the energy of interaction vs. translational position vs. rotational position of the solute with respect to the CD.

such stabilizing forces were occurring. Moreover the shape of the CD is not a cylinder but more like a bowl, with the bottom portion being smaller. Some of the atoms of the solute could be seen "crashing" into atoms of the CD giving some of the very poor interaction energies that are apparent around 0-1 Å. Unfavorable steric forces undoubtedly play a role as the solute is forced into this smaller area.

Another noteworthy aspect of these plots that is that each of the 4320 points explored during docking yielded its own unique energy conformation. In other words, no two CD-solute starting positions were found to minimize to the same configuration. If two starting points were close enough to each other and minimized appropriately, the CD-solute structure should minimize to the same low energy conformation. This brought up the possibility that problems with local minima were keeping this method from finding the appropriate true low energy conformers. If the translational and rotational increments could be reduced to a small enough size, or if the minimization iterations could be increased sufficiently would this then be enough to overcome these local minima? Increasing the number of iterations was found to not be immediately feasible given the computing power on hand at the time. Increasing the translational and rotational increments by only one order of magnitude would result in 432,000 points in a single docking experiment, which is also prohibitively time consuming. When additional computing power became available later, experiments were designed to address these issues and will be discussed further later in this chapter (comprehensive minimization).

The data from the output files was also imported into Microsoft Excel for calculation of the interaction energy between solute and CD. To determine the energies of the conformers found in all the docking experiments, the energy of the CD and solute

before docking was subtracted from the computed energy of each conformer. This allowed for comparisons between solutes by accounting for the different starting energies of each. Next the energies, e_i from all docking positions, i, were entered into Equation (4.1) to give an average solute-CD interaction energy, E_{MM}, or <e>.

$$\mathbf{E_{MM} = \langle e \rangle = \frac{\sum e_i \exp(-e_i/RT)}{\sum \exp(-e_i/RT)}} \qquad (4.1)$$

In calculations using Equation 4.1, the gas constant R was multiplied by room temperature, T = 298 K; any temperature increases in CE applications due to Joule heating were ignored. This equation considers all points but allows for conformers of the most favorable energies to contribute the most to the calculated interaction energy.

Conversion between energy and distribution coefficients (K_d) was done using the equation:

$$\Delta G \approx \langle e \rangle = -RT \ln (K_d / [CD]_o) \qquad (4.2)$$

To use this equation in such a manner, it is assumed that ΔH is a good approximation of <e> and entropy is ignored in the equation:

$$\Delta G = \Delta H - T \Delta S \qquad (4.3)$$

Since all of the solutes exhibit C2 axes and have similar symmetry, we can expect the differences in ΔS to be small. The experimentally determined K_d value of 2,7-DNN was used to scale the calculated interaction energies since these values have no physical meaning and only the relative differences in calculated interaction energy between solutes are important. The results are shown in Table 4.2. While the ordering of the K_d values was consistent with the observed elution order, the agreement between experiment

Table 4.2: The calculated interaction energy <e> with the calculated inclusion constant (K_d), compared with the experimental inclusion constant.

Solute	<e>, kcal/mol	K_d	K_d Experimental
1,5-DNN:	+1.64	6.3×10^{-2}	47
1,8-DNN:	+0.69	3.2	65
2,7-DNN:	- 2.70	96	96
1,5-DMN:	- 4.83	3.5×10^{3}	130
1,5-DHN:	- 8.07	8.4×10^{5}	490

and calculated K_d values did not permit rigorous simulation of the separation, deviating substantially from the experimental values.

Close Valley Inspection

It was evident from the 3-dimensional energy plots that there were only certain translational and rotational regions energetically favorable enough to be significant in the calculation of the interaction energy. Although it is seen from Equation 4.1 that all points are considered, the contribution to the <e> from the higher "ridges" region of the plots is negligible. The lowest energy regions are the most important areas and were selected for "close valley inspection."

Using the 3-dimensional plots and the numerical output data from the previous modeling experiment, the regions producing the best interaction energies were selected for each solute. The regional selections were found by using the Sigma Plot software to set the lower limit of the energy scale just above the values of best interaction. This resulted in the targeted regions becoming clearly evident as shown in Figure 4.6. The range selected for each solute was generally in the translational range of -4.0 to –1.5 Å, and in the rotational "valleys" between 120 - 200 degrees and 340 - 20 degrees.

New macro programs were written to dock the solute molecules in only these selected positions. In this procedure, the selected docking positions were probed more in-depth by changing the rotational increment from 5 degrees to 1 degree. Also, the energy of the complex was more extensively minimized by increasing the number of minimization iterations to 250. All other minimization parameters remained the same. This was conducted to attempt to overcome local minima issues and to more thoroughly search for the best low energy configurations of the solute-CD complex. The number of

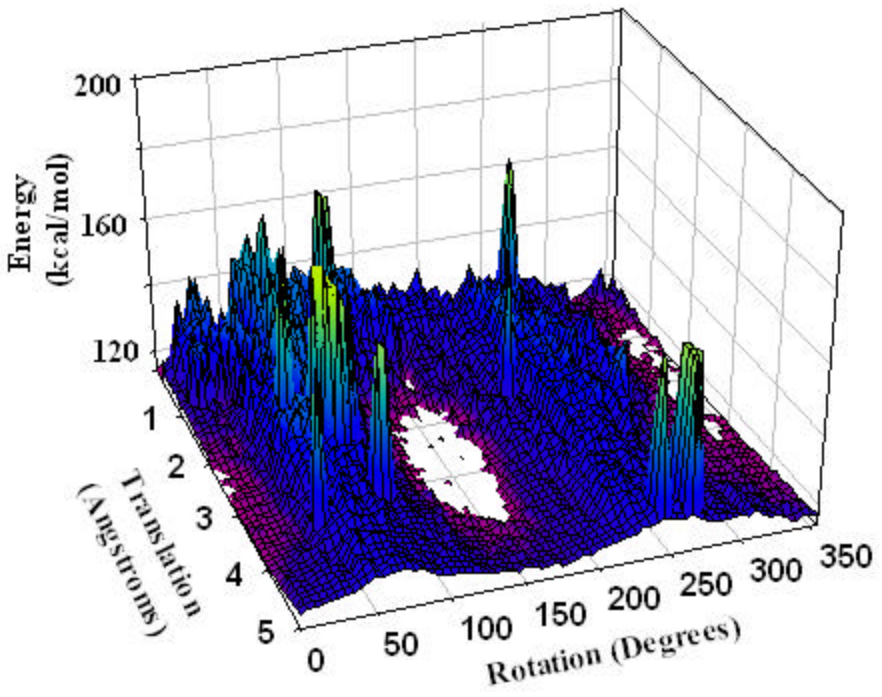

Figure 4.6. Graphical plots such as this were used to find the lowest energy translational and rotational regions, which were then targeted for more in depth minimization experiments.

data points considered for each of the solutes in this procedure was the same, allowing for valid comparisons of the <e>. The calculated <e> and K_d values for this experiment are listed in Table 4.3**.**

It can be seen that although the calculated values of K_d for this experiment are still relatively far from the experimental results, the proper elution order is still predicted. The K_d values are also significantly closer to their mark, indicating that this approach was a successful step toward achieving a more functional model.

Flat Docking and Solute Offset Docking

Other attempts were made to more carefully address the full interaction space between solute and CD and also incorporate higher degrees of freedom into the model. Molecular computer aided design (MolCAD) representations of the solutes and CD indicated that hydrogen bonding is likely to occur between the functionalities on the solutes and the hydroxyl groups on the rim of the CD structure. MolCAD is a tool in the Sybyl software that allows a 3 dimensional picture of the electron density to be displayed. Several different properties (lipophilicity, hydrogen bonding potential, electrostatic) can then be mapped on the electron density surface and visualized. Representations of the hydrogen bonding potential of the solutes and CD indicated that there might be important stabilized conformations found by lining up both functionalites of the solutes with the CD rim during docking (see Figure 4.7). Confirmation that hydrogen bonding could take place in this manner was achieved by using the graphical interface of a Sybyl software module specifically designed to reveal hydrogen bonding.

Based on this information, docking experiments were designed and performed where the solute molecules were docked into the CD “flat”, as opposed to being inserted

Table 4.3: Calculated and experimental K_d values for "close valley inspection".

Solute	<e>, Kcal/mol	K_d	K_d Experimental
1,5-DNN:	- 1.68	17	47
1,8-DNN:	- 1.76	20	65
2,7-DNN:	- 2.70	96	96
1,5-DMN:	- 6.31	4.3×10^4	130
1,5-DHN:	- 7.91	6.4×10^4	490

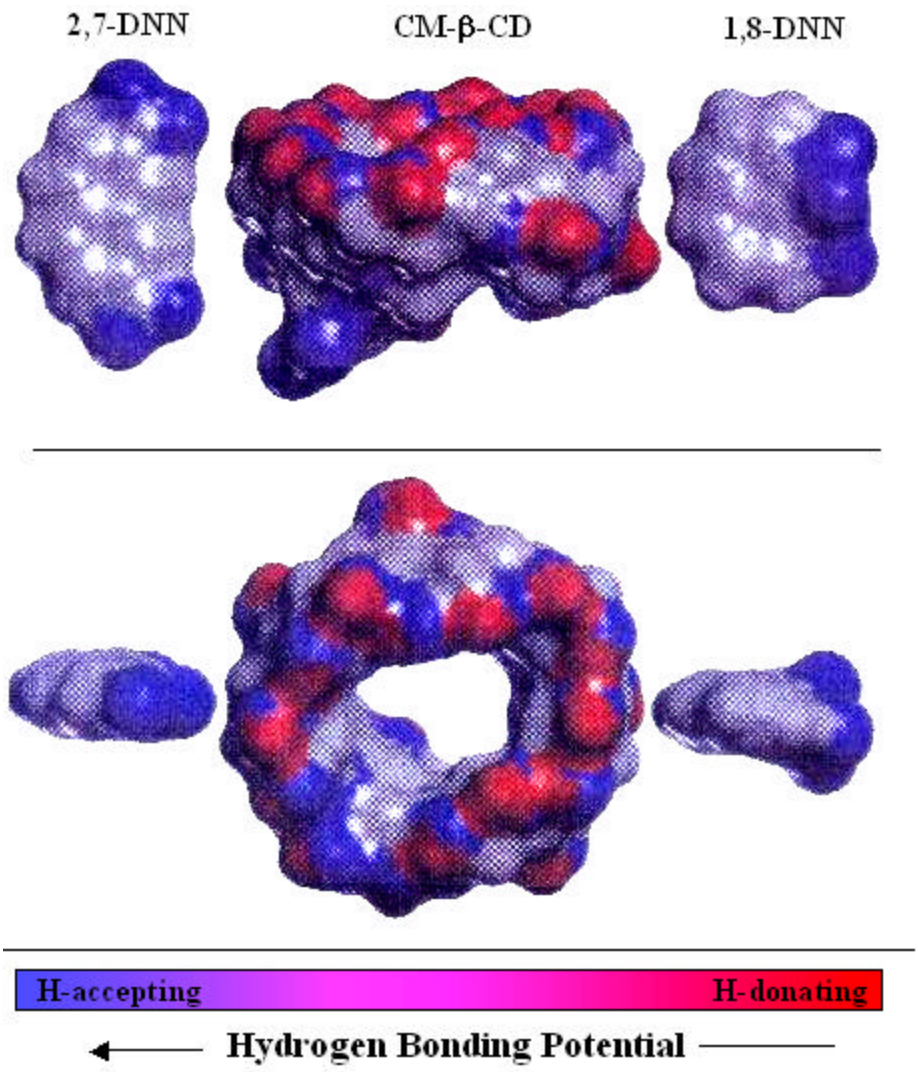

Figure 4.7. The hydrogen bonding potential of 2,7-DNN, CM-β-CD, and 1,8-DNN is shown.

lengthwise. However, these attempts did not yield any conformations that were energetically favorable enough to be significant in the calculation of any of the solutes' interaction energies.

Another set of experiments was performed which involved offsetting the solute relative to the center of the CD prior to docking (see Figure 4.8) . The solutes were moved ± 0.1 and ± 0.2 Å away from the center along the x and y axes before docking. The docking was then conducted as usual, but this time exploring the interaction energy space offset from the central z-axis. It was found that there were some lower energy conformations discovered in this manner, but the ones that were observed were not significant enough to change the predicted elution order.

Solvent

In order to try to more closely mimic the actual separation environment, experiments were performed attempting to incorporate the aqueous environment in the model. The docking programs were modified to instruct the Sybyl software to include a "droplet" of water molecules around solute and CD. This droplet consisted of exactly 168 water molecules arranged in a sphere around the center of the CD-solute system and was included at each of the translational and rotational points during docking.

It was discovered that with the solvent present in the docking sequence, the 100 minimization iterations used was barely even enough to finish the initial Simplex method for minimizing the structure. The minimization procedure was now taking into account all of the additional 168 water molecules combined with the structure of the CD and solute. 100 iterations was simply insufficient for this computationally intensive task. The number of iterations was increased to 1000 and the experiments were performed

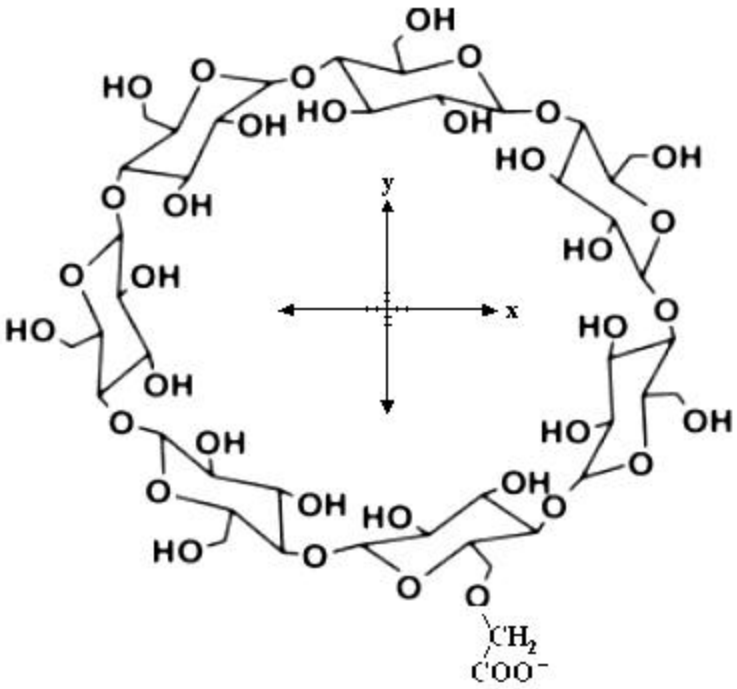

Figure 4.8. Solutes were docked into the cavity starting at positions offset from the center in the x and y direction.

again. It was found that even after 1000 iterations the minimization sequence was still making large changes to the system's structure each step. It was discovered that by taking the same solvated complex and simply altering the position of a single solvent molecule prior to minimization, the computed energy would vary by as much as 15 kcal/mol, indicating that the environment was no where near being energetically minimized. In addition, the Tripos force field considers all atoms in the environment simultaneously. With the additional 504 atoms from the solvent, the computing is tremendously stretched out and slowed down making its use with this docking technique completely impractical. Indeed it was observed in further experimentation that even after 100,000 iterations, the structures were still being rearranged quite significantly by the program.

It was also observed from the analysis of the solvated docking data that the 3-dimensional energy maps showed absolutely no discernable features the way previous "dry" docking experiments had. In fact as shown in Figure 4.9, the energy maps simply look like noise, with no useful interaction information apparent. It is believed that since the program has to address each of the additional water molecules at hand, that the amount of error present in each of their incompletely minimized structures is additive and thus totally masks any features of the interaction between CD and solute.

Comprehensive Minimzation

The results of the previous experiments indicated that the results of the modeling improved as higher minimization iterations were utilized and as finer increments of the grid search were explored. With the addition of a 3rd more powerful and modern Silicon Graphics workstation to the computing workforce, a more comprehensive approach to the grid search docking was possible.

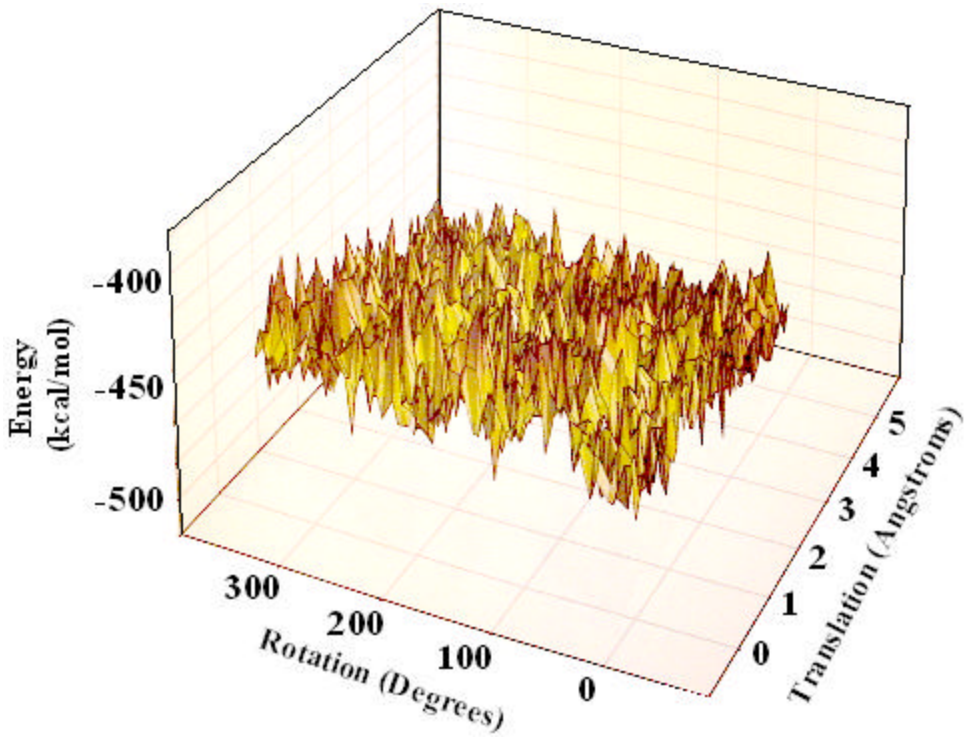

Figure 4.9. Energy plot of 1,5-dinitronaphthalene docking into CM-β-CD surrounded by a solvent environment.

As noted from Figure 4.5 and the results of the experiments using 100 and 250 minimization iterations, each of the starting points in the docking minimized to its own unique energy. The possibility that local minima were blocking the discovery of all low energy conformers precipitated experiments to test this and explore the feasibility of using finer docking increments. Programs were written using both 100 and 250 minimization iterations where the translational component of the docking solute was reduced to smaller and smaller increments until no change could be observed. A small 10 x 10 grid was then selected for each solute in which this miniature version of the docking sequence was performed, using 10^{-2} Å through 10^{-5} Å increments. It was discovered that no two points were found to minimize to the same energy until the increment was reduced to 10^{-3} Å. Not until the translational change was set to 10^{-5} Å did all of the docking points yield the same conformation.

It is apparent that even with expanded computing power, it would not be possible to compute the millions of points required by lowering the increments to 10^{-3} Å. However, higher minimization iterations were still an achievable improvement. Some programs were written that took selected docking points from different solutes and minimized them as fully as possible. In other words, the minimization was not set to stop with 100 or 250 iterations, but to continue indefinitely until no further decrease in energy was possible. Once such a state was achieved, the Sybyl software was instructed to automatically terminate the minimization sequence and record the output to a file.

The data was plotted as energy vs. minimization iterations as illustrated by the example in Figure 4.10. The application of the Simplex Method can be seen in action in

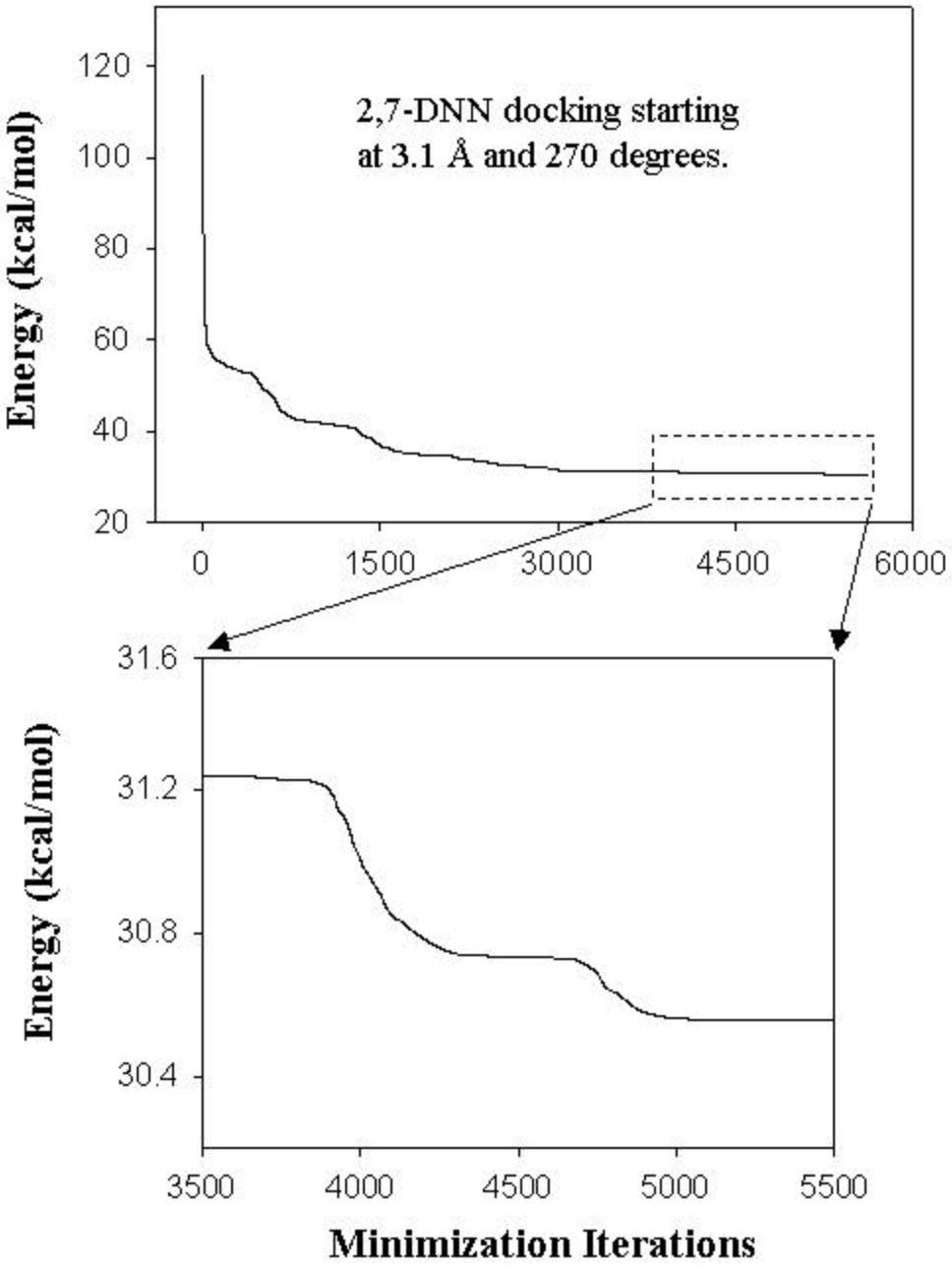

Figure 4.10. Typical plot of the CD-solute complex energy vs. the number of minimization iterations.

the first 10 iterations as the energy rapidly decreases. The Powell Method then fine tunes the complex structure and takes the minimization process the rest of the way. As evident in the figure, important minimization activity was found to occur even after 4000 iterations, and was noted at 7500 iterations in some cases.

With calculations from this data revealing that the application of comprehensive minimization to the docking procedure was achievable within a period of months, the docking programs were modified to include this measure. The programs were run for each solute and the data collected was again used to generate 3-dimensional energy plots.

The 3-dimensional plots revealed a remarkable development. Most of the starting coordinates for the solute were now found to minimize to the same energy rather than its own unique energy as in the previous methods ('100 min' and '250 min'.). This strongly suggests that the local minima energy barriers or incomplete minimization problems are overcome with comprehensive minimization, and the true preferred CD-solute conformations are being identified.

This is illustrated in Figure 4.11 where many of the points with unique energies from the 1,5-DNN docking under 250 iterations conditions (a) can be seen converging to the same energy after comprehensive minimization (b). This is again clearly illustrated in Figure 4.11, which shows graphical screen shots of 1,5-DHN at two different starting locations in the docking grid and arriving at the same preferred conformation.

Despite the fact that the two starting points of 1,5-DHN depicted in Figure 4.12 are 4 Å and 80 degrees away from each other, this method was found to overcome most energy barriers in minimization and rearrange the complex to the nearest low energy conformation. The effects of the elliptical CD can still be observed, but acting more as a

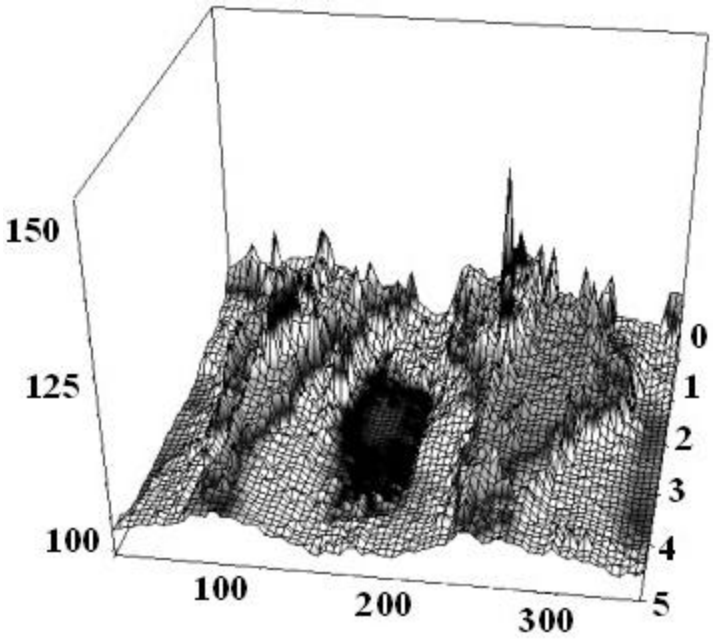

a. 1,5-DNN; 250 min.

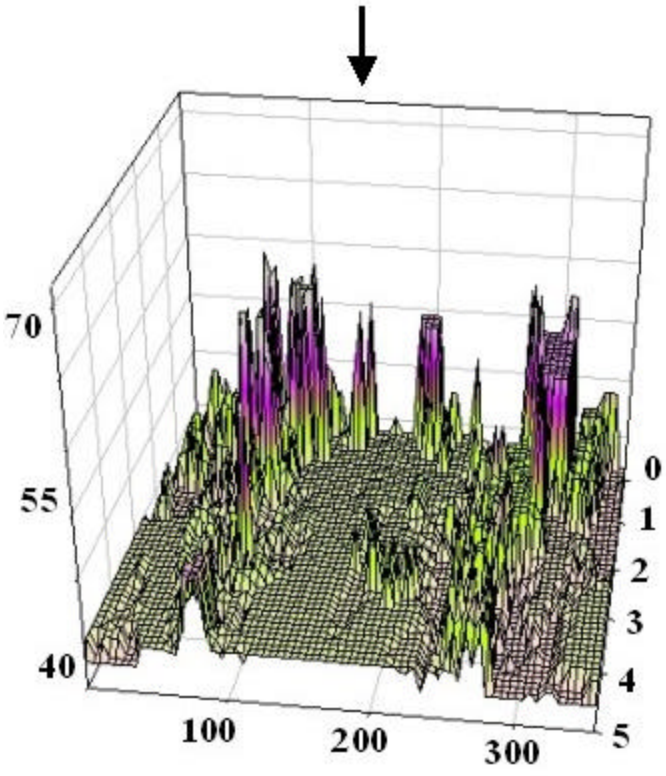

b. 1,5-DNN; Comprehensive min.

Figure 4.11. Plot of the solutes rotation (x-axis, degrees) vs. translation (y-axis, angstroms) vs. energy (z-axis, kcal/mol) from docking with the CD.

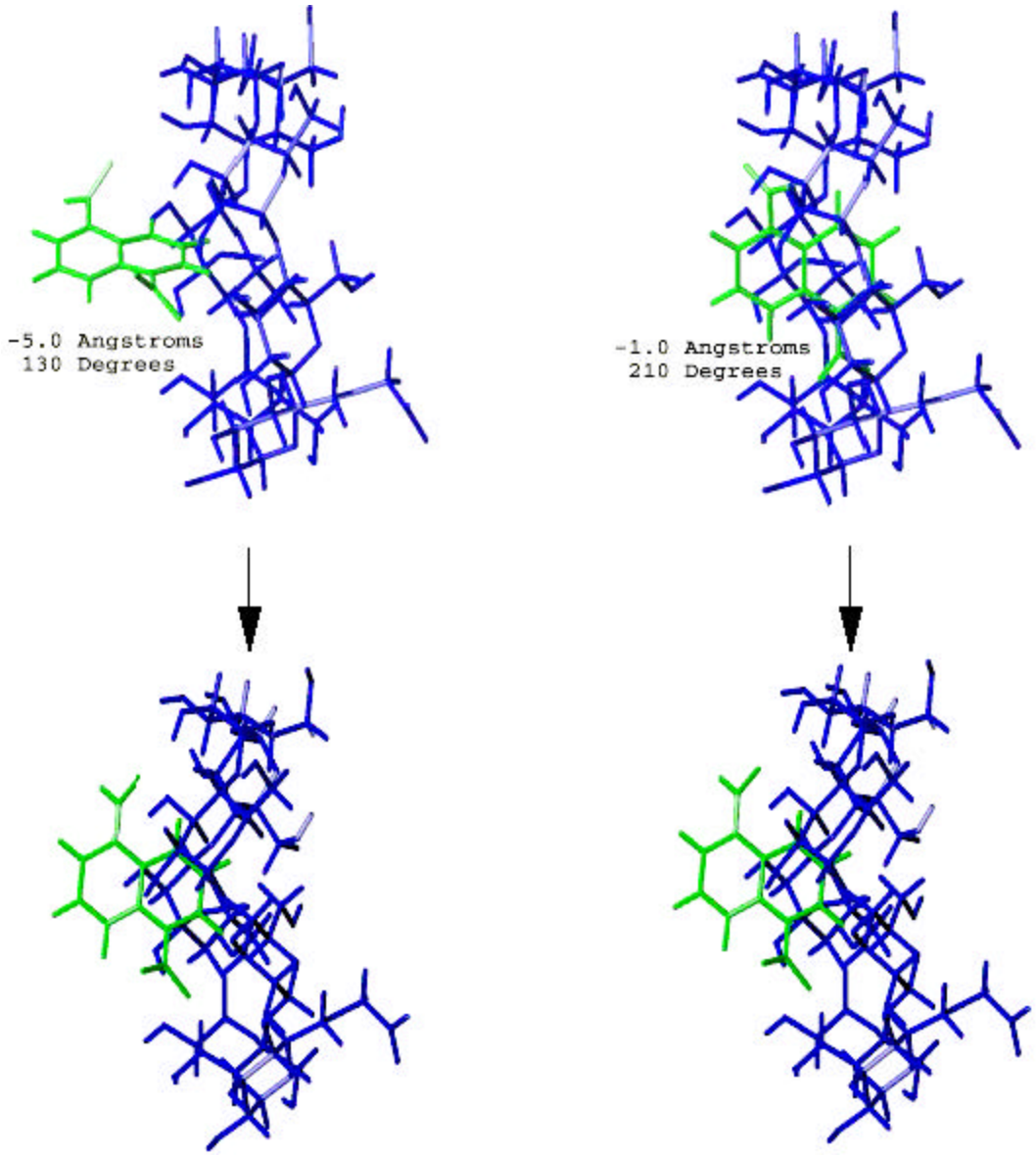

Figure 4.12. Graphical screen shot depiction of 1,5-DHN starting at two different docking points and minimizing to the same conformer.

boundary between certain conformational energy basins in the comprehensive minimization case.

This phenomenon clearly demonstrates that there is no need to attempt smaller translational and rotational increments to overcome local minima. The results of this comprehensive minimization experiments show that not only are merely the specific starting points of the programmed docking sequence being addressed, but effectively the entire interaction space between the solute and CD is being probed. Adding degrees of freedom by tilting the solute or offsetting the initial docking vector will still at best only yield the same low energy conformations that are found with the solute docking straight down the middle. Since the procedure will take the solute and rearrange it (by tilting or moving along x and y axes), it is effectively addressing all these configurations without the need to dock them. This is again demonstrated well in Figure 4.12, where both of the starting positions of the 1,5-DHN are moved and tilted significantly from their original configurations to give the same low energy conformation pictured below.

These features were mirrored with the other solutes that were minimized under comprehensive conditions, as can be seen in Figure 4.13. The energy plots of 1,8-DNN and 2,7-DNN are shown in Figures 4.13 (a) and (b) respectively.

The data indicates that most of the 2,7-DNN conformers are lower in energy than the 1,8-DNN conformers. This is consistent with the experimental findings that 2,7-DNN has a better inclusion constant with the CD than does 1,8-DNN. It was also determined that the conformations of 2,7-DNN that were found are fewer in number but resulted from much larger areas of starting coordinates. This indicates that the 2,7-DNN is less inhibited in its rearrangement during minimization. This can be attributed to the fact that

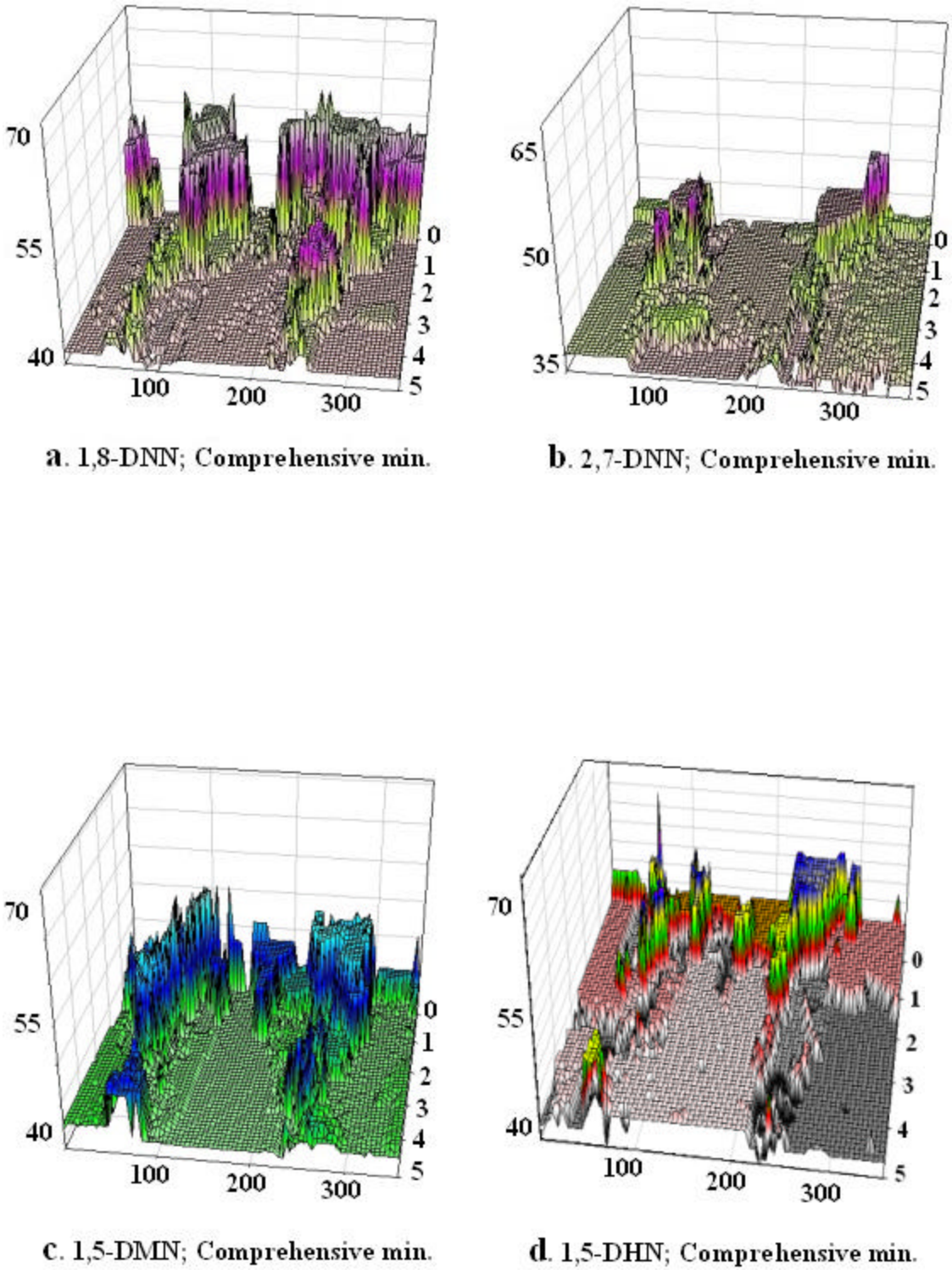

Figure 4.13. Plot of the solutes rotation (x-axis, degrees) vs. translation (y-axis, angstroms) vs. energy (z-axis, kcal/mol) from comprehensively docking with the CD.

the long slender 2,7-DNN with the functional groups on the ends can more freely rotate and move around inside the CD cavity, and is less likely to be caught in a configuration of higher energy than the wide 1,8-DNN. This effect is again observed with the smaller more compact 1,5-DHN (Figure 4.13 d) which can more easily rearrange its position in the CD cavity than the bulky 1,5-DMN (Figure 4.13 c).

Dielectric Constant

While we have gained confidence that true conformers are being found for the modeled system, the model does not fully represent the true experimental system since solvent is not explicitly considered. Ideally, it would be desirable to include the solvent in the modeling system to more realistically mimic the actual molecular environment. However, as discussed earlier several problems make this approach unfeasible, and solvent effects must be accounted for by relying on the more simplistic method of manipulating the dielectric constant. Given that all of the solutes are very similar in nature it is believed that much of the role that the solvent plays in this environment would be the same for each solute, and this more simplistic treatment may be justified for this work.

The comprehensive minimization experiments were performed at a dielectric constant (e) value of 20. The value of ε influences the electrostatic energy term (E_{ele}) of the Tripos force field.[150] By increasing e from the default value of 1, the contribution of the electrostatic energy term in the force field is decreased, simulating the shielding effect the solvent molecules might have between the solute and CD. At many docking points where the solute is deep inside the CD cavity, there is insufficient space for solvent

molecules to fit between two interacting species, and e is effectively 1. Conversely, when the solute is far away from the CD, e may be better represented by a value of 80 (that of water).

To study the effect that changing the dielectric constant has on the comprehensive model, some of the solutes were docked into CM-ß-CD with e = 1, 20, 40, and 80. As shown in Figure 4.14, the conformations found when the dielectric = 80 (b) were fewer and from larger docking grid areas than the conformers found with e set to 1 (a). This can be attributed to the fact that at high dielectric values, the solute is shielded enough from restraining forces within the CD cavity to rearrange and move about relatively freely. It was determined by analyzing the individual electrostatic energy terms from many docking points and other data in this experiment that a e of 20 provides a good balance by preventing dominating electrostatic contributions when e = 1, and excessive shielding effects when e = 80. This value was also determined to be appropriate by Jørgensen and Christensen in other research.[160]

To calculate the <e> for the solutes in the comprehensive minimization experiments, Equation 4.1 was modified to Equation 4.4 to account for the degeneracy, g_i, in the data.

$$\langle e \rangle = \frac{\sum g_i e_i \exp(-e_i/kT)}{\sum g_i \exp(-e_i/kT)} \qquad (4.4)$$

The g_i is defined here as the number of micropositional (translational and rotational) starting points that minimize to a given conformer and e_i. This approach may be compared to that used by Stillinger and Weber to map the "quenching" of molecular

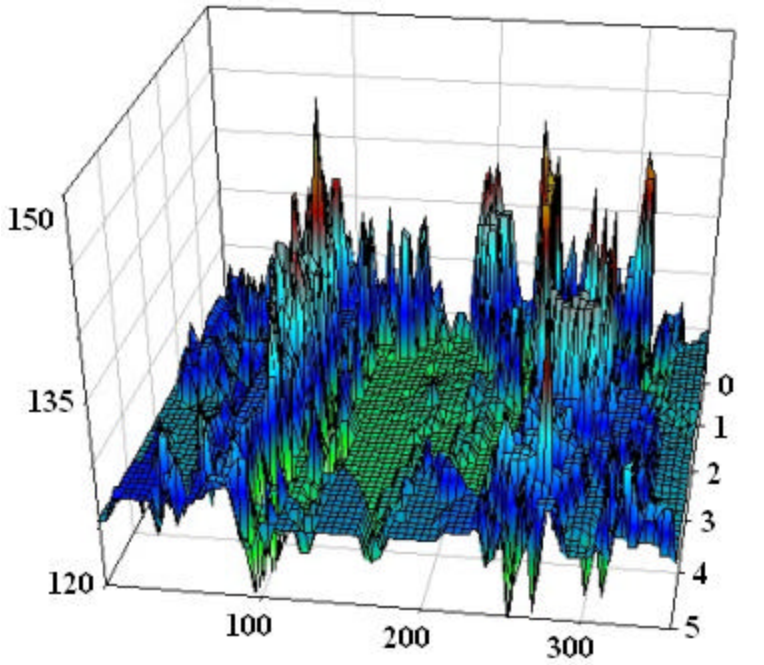

a. 1,5-DNN; ε = 1

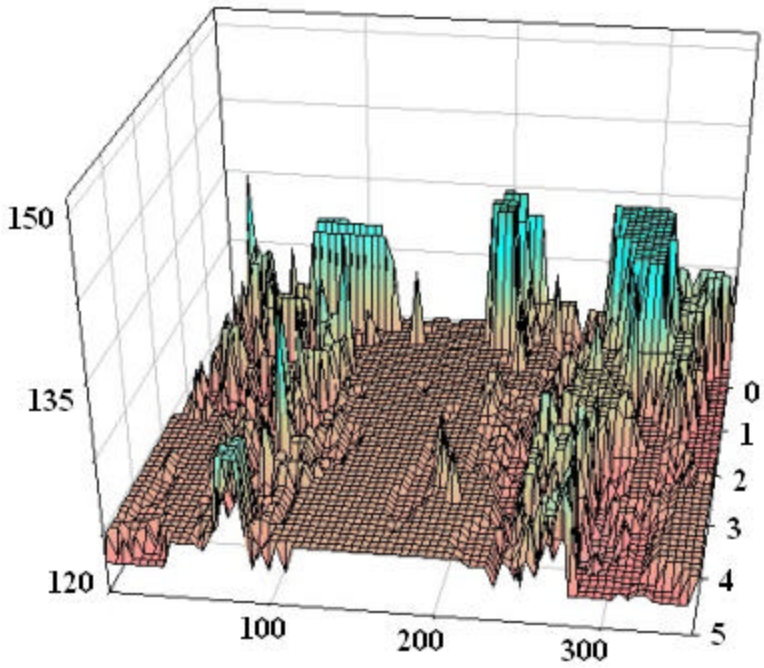

b. 1,5-DNN; ε = 80

Figure 4.14. Plot of the solutes docking with different dielectric constants (ε). a) 1,5-DNN; ε=1, b) 1,5-DNN; ε=80.

positions to relative minima on the potential energy hyperspace of a many-body system.[161] The absolute value of g_i is somewhat arbitrary, as smaller incremental changes in starting positions when performing the grid search, will yield larger g_i values. However, the relative magnitudes of g_i between different conformers should remain approximately constant for a given solute-CD system when increments are reduced. It is clear (as shown in Figure 4.13) that all of the additional micropositional starting points that would be present from reducing increments would simply add proportionately to their respective energy plateaus and basins, and not change the relative g_i values.

Equation (4.5) is employed to convert <e> to K_d. The CM-β-CD concentration used in these studies was 10 mM. Because the solutes are injected as dilute solutions, the free concentration of CD in the region of solute bands may be assumed to be this concentration.

$$\langle e \rangle \sim -RT \ln (K_d / [CD]_o) \qquad (4.5)$$

$$K_d = [\text{solute-CD}] / [\text{solute-RB}] \qquad (4.6)$$

The rigorous use of Equation 4.5 requires an equivalency between <e> and the free energy change associated with the exchange of solute between running buffer and CD. Although this equivalency is not strictly valid, the various potential energy terms present in the force field (see appendix A.2) are implicit in <e>, and entropy information is represented by g_i. The solutes used in this case all exhibit similar symmetry and, thus, differences in the entropies of the free solutes may not be large. Moreover, the <e> values are normalized based on the experimentally determined K_d of one of the solutes (2,7-DNN). In this regard, it is only necessary that values of K_d obtained via Equation 4.5

scale with true values of K_d. Further discussion of the validity of this type of calculation can be found in the *Energy Calculation* section of Chapter 3.

Table 4.4 shows the K_d values for the comprehensive minimization calculations vs. the experimental K_d. It can be seen that not only is the proper elution order still predicted, but the calculated K_d values are remarkably closer to the experimental K_d values than was observed with the '100 min' and '250 min' experiments.

While an impressive improvement in the calculated K_d was observed with the comprehensive minimization, it is important to consider different approaches to the data analysis to determine which approach might most closely match the experimental data. As evident from Figure 4.11, the traditional energy "ridges" arising from the elliptical CD shape evolve into energy "boundaries", separating the plateaus and basins. The algorithm for minimization does not drastically rearrange the structures to overcome large energy barriers present. However this is desirable because an algorithm that could overcome any energy barrier (even very large ones) would eventually yield a completely flat 3-dimensional energy plot, with every starting point arriving at only one absolute lowest conformation.

In reality, there is not a single complex that dictates the inclusion constant, but an group of low energy structures that collectively determines the strength of inclusion. During a CDCE separation, the solute has been shown to enter the CD on the order of thousands of times per second.[76] Of those 1000s of entries, the nature and strength of the interaction will be the most dependant on the collective contributions of the different low energy conformations that are experienced. Conformations with lower energies and greater numbers of points (g_i) are weighed more strongly in Equation 4.4, and the top 5

Table 4.4: Calculated values of K_d for the comprehensive minimization experiments, compared to the experimental values.

Solute	<e>, Kcal/mol	K_d	K_d Experimental
1,5-DNN:	- 1.68	18	47
1,8-DNN:	- 1.76	35	65
2,7-DNN:	- 2.70	96	96
1,5-DMN:	- 6.31	1000	130
1,5-DHN:	- 7.91	3300	490

contributors make up most of the calculated <e> as can be seen by the example in Table 4.5. The regions of these contributors are graphically represented in Figure 4.15. These top 5 conformers leading to the calculated interaction energy of 1,5-DHN contribute nearly 80% to the final interaction energy (-36.034 kcal/mol), indicating that they are the most preferred conformations.

With this in mind, two additional approaches to the calculation <e> were considered. First, the top 5 conformers contributing to the final <e> were determined for each solute and averaged together to get a new <e> value (called 'Approach 1'). Approach 2 consisted of calculating <e> according to Equation 4.1, but considering each point as a unique energy ($g_i = 1$), rather than using the actual g_i values. The conventional use off Equation 4.1 was called Approach 3.

Table 4.6 shows the resulting K_d values calculated from each approach along with the results from the other two previous experiments for comparison. As seen in the table, Approach 1 and 2 yield an incorrect elution order. However, when consideration is made of all the statistically accessible micropositional states that can quench into the observed conformer energies (Approach 3), the correct elution order is observed and the relative magnitudes of K_d values among the solutes are reasonably close to the experimental values. It is important to note that a difference in energy of only 0.3 kcal/mol results in a 2-fold change in K_d, leaving little margin for error.

It can be seen from Table 4.5 (conformers for 1,5-DHN) that the contribution of the 2nd best conformer is very small relative to the 3rd conformer, if g_i values are ignored. Conversely, the 2nd conformer's contribution to <e> is larger than the 3rd when degeneracy is considered. Thus, Approaches 2 and 3 are decidedly different. The

Table 4.5: The top five conformers and percent contribution to <e> for 1,5-DHN.

Conformer	Energy (kcal/mol)	# of Points	% Contribution
1	-36.954	40	41 %
2	-34.819	701	18 %
3	-36.445	18	8 %
4	-35.316	117	7 %
5	-36.389	14	5 %

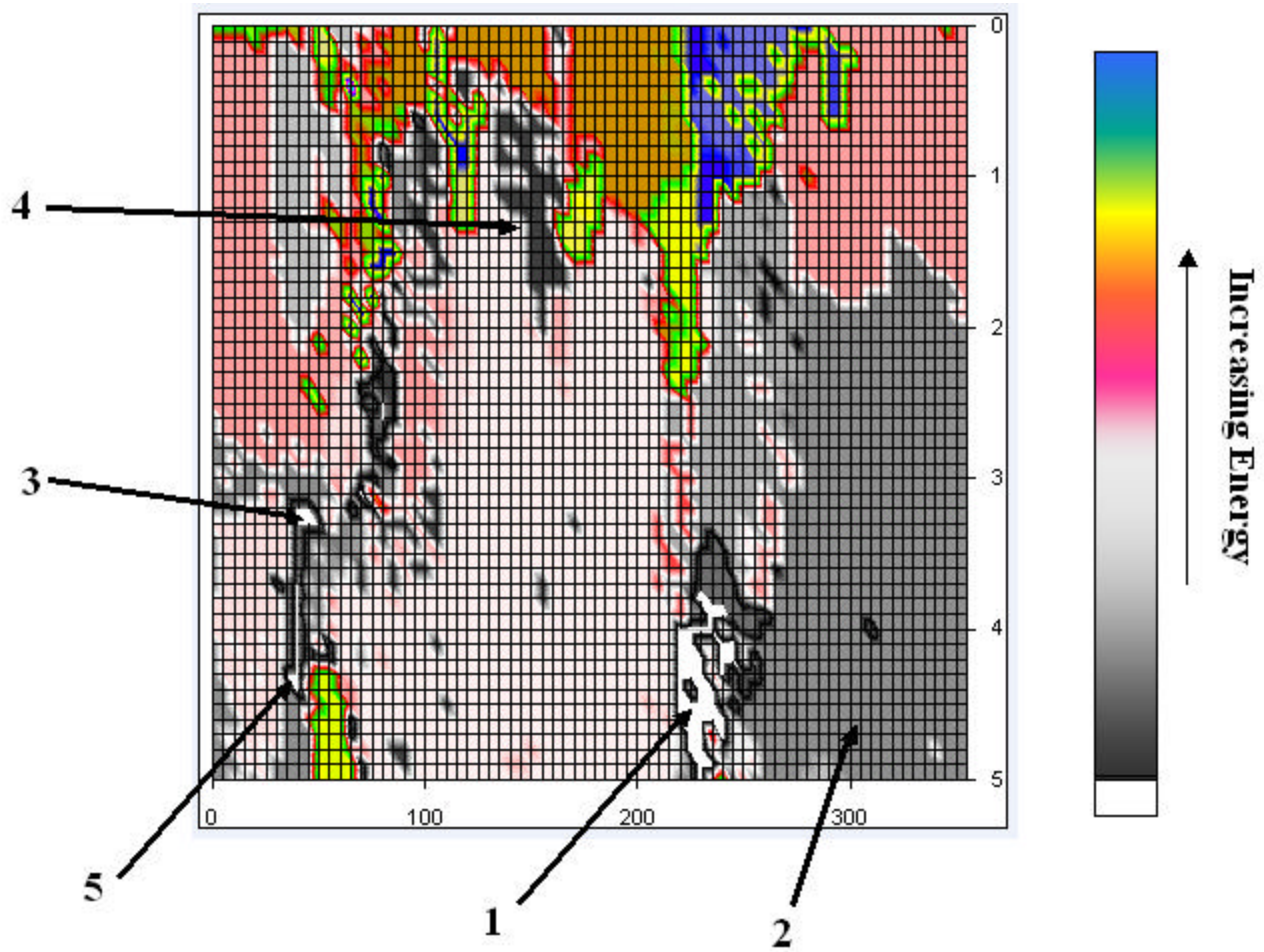

Figure 4.15. Two dimensional representation of the 1,5-DHN energy data from Figure 4.13 (d). The top five regions contributing to the calculation of <e> are shown. Energy values for the regions are found in Table 4.4.

Table 4.6: Resulting K_d values from each calculation approach for comprehensive minimization, compared with results from the previous two experiments.

Solutes	Expt.	'100 min'	'250 min'	Approach 1	Approach 2	Approach3
1,5-DNN	47	$6.3x10^{-2}$	17	450	36	18
1,8-DNN	65	3.2	20	230	31	35
2,7-DNN	96	96	96	96	96	96
1,5-DMN	130	$3.5x10^{3}$	$4.3x10^{4}$	$4.2x10^{4}$	3100	1000
1,5-DHN	490	$8.4x10^{5}$	$6.4x10^{4}$	$4.6x10^{4}$	4700	3300

improvement in correlation with consideration of g_i may indicate that molecular rearrangements (quenching) occurs rapidly relative to solute-CD exchange rates. Like Approach 3, the '100 min' and '250 min' cases also consider all the available grid search data and yield the correct elution order. However, the range of K_d values is enormous compared to the experimental values, and it is clear that the comprehensive minimization of Approach 3 is the most successful model considered. The predicted migration times that result from comprehensive minimization, Approach 3, are shown in Figure 4.16.

Conclusion

These studies indicate the effectiveness of this modeling approach to studying the strength of solute-CD interactions as they influence migration behavior in CD-modified CE. Each of the three techniques presented here correctly predicts the experimentally observed elution order. It was found to be very important to extensively geometrically minimize solute-CD configuration to find reliable conformers. Further, it was determined that it is important to weight the conformers based on the interaction space that can quench to the conformer.

It is evident in the 3D-plots and data that this method is indeed finding legitimate conformations of the CD-solute complex, and that the energies of these conformers can closely approximate the actual interaction energies experienced by the species in experimental separations. A significant step has been made toward the ultimate goal of computationally determining and manipulating selectivity in CD systems.

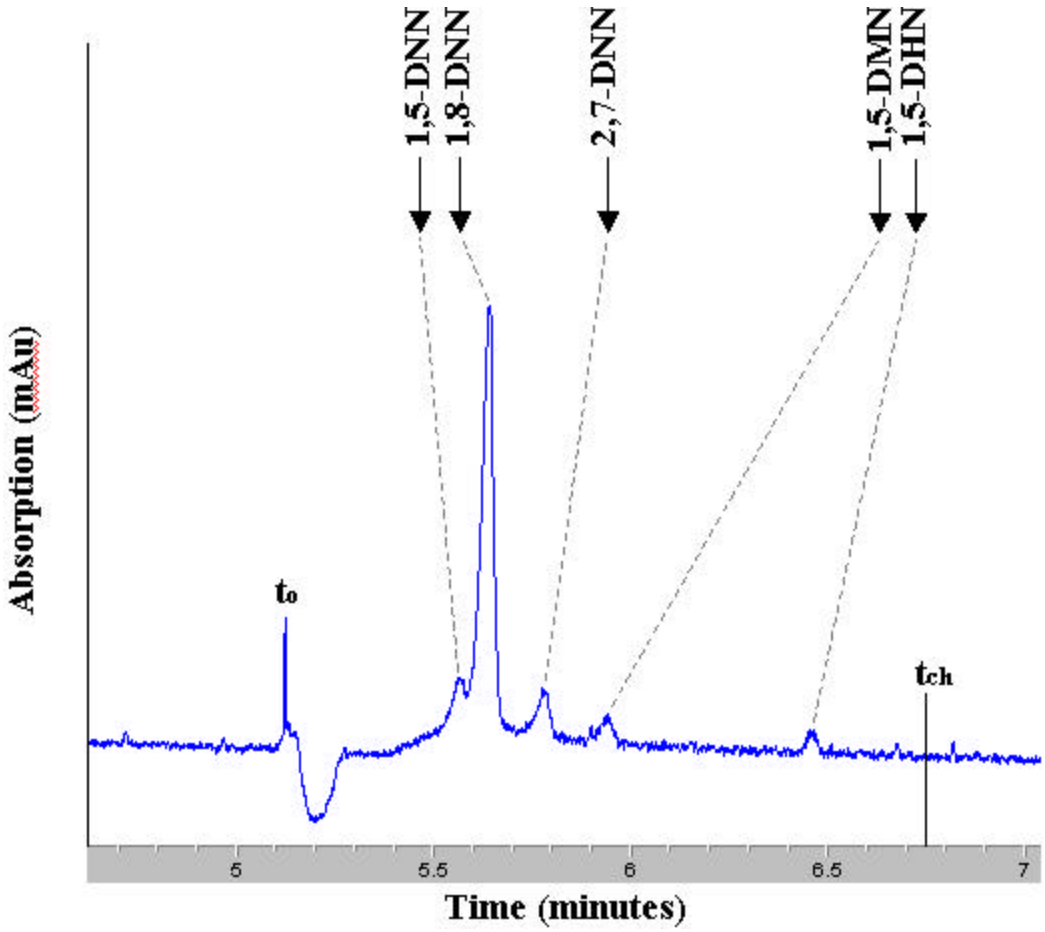

Figure 4.16. Predicted peak elution times based on modeling calculations are shown in arrows on the experiment electropherogram.

CHAPTER 5

MOLECULAR MODELING APPLICATIONS: SYNTHESIS OF A NEW CYCLODEXTRIN, AND STUDIES OF THE CHIRAL SEPARATION OF DANSYL AMINO ACIDS

Part 1: Design of a New Cyclodextrin

Introduction

Cyclodextrins lend themselves very well to derivatization, and serve as effective molecules with which to build a wide range of useful hosts. Because of this flexibility in derivatization, CDs geometries and functionality can be specifically tailored to meet the requirements of a particular guest. Improvements in molecular recognition and chemical separation are possible by customizing the host to optimize complexation for the guests.

The hydroxyl groups on the native CDs are the sites through which derivatization can take place. There are primary hydroxyl groups at the C6 position and secondary hydroxyl groups at the C2 and C3 positions of each glucopyranos unit (see Figure 1.6), meaning that there is a abundance of sites for reaction. However, given the large number of hydroxyl groups, products tend to form complex mixtures of isomers and different products. The reactions can be controlled in various ways however, such as by the use of protecting groups, or by exploiting the different reactivities of the primary and secondary hydroxyl groups.[162-164] Acylation or sulfonation are frequently used to place functional groups on directly, or intermediate halides and sulfonates can be made which the functional groups can replace through SN1 or SN2 reactions.[165, 166]

In the first part of this chapter the design, synthesis, and evaluation of a new cyclodextrin, heptakis (6-O-carboxymethyl-2,3-dimethyl)-β-cyclodextrin (HDMCM-β-CD), will be presented, along with the molecular modeling methods used to support and initiate this effort.

HDMCM-b-CD

The design of any new CD needs to meet several criteria to be a successful resolving agent as a CE additive. First, it must be somewhat soluble in aqueous environments since CE experiments are frequently conducted as such. Second, the CD should be amenable to forming complexes with the analytes of interest. Third, if neutral analytes are to be resolved, the CD must have a charge with which to impart selective mobility changes to the solutes. And fourth, the CD must be reasonably attainable by synthetic methods.

Additionally, there were further criteria that would influence the design of the CD for this work. First, this charged CD needed to be a single isomer. This is necessary in order to conduct quicker and more accurate molecular modeling, as well as to eliminate separation problems that can be experienced with multiple-isomer mixtures. Second, it was desirable to make the CD highly charged to maximize its mobility against EOF and provide a large elution window for the separation of neutral analytes.

Further influence on the CD design came from prior achievement of the commercial CM-β-CD at resolving neutral organic species in CE (as demonstrated in Chapter 4), and Vigh's successes with his highly charged heptakis(2,3-dimethyl-6-

sulfato)-β-cylodextrin (HDMS-β-CD).[116,117] The new CD that was decided upon was heptakis (6-O-carboxymethyl-2,3-dimethyl)-β-cyclodextrin (HDMCM-β-CD); its MolCAD structure is shown in Figure 5.1.

HDMCM-β-CD is highly charged, single isomer species, like Vigh's HDMS-β-CD. The methyl groups attached to the C(2) and C(3) were necessary to protect those positions from further substitution during a synthesis, but also to provide a more hydrophobic cavity entrance with which to facilitate inclusion of non-polar analytes.

Experimental

The HDMCM-β-CD was synthesized using using established, multi-step procedures.[167-170] The reaction scheme for the synthesis of HDMCM-β-CD is shown in Figure 5.2; all synthetic work was performed by Mustafa Culha.[171] The running buffer in the experiments was a 10 mM phosphate solution with a 5 mM concentration of the CD to be evaluated. The pH of the buffer solutions was adjusted to 5.0 using an Orion Model SA520 pH meter operating under a two-standard calibration. The buffer was sonicated and filtered through a 0.22 μm nylon filter before being placed under vacuum conditions to remove dissolved gases. To slow the growth of microorganisms, the buffer solutions were stored in the refrigerator.

The samples were prepared by diluting stock methanol solutions of the analytes with the running buffer to give concentrations in the range of 10^{-5} to 10^{-6} M. All CE experiments were performed using a Hewlett Packard HP^{3D}CE automated capillary electrophoresis instrument interfaced to a HP Pentium I personal computer. Fused silica capillaries (50 μm i.d. x 360 μm o.d.) were obtained from Polymicro Technologies, Inc.

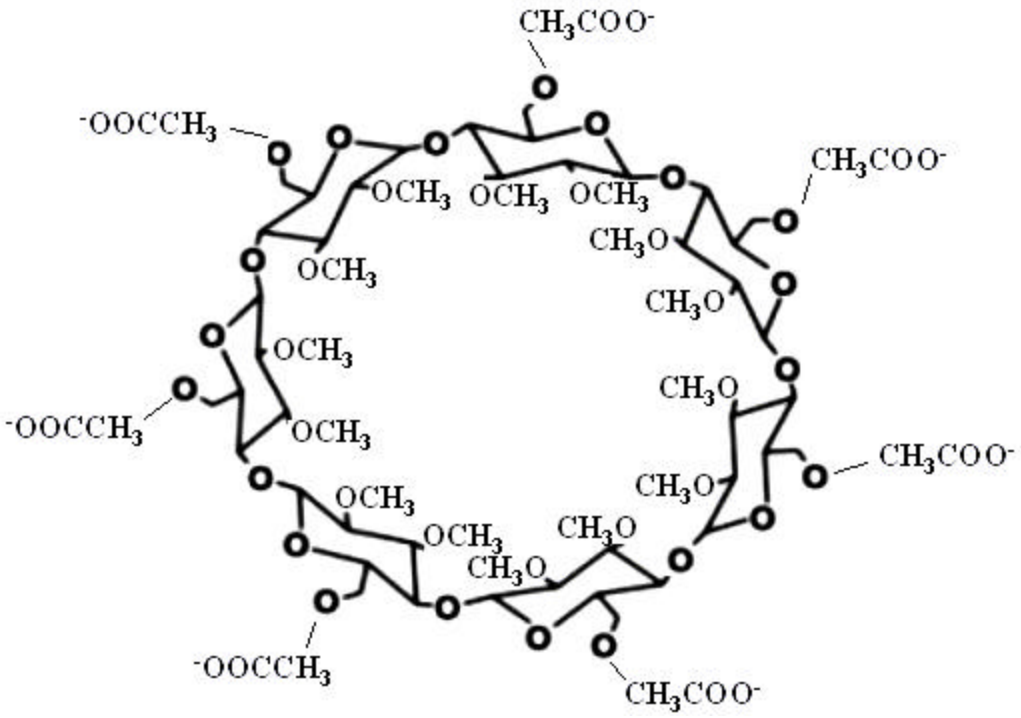

Figure 5.1. Heptakis (6-O-carboxymethyl-2,3-dimethyl)-β-cyclodextrin (HDMCM-β-CD), shown in its deprotonated form.

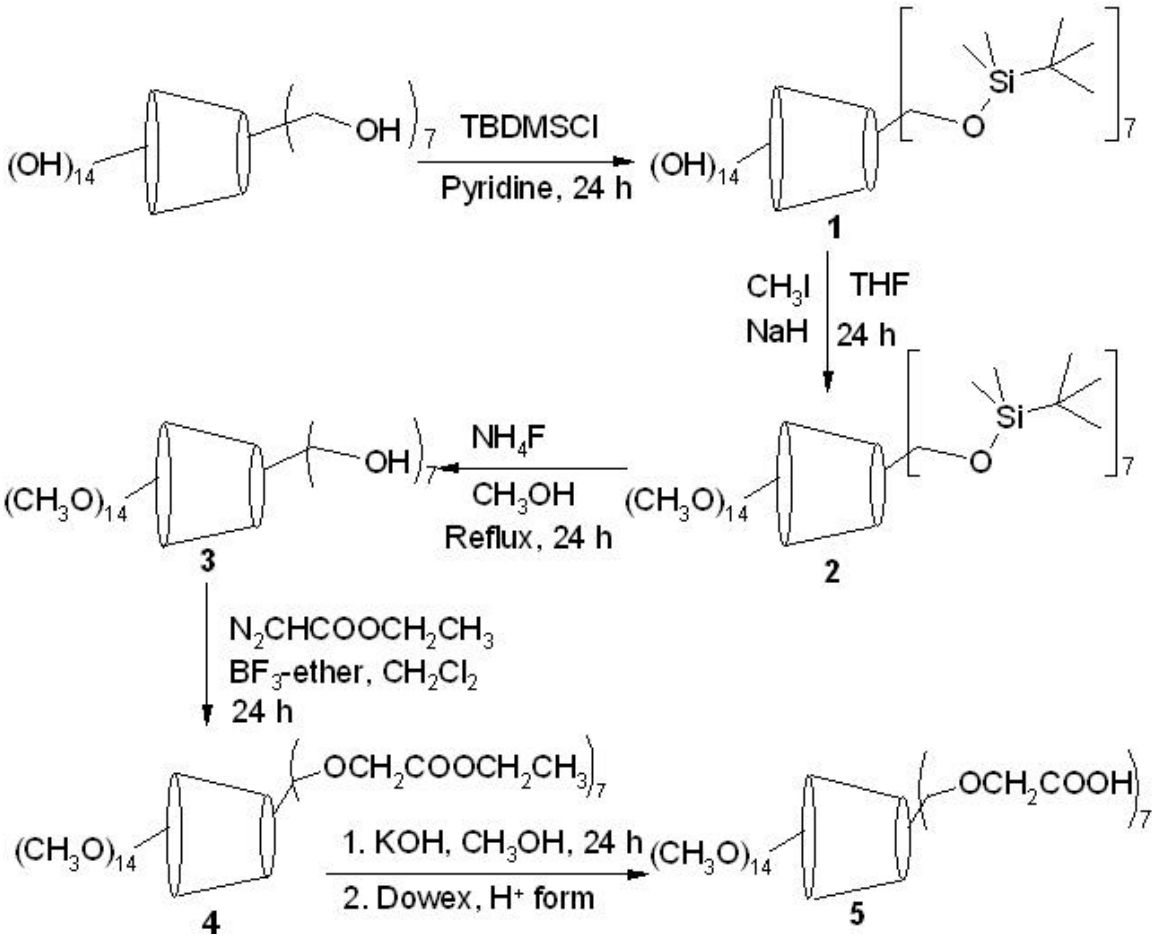

Figure 5.2. The reaction scheme for the synthesis of HDMCM-β-CD.

(Phoenix, AZ). The capillary was cut to a total length of 48 cm, and approximately 1 cm of polyamide coating centered at 39.5 cm was removed to create an optical detection window.

Injection was achieved by the application of 10 mbar of pressure for 6 seconds to the inlet buffer vial. The applied potential for all CE experiments was 15 kV. UV absorbance detection was performed at wavelengths ranging from 205 to 254 nm for all the test solutes. All experiments were conducted at room temperature ($24 \pm 1\ ^{o}C$).

Results and Discussion

Molecular Modeling to Support Synthetic Target

Molecular modeling was used in support of the efforts to design HDMCM-β-CD. Studies using MolCAD were performed to compare its predicted properties to that of other known CDs. Electron density surfaces were created for β-CD, HDMCM-β-CD, HDMS-β-CD, and heptakis(2,3-diacetyl-6-sulfato)-β-cylodextrin (HDAS-β-CD). Mapped on the surfaces of each of these molecules were different properties, such as hydrogen bonding potential, electrostatic potential, and lipophilicity. These studies revealed that although HDMCM-β-CD is absent of the hydrogen bonding possible from secondary hydroxyl groups, it is very lipophilic around this area of the molecule (see Figure 5.3), which should make it more conducive toward the association with non-polar organic analytes.

The modeling also showed that the cavity structure of the HDMCM-β-CD remained roughly equivalent to the shape of β-CD, without undergoing much distortion. When the CD was compared to the commercially available HDMS-β-CD using

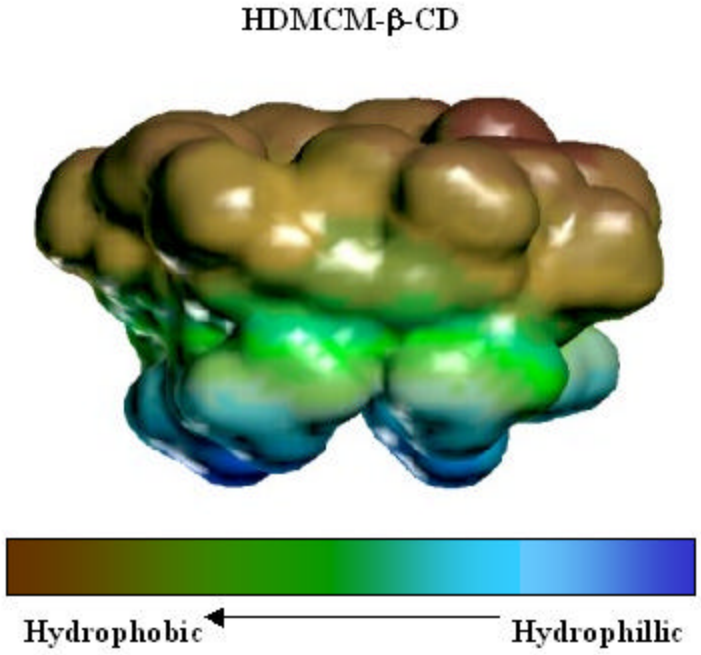

Figure 5.3. MolCAD representation of HDMCM-β-CD is shown with the lipophilic property mapped to an electron density surface. Brown indicates hydrophobic portions of the molecule (methoxy groups at C2 and C3 positions), while blue indicates hydrophilic areas (carboxymethyl groups at C6 position).

MolCAD, it was apparent that the cavity shape of HDMCM-β-CD was much more open and accessible. The sulfato groups on the HDMS-β-CD were found to be positioned inward, essentially truncating the bottom of its cavity (Figure 5.4). This evidence lent support to the premise that HDMCM-β-CD would be better at resolving the hydrophobic target analytes of interest than the HDMS-β-CD.

Docking experiments were performed to compare the computed interaction of the analytes with HDMCM-β-CD to the interaction with HDMS-β-CD. The analytes were the same substituted naphthalene compounds used in the work described in Chapter 4: 1,8-DNN, 2,7-DNN, 1,5-DNN, 1,5-DHN, and 1,5-DMN. The CDs were created by using the SKETCH function of Sybyl to modify a β-CD obtained from the Cambridge Crystallographic Data Center's structural database. These CDs were minimized with 1000 iterations in a water environment using the MAXIMIN2 command in Sybyl with the Tripos force field. The structures were then saved to the computers hard drive after removing the water molecules.

Programs were written in Sybyl Programming Language to dock the solutes into each CD using the grid conformation-searching modeling technique described in Chapter 4. The solutes were translated toward the cavity from –5.0 Å away in 0.1 Å increments, and rotated at each increment by 5^{o}. At each of these points the structures were minimized using MAXIMIN2 with 500 minimization iterations, and the energy was saved to an output file. The data was imported into Microsoft Excel and the computational interaction energy of each of the solutes with the CDs was determined. It was found that the complexes the solutes formed with HDMCM-β-CD were an average

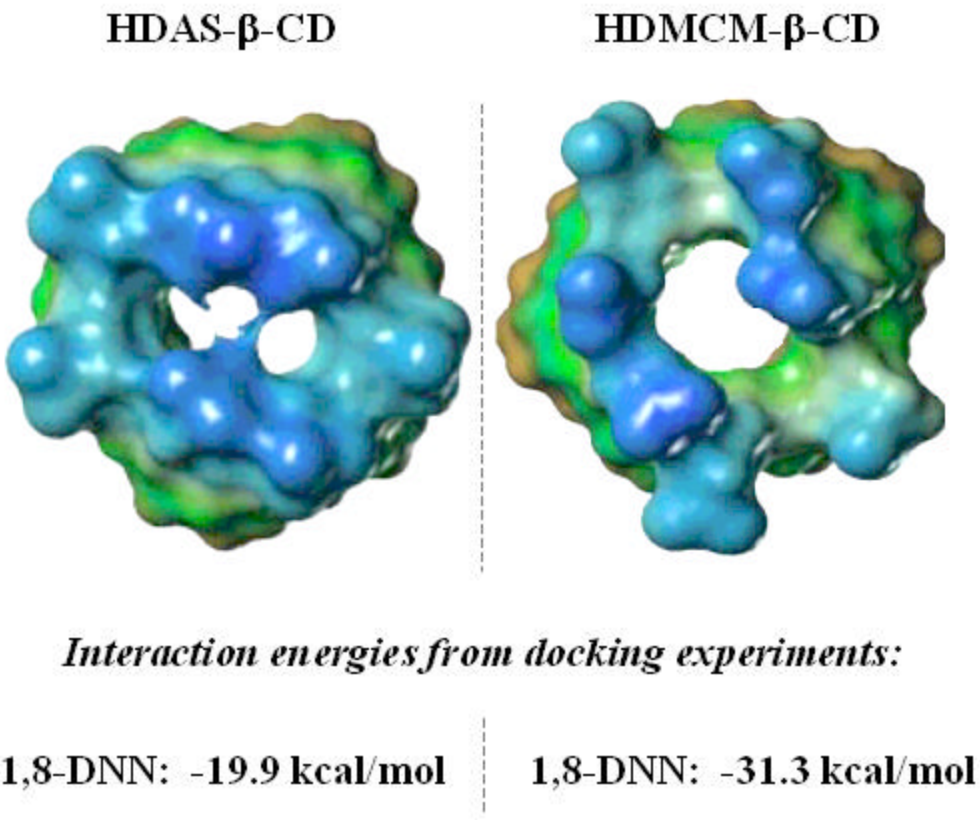

Figure 5.4. The lower part of the Sulfato-CD cavity (left) shows strong negative potential and truncation. The cavity of the Carboxymethyl-CD appears more compatible with insertion of the solute compounds under study. Modeling <e> values support superior inclusion of solutes into the HDMCM-β-CD, guiding its synthesis as a new reagent.

of 8 kcal/mole more favorable than those complexes formed with HDMS-β-CD.

An additional docking experiment was conducted to further investigate the ability of HDMCM-β-CD to complex the analytes, relative to HDMS-β-CD. Using 1,8-DNN, a program was written to dock the solute into the CDs using comprehensive minimization. The interaction energy was calculated for the 1,8-DNN with each CD. It was found that the interaction energy of the solute with HDMS-β-CD was –19.9 kcal/mol, while it was –31.3 kcal/mol for HDMCM-β-CD. This -11.4 kcal difference is substantial, and a strong indication that HDMCM-β-CD would indeed be superior to HDMS-β-CD for these analytes.

Experimental Separation

The results of the experimental separations are shown in Figure 5.5. Although both CDs are shown to be able to separate the analytes, it is apparent that the solutes experience a much greater affinity for the HDMCM-β-CD than for HDMS-β-CD. The solutes in separation are significantly more retained with the HDMCM-β-CD, as evidenced by their longer elution time. Since the elution window (time between EOF marker and the charged CD elution) is roughly the same for the two CDs due to their similar charge to size ratio, it can be concluded that HDMCM-β-CD is a much better at complexing the analytes than HDMS-β-CD. These results are in agreement with the molecular modeling efforts which showed through MolCAD and docking experiments that the HDMCM-β-CD would yield superior inclusion ability.

It is interesting to note that the although the solutes clearly prefer HDMCM-β-CD over HDMS-β-CD, the elution order of the solutes is equivalent in both separations. This

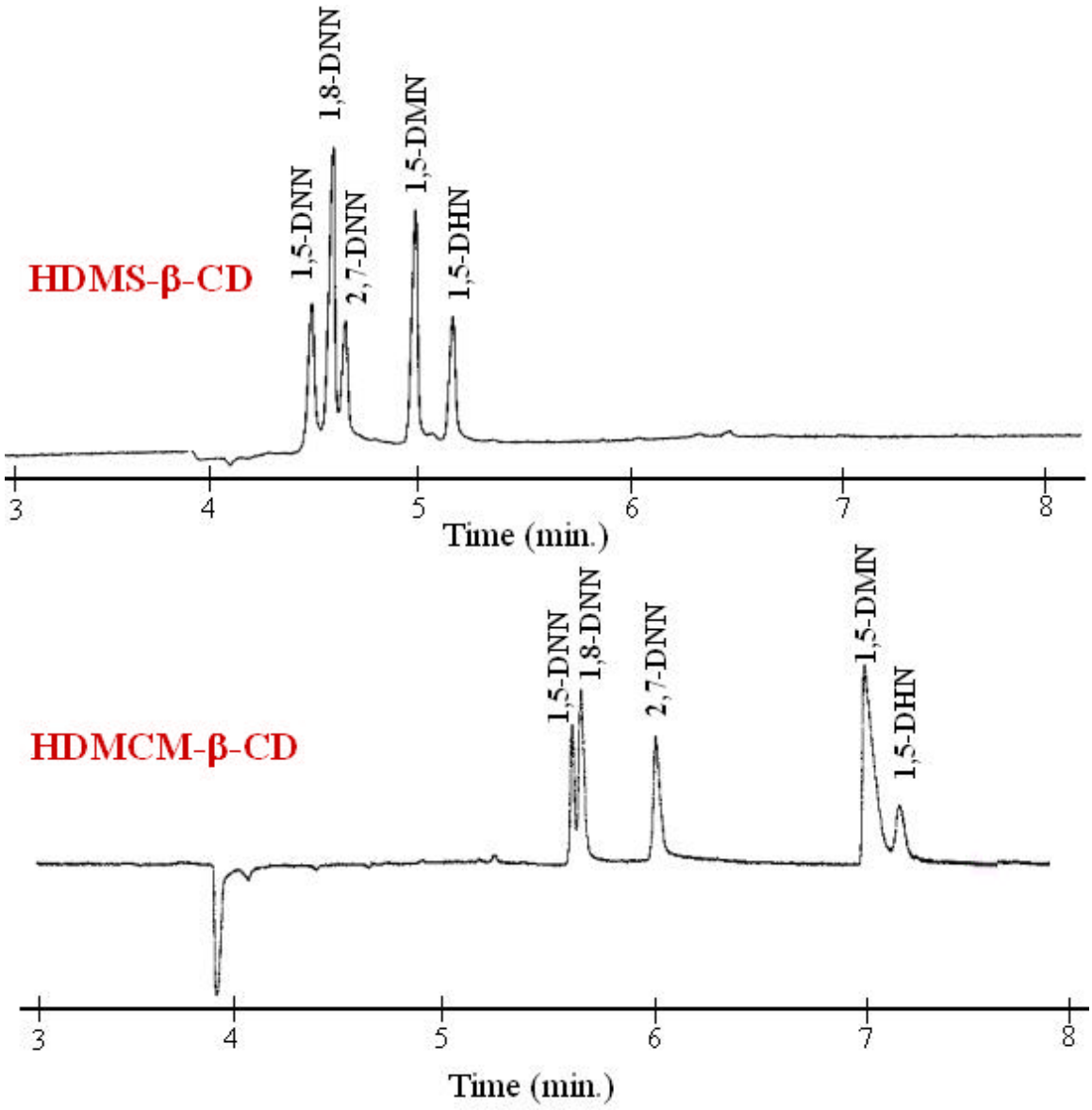

Figure 5.5. The separation of analytes using HDMS-β-CD and HDMCM-β-CD is shown.

may be because both the CDs are very similar chemically, with a highly charged polar side and a strongly hydrophobic methyl side. The difference in inclusion ability between the two may then be a result of the different charged groups; HDMCM-β-CD is lined with carboxymethyl groups while HDMS-β-CD contains sulfato groups. As the modeling showed, the sulfato groups appear to take on a more inward orientation, which may truncate the cavity and diminish inclusion.

Molecular Modeling in Support of Separation Behavior

In cyclodextrin distribution capillary electrochromatography (CDCE), mixtures of CDs are employed in the running buffer with which the analytes will selectively partition. The utility and predictability of incorporating multiple CDs in the CE buffer depend upon the assumption that the CD selectors act independently of each other. However, this is not always the case, given that some CDs contain numerous sites with which to hydrogen bond with each other.[172]

In additional experimentation, CDCE experiments were conducted separating the naphthalene derivative solutes. The charged HDMS-β-CD was mixed with β-CD in the running buffer, and all other experimental conditions were held the same as described above. The results revealed that adding β-CD to the buffer did not affect the observed elution behavior. Even as the β-CD concentration was increased relative to the HDMS-β-CD to a 5:1 ratio (which should cause the solutes migration time to converge on t_o), little effect was observed on the elution pattern. This puzzling finding initiated an effort to understand the nature of this phenomenon using molecular modeling.

After generating MolCAD representations of HDMS-β-CD and β-CD with the hydrogen bonding potential mapped on the electron density surface, it was apparent that there were numerous sites on both CDs where such interactions could occur.

Using the Sybyl software two structures β-CD were displayed. A function of the Sybyl software was then used, which calculates and draws hydrogen bonds between two molecules as they are moved relative to each other. One β-CD was then lined up with the other in a top to bottom arrangement, and the two were slowly brought together. As expected, significant hydrogen bonding was observed between the primary and secondary hydroxyl groups of the CDs, with as many as 5 hydrogen bonds appearing under certain alignments. This is consistent with observations by Coleman et al., who previously has shown that CDs can exist as aggregates in solution, bound by a network of hydrogen bonds.

This procedure was next applied to HDMS-β-CD and β-CD. The HDMS-β-CD, was aligned so that the sulfato groups were oriented toward the secondary hydroxyl groups on the top of the β-CD. As the two molecules were brought together, a multitude of hydrogen bonds were observed, with as many as 20 being present at one time (see Figure 5.6). The sulfato groups on the HDMS-β-CD were found to have many more hydrogen bonding sites with which to interact with β−CD than a second β-CD does with its primary hydroxyl groups. With the strength of hydrogen bonds generally in the range of 5-10 kcal/mol, the extensive interaction observed between the HDMS-β-CD and β-CD approaches or exceeds the strength of a covalent bond (100-150 kcal/mol). Clearly, CD-CD interactions of this magnitude effectively block the action of the β-CD, as its cavity

HDMS-b-CD b-**CD**

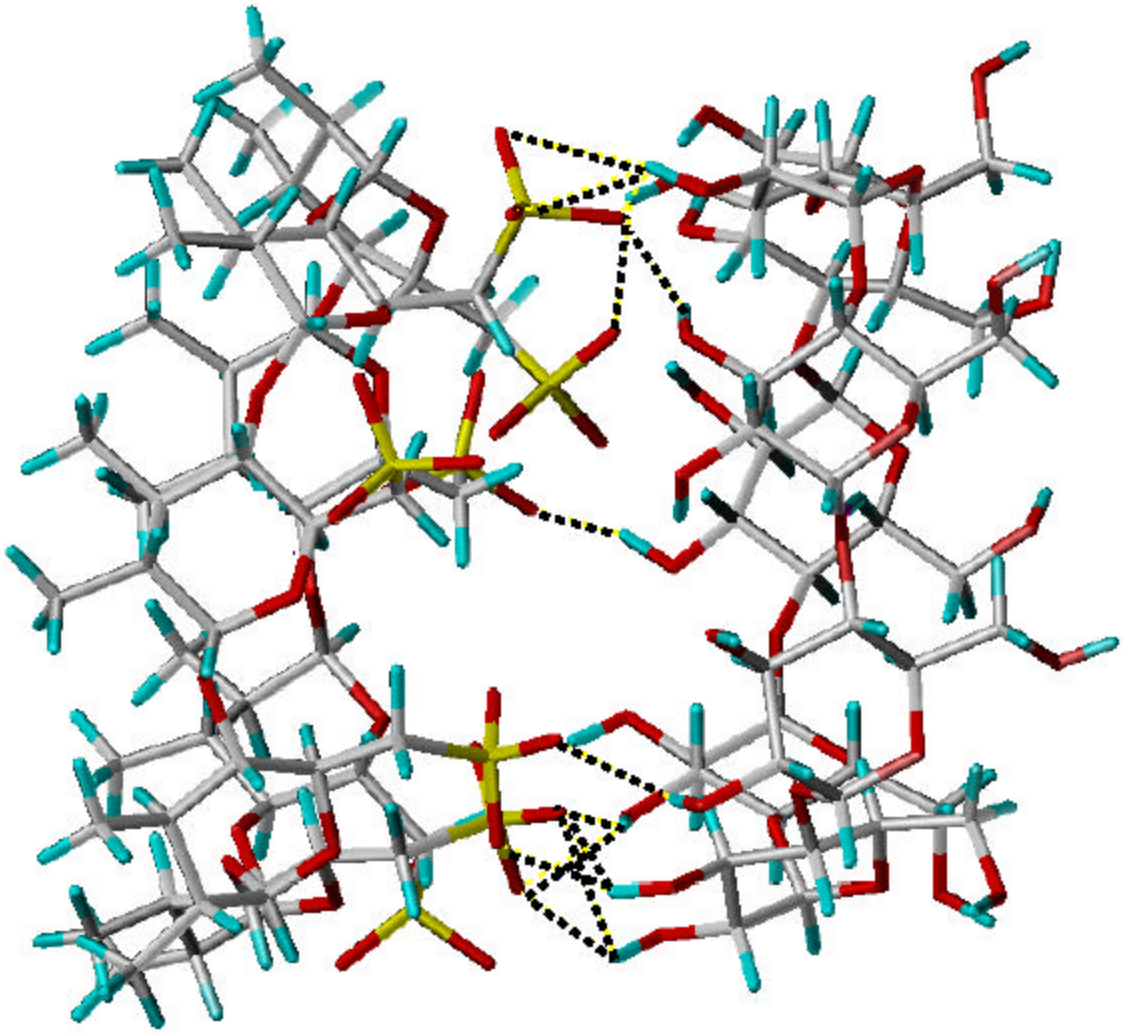

Figure 5.6. Significant hydrogen bonding between the sulfato groups of the HDMS-β-CD (left) and the secondary hydroxyl groups of β-CD (right) is shown by dotted black lines.

would most likely be blocked by an HDMS-β-CD molecule in solution.

Additional modeling work was conducted to support this finding. Docking programs were created so that β-CD could "dock" toward another β-CD, with the primary hydroxyl groups of one being aligned with the secondary hydroxyl groups of another. The first CD was systematically translated (0.1 Å steps) and rotated (5^o increments) toward the second CD from 20 Å away. At each step the energy was minimized with 250 iterations using the MAXIMIN2 command, and stored to a data file. This docking procedure was repeated with the HDMS-β-CD docking toward a β-CD.

The interaction energy of the CDs from both docking experiments was determined (as described procedures in Chapter 4). It was found that the interaction of HDMS-β-CD with β-CD was approximately 10 kcal/mol stronger than that experienced by the interaction of two β-CDs. These results provided further evidence that significant intermolecular interactions can occur in solution between CDs and considerably affect separation results.

Part 2: Application of Molecular Modeling to the Separation of Dansyl Amino Acids.

Introduction

Advances in both the science and technology of direct enantiomer resolution over the last two decades has made the separation of a wide range of enantiomers routine today.[173-181] Different phases have been used to achieve enantioselectivity in separations. Bovine serum albumin, α_1-acid gycoprotein, ovomucoid, and casein have been successfully used to achieve the task.[182] Kuhn and coworkers[183,184] have shown the utility of a chiral crown ether (18-crown-6-tetracarboxylic acid) for chiral recognition.

The macrocyclic antibiotic vancomycin was successfully used in CE separations,[185,186] and amino acids have been separated using CDs as CE buffer additives.[187] Vigh and coworkers have synthesized a sulfated γ-CD reagent that was successfully used to separate several amino acid enantiomers.[116,117] The single isomer highly charged CD takes advantage of a large separation window.

There have been some efforts to use molecular modeling to study enantiomeric separations, but few ambitious or accurate enough to attempt predictions of enantioselectivity. Sepaniak et al. used molecular mechanics to study separations of derivatized amino acids by cyclodextrin-modified CE.[189] Sepaniak and Sun later successfully applied this computational work to CE separations using calix[n]arenes as reagent phases.[190] Molecular dynamics has been used in a pioneering work by Konigh and coworkers to study GC results.[191] Koen et al. used a combined molecular dynamics and molecular mechanics technique to explain trends in qualitative GC separations.[192] Armstrong and coworkers have used MM to calculate the binding enthalpy, ΔH, for CD hosts and enantiomer guests.[193]

In other efforts, molecular modeling was used by Kobor et al. to study the binding of polar and non-polar solutes to CDs in GC experiments.[194] In order to design better chiral stationary phases, Bradshaw et al. used MM to study how enantiomeric amines were separated with new crown ethers.[195] Molecular graphics studies have been conducted by Armstrong and co-workers to assist in understanding how β-CD separates diastereomers[196] and enantiomers.[197,198] Their work revealed that enantiomeric resolution is somewhat dependant on the 2- and 3- hydroxyl groups, and allowed them to attempt

rational CD designs to achieve optimal separations.

Experimental

Reagents

Five different amino acids (AA) were chosen to be separated by cyclodextrin modified CE. The AAs were selected based on their differing properties. Dansyl-glutamic acid (Glu) and dansyl-aspartic acid (Asp) were selected due to their acidity. dansyl-serine (Ser) was chosen because it is a more polar compound, and dansyl-leucine (Leu) and dansyl-Valine (Val) were included because they are more hydrophobic in nature. Each of the AAs were acquired from Sigma Chemical Company (St. Louis, MO). The structures of the AAs are shown in Figure 5.7.

The separation of these AAs is not trivial because there are 10 possible separate bands to be separated, and there are three different classes of AAs selected that differ significantly in their chemical properties. Additionally, it is important that the enantiomers be separated, but not overly so. This is because with all the other solutes present it is possible for enantiomer bands from two different AAs to coelute.[189,199] Five different cyclodextrins were selected to evaluate their effectiveness for this chiral separation.

Five different cyclodextrins were chosen to evaluate their effectiveness for this particular separation. The 5 CDs used in these experiments were β-CD, γ-CD, CM-β-CD, heptakis-(2,3-dimethyl-6-carboxymethyl)-β-CD (HDMCM-β-CD), and octakis-(2,3-dimethyl-6-hydroxy)-β-CD (16-me-γ-CD). β-CD was obtained from Sigma Chemical Company. γ-CD was purchased from Cyclodextrin Technologies Development, Inc.

Dansyl Amino Acids

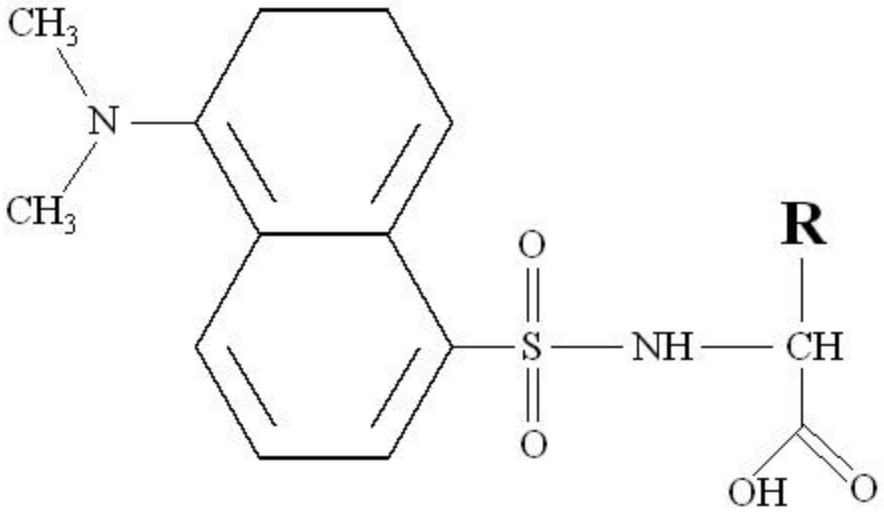

Serine:	$R = CH_2OH$
Valine:	$R = CH(CH_3)_2$
Leucine:	$R = CH_2CH(CH_3)_2$
Glutamic Acid:	$R = (CH_2)_2CO_2H$
Aspartic Acid:	$R = CH_2CO_2H$

Figure 5.7. The structures of the 5 dansyl amino acids are shown.

(Gainsville, FL.) CM-β-CD was acquired from Advanced Separation Technologies Inc. (Whippany, NJ). The HDMCM-β-CD and 16-me-γ-CD were synthetically produced in our laboratories.[200]

The charged cyclodextrins used in these experiments were chosen because they presumably were single isomer species. This precludes the need to model several different isomers in the molecular modeling studies. Additionally these single isomer reagents facilitate reproducible separations. Most commercial CD derivatives are made of mixtures that have different degrees of substitution. The electropherograms appearing in this chapter were generated by James Schaeper.[201]

Separation Conditions

Separations were performed using a Hewlett Packard automated Capillary Electrophoresis system ($HP^{3D}CE$) with a diode array detector interfaced to a Pentium I personal computer. All experiments were conducted with an applied potential of 16 kV at a constant temperature of 24°C. The degassing of the buffers and the preconditioning steps for the capillary were conducted as described previously in Chapter 4. Detection was achieved with a diode array by measuring the absorbance at 214 nm.

The fused silica capillaries that were used were obtained from Polymicro Technologies Inc. (Phoenix, AZ). The dimensions of the capillaries were 50 μm i.d. and 360 μm o.d., and they were cut to a total length of 60 cm. A detection window was prepared at 51 cm by removing the polyamide coating. The void time of the separation (t_o) was determined by including mesityl oxide in the injected sample, which caused a baseline disturbance upon elution.

The running buffer in all experiments was a solution of 0.01 M sodium phosphate and 0.006 M sodium borate, adjusted to a pH of 8.1. The different cyclodextrins were mixed into this solution as buffer additives at a concentration of 5 mM.

Modeling Experiments

The modeling experiments in this work are not intended to rigorously predict the elution order between two enantiomers. To study the enantioselectivity the subtle differences in the interactions between CDs and enantiomer pairs would require extremely long, comprehensive modeling approaches. Rather, these efforts were performed concomitantly with the separations to elucidate the general nature of interactions, and at the same time expand and explore the utility of the grid conformation-searching modeling technique to more CDs.

The structures for β-CD and γ-CD were obtained from the Cambridge Crystallographic Data Center's structural database. CM-β-CD and HDMCM-β-CD were constructed from the β-CD structure using the SKETCH feature in Sybyl. The 16-me-γ-CD was obtained by modifying the γ-CD structure with SKETCH. Each CD was minimized 1000 times in an aqueous environment using the Tripos force field. The waters were then removed, and the structure of the CDs were saved for use with the docking programs.

Macro programs were written in Sybyl Programming Language to dock the AAs into the CDs. The AAs were systematically translated toward the CDs from –10 Å away to 0 Å inside the cavity, in increments of 0.1 Å. At each of these translation points the

solute was rotated 360 degrees in 5 degree increments. The energy was minimized at the points using the MAXIMIN2 function utilizing 250 iterations.

A depiction of the docking and orientation of the AAs is shown in Figure 5.8. This orientation was selected based on findings from MolCAD visualization studies. The most likely docking position for the AA was found to be that of the aromatic portion of the molecule entering the hydrophobic cavities of the CDs, with the functional groups on the remaining part the molecule experiencing stabilizing interactions with hydroxyl groups on the rims of some of the CDs. MolCAD representations of the CDs are shown in Figure 5.9, with the hydrogen bonding potential mapped on the electron density surface.

The dielectric constant was set to 20 for calculations in these experiments. The energy data from all of the 7920 grid points was saved to an output file and imported into Microsoft Excel and Sigma Plot for analysis.

Results and Discussion

The different cyclodextrins in these experiments separate the AAs by modifying their effective mobilities via selective inclusion into their cavities. Some of the CDs are charged and influence the effective elution window. As can be seen in the expression of Equation 5.1, the observed mobility (μ_{obs}) for the solute is dependant on its distribution between the free and complexed forms:

$$\mu_{obs} = \frac{\mu_f + \mu_c K_{CD} [CD]}{1 + K_{CD} [CD]} \qquad (5.1)$$

where μ_f is the free mobility of the solute, and μ_c is the mobility of the CD-solute

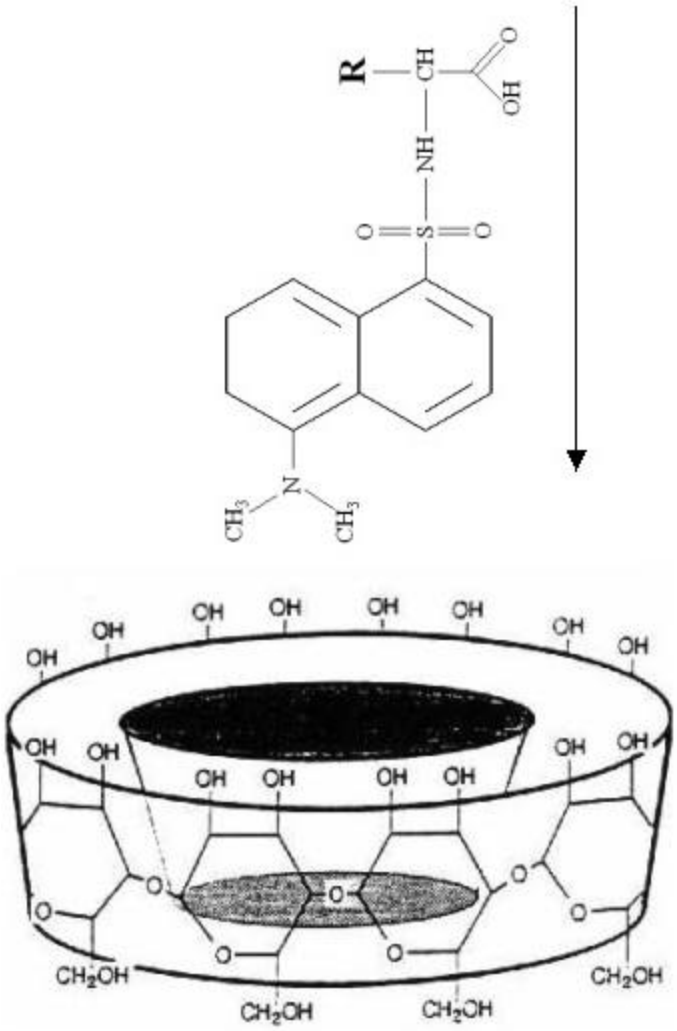

Figure 5.8. The orientation of the dansyl amino acids docking into the CD is shown.

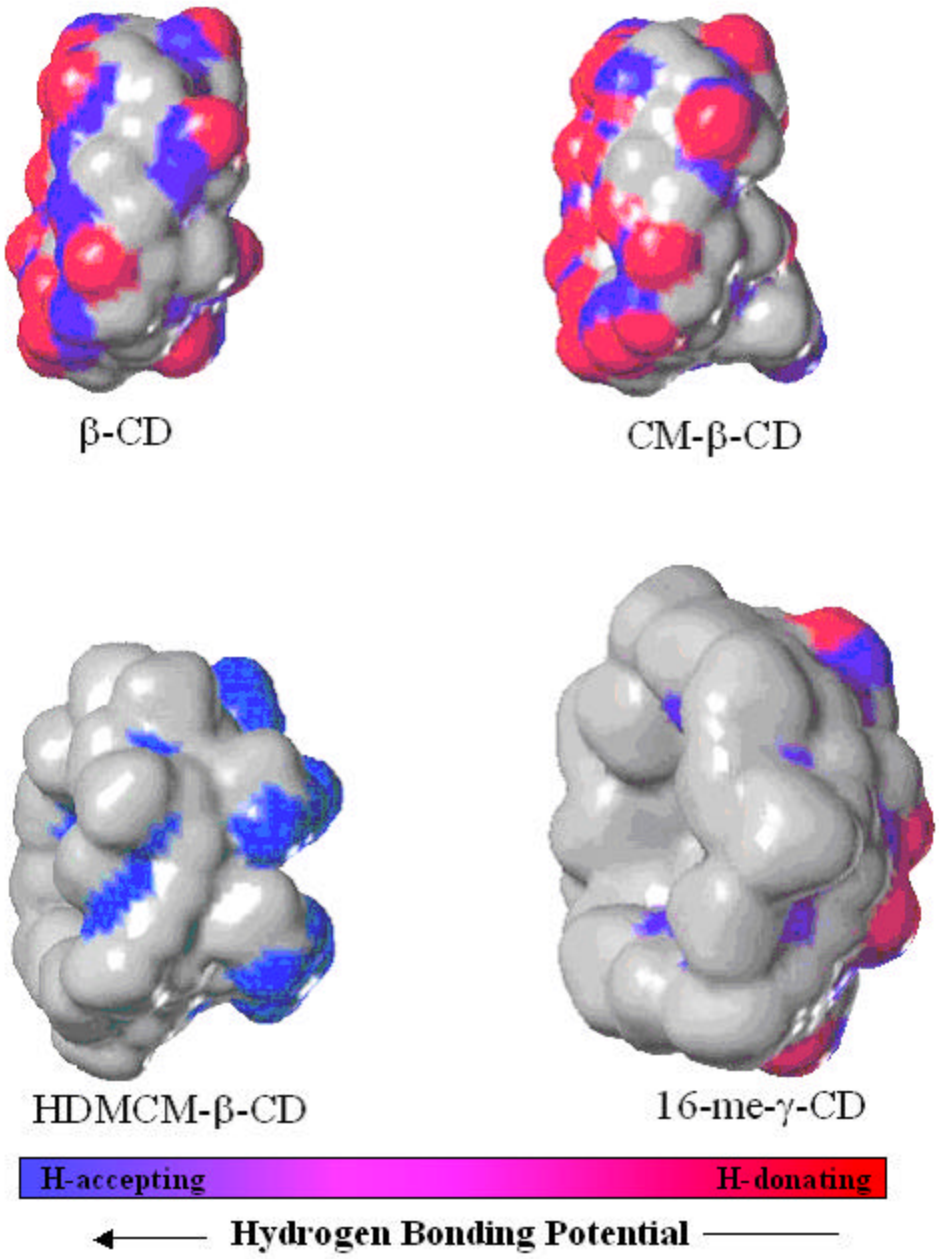

Figure 5.9. Electron density surfaces are generated for the cyclodextrins using MolCAD within the Sybyl software, and hydrogen bonding potential is mapped on the surface. γ-CD is not shown; it is structurally the same as β-CD except that it has one more cyclic glucose unit in its structure. Red designates hydrogen donating regions and blue represents hydrogen accepting regions.

complex. The inclusion constant, K_{CD}, is given by Equation (5.2):

$$K_{CD} = \frac{[\text{CD-solute}]}{[\text{CD}]\ [\text{solute}]} \qquad (5.2)$$

Elution Window Considerations

Depending on the pH, the amino acids can be charged or neutral. The pH used in these CE experiments was 8.1, a value at which all of the AAs that were used are negatively charged. In the electric field, the AAs have an electrophoretic mobility that is opposite that of EOF. Since the AAs are "swimming upstream", they elute later than t_o in their free, uncomplexed form.

Figure 5.10 is a graphical illustration of the elution time of the AAs, and how it is affected by different cyclodextrins present in the running buffer. The elution time of the free amino acid ($t_{f.a.a.}$) will be much later than t_o because of its mobility opposite EOF, as described above. The elution time of the AAs completely complexed with a neutral CD ($t_{c,\beta\text{-cd}}$) is much earlier than the free AA, because the charge to size ratio of the complex is much smaller. The AAs in a CE separation using neutral CDs can therefore elute within a range of time between $t_{f.a.a.}$ and $t_{c,\beta\text{-cd}}$, depending on the relative affinities of the AA for the CD. If HDMCM-β-CD is considered, the elution time of this CD-AA complex ($t_{c,\ \text{HDMCM-}\beta\text{-CD}}$) will be much *later* than that of the free amino acid. This is because the highly charged CD has a very strong mobility opposite EOF, and charge to size ratio of the complex is greater than the free AA. The elution range using the HDMCM-β-CD then will be between $t_{f.a.a}$ and $t_{c,\ \text{HDMCM-}\beta\text{-CD}}$. In the case of CM-β-CD, it is only

Representation of Elution Ranges

t_0 = time for electroosmotic flow marker to elute

$t_{c,\beta\text{-CD}}$ = time for amino acid complexed with β-CD to elute

$t_{c,1\text{-CM-}\beta\text{-CD}}$ = time for amino acid complexed with CM-β-CD to elute

$t_{f.a.a.}$ = time for free amino acid to elute

$t_{c,HDMCM\text{-}\beta\text{-CD}}$ = time for solute complexed with HDMCM-β-CD to elute

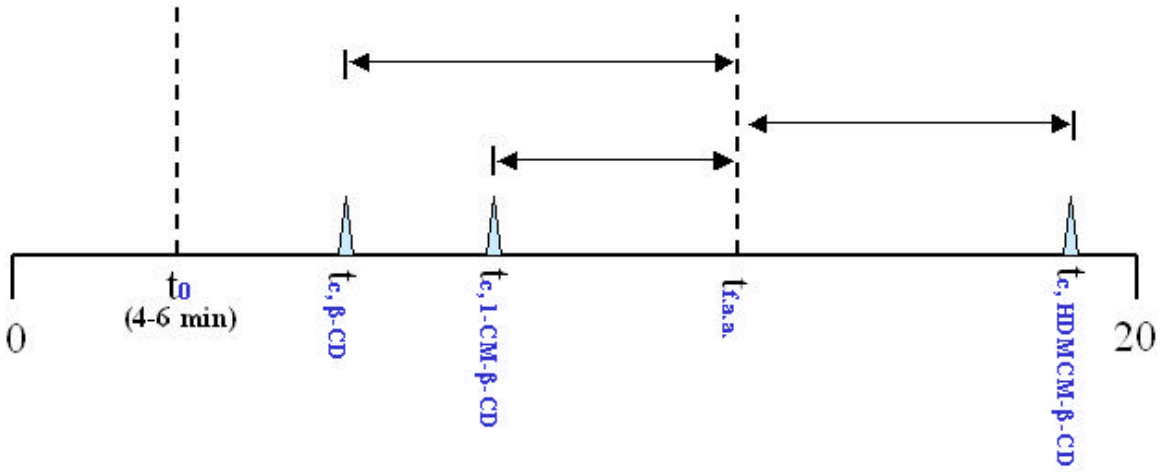

Figure 5.10. The elution ranges of the amino acid with different CDs is shown.

minimally charged. Partitioning into this phase will cause the AA to elute earlier than normal, between $t_{f.a.a}$ and $t_{c,CM\text{-}\beta\text{-}CD}$, because the charge to size ratio of the complex is still much lower than the free AA. β-CD and HDMCM-β-CD can achieve the largest elution ranges for the AA, as Figure 5.10 illustrates. Note that the migration times shown in Figure 5.10 are rough typical values for these systems and change depending on parameters such as pH and applied field.

Electropherograms

The resulting electropherograms of the AA separations with each of the CDs is shown in Figures 5.11-5.13. Interaction energies, <e>, were calculated using Equation 4.1.

From the electropherograms it is seen that only β-CD was able to achieve any chiral recognition between the different enantiomers. Elution times were the fastest with the β-CD because it retards the negative migration of the charged amino acids. Additionally, the inclusion is very strong in the β-CD as evidenced by the quick elution times.

The results from the molecular modeling support this. As seen in Table 5.1, the calculated interaction energy, <e>, for β-CD with the two modeled AAs is lowest (most negative) of all CDs for Val, and second lowest for Glu. Using visualizations in Sybyl, hydrogen bonding could be seen occurring between the polar ends of the AAs and the hydroxyl groups on the rim of β-CD as the non-polar rings were included into the cavity. This additional stabilization mechanism is evident in the low calculated <e> values. Interaction of the analyte with the secondary hydroxyl groups of the CD has been shown to play a major role in the achievement of chiral recognition.[197,198,202] The presence of

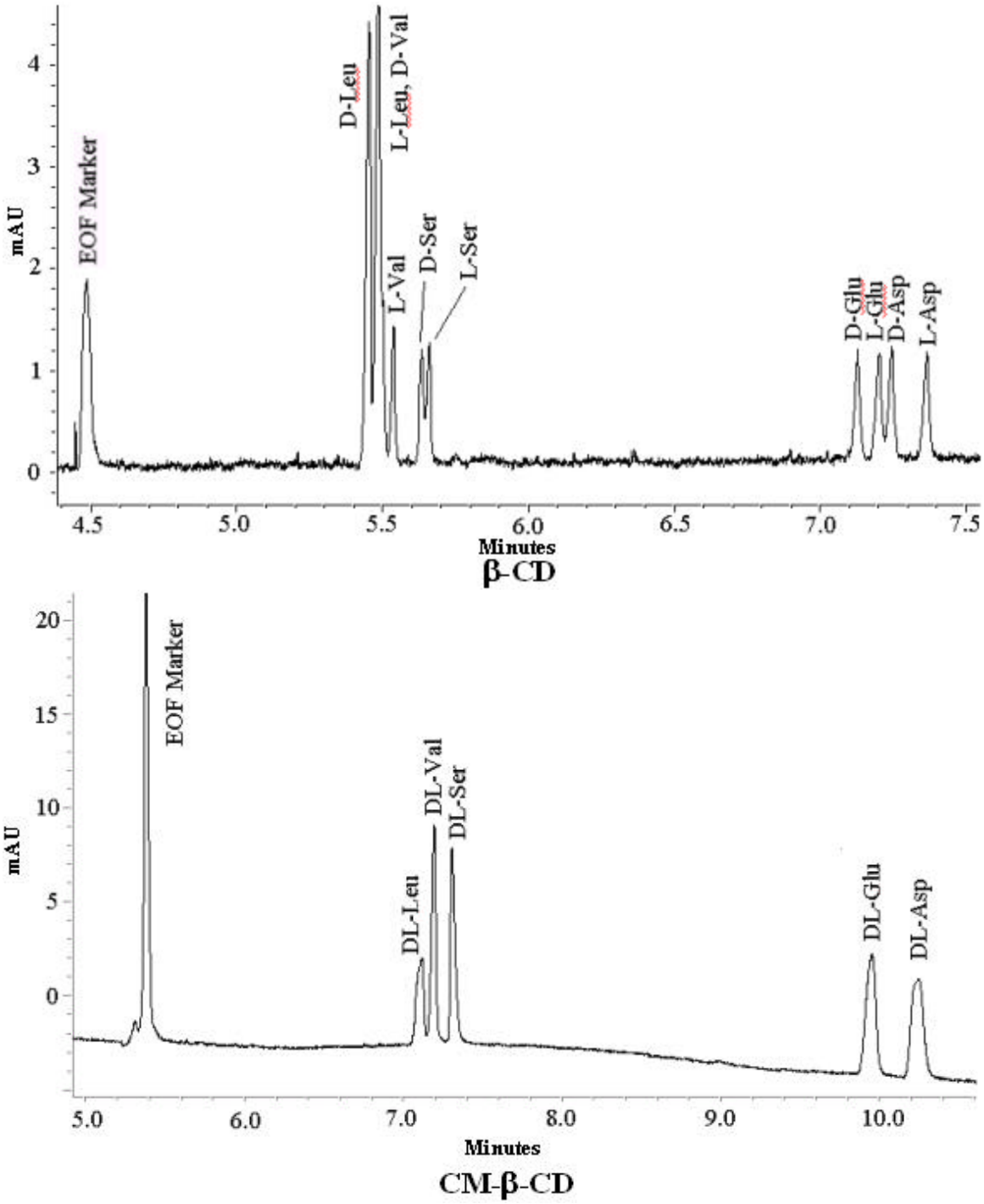

Figure 5.11. Electropherograms are shown of the separation of dansyl amino acids with 5 mM β-CD (above) and 5 mM CM-β-CD (below).

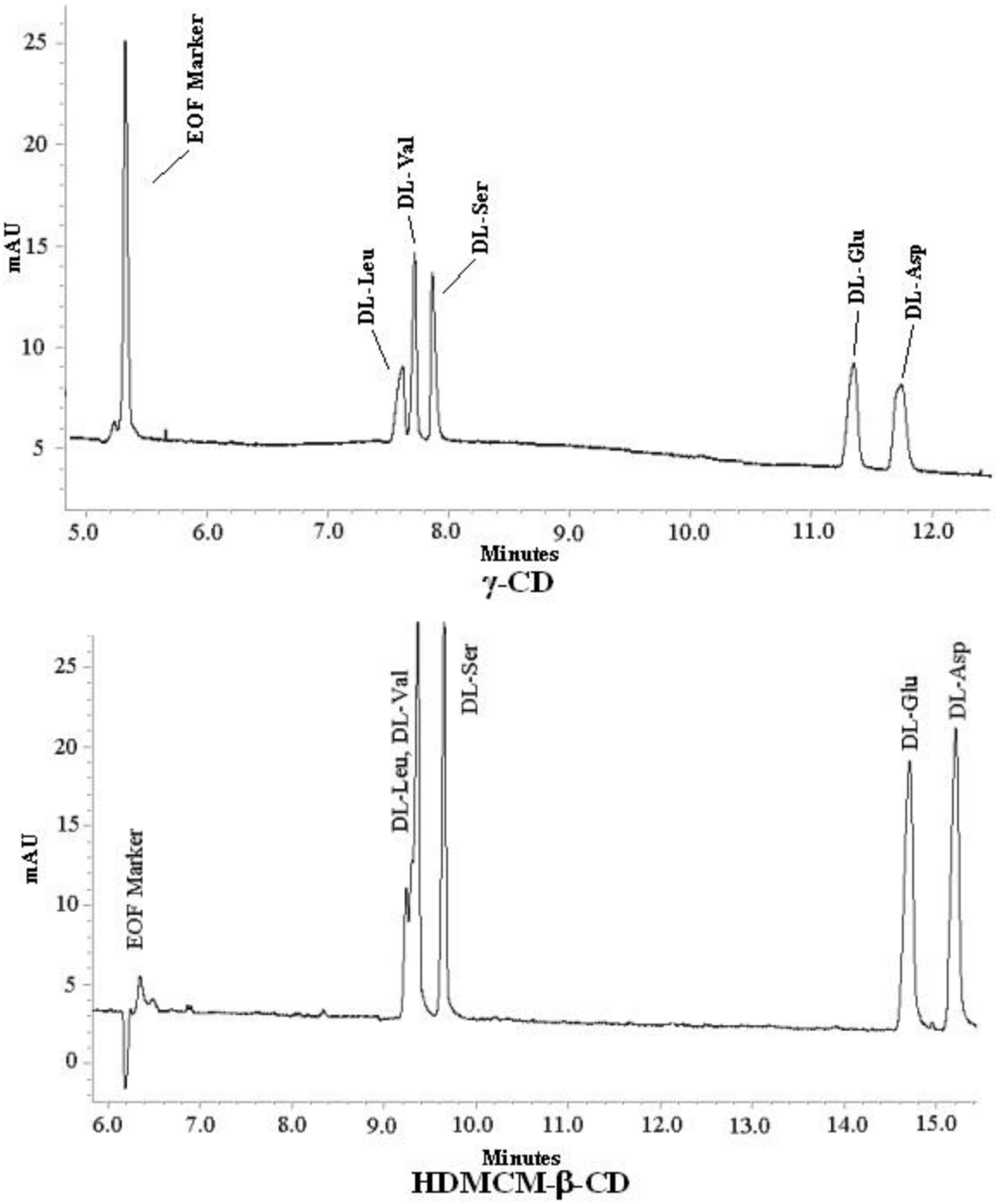

Figure 5.12. Electropherograms are shown of the separation of dansyl amino acids with 5 mM γ-CD (above) and 5mM HDMCM-β-CD (below).

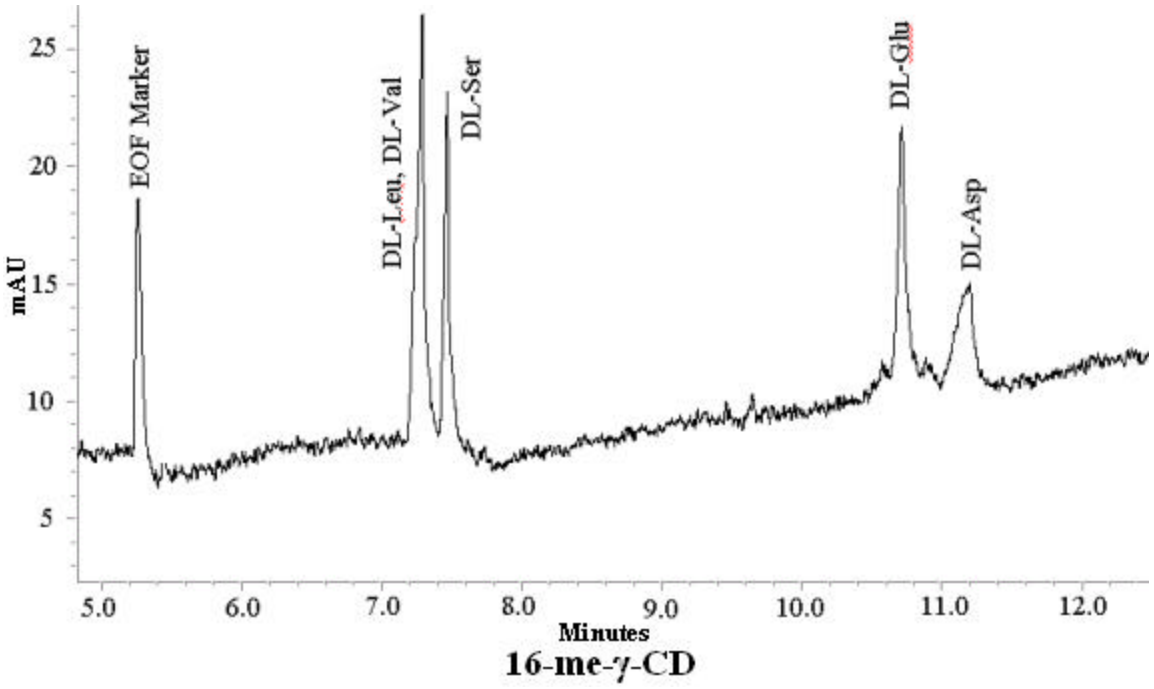

Figure 5.13. Electropherogram of the separation of dansyl amino acids with 5 mM 16-me-γ-CD is shown.

Table 5.1: Interaction energies, <e>, (kcal/mol) calculated from the molecular modeling for each of the CDs with Valine and Glutamic Acid.

CD	Glutamic Acid	Valine
CM-β-CD:	- 31.4	- 29.3
HDMCM-β-CD:	- 10.3	- 17.3
β-CD:	- 33.8	- 36.3
γ-CD:	- 37.9	- 35.0
16-me-γ-CD:	- 27.9	- 28.4

separation in Figure 5.11 shows agreement with the modeling, as evidenced by the much longer elution times. The poorer inclusion of the AAs in the CD allows their negative migration to extend their elution time considerably. Another factor working against CM-β-CD is its charge. The negatively charged CD electrostatically repels the negative AAs, further decreasing their affinity. This CD also has a smaller elution window with which to work than β-CD does, given its own negative mobility (see Figure 5.10).

Negative mobility is not a problem for the HDMCM-β-CD (Figure 5.12). The charge to size ratio for this –7 charged CD is so large that it very strongly migrates these groups on β-CD and the strong inclusion allow for the enantioselectivity to occur exclusively with this CD.

Perhaps the question now is, why is CM-β-CD not successful in separating the enantiomers given that it too has secondary hydroxyl groups on the rim? The modeling indicates that the interaction of the AAs with CM-β-CD is not as strong as with β-CD, which may limit its ability to achieve chiral recognition somewhat. The CM-β-CD against EOF much faster than even the AAs. This extends a wide elution range in the other direction, enabling it to successfully separate the AAs. The elution times using this reagent are longest of all the CDs, because any complexation of the AAs with the CD will carry them in the opposite direction of EOF as the CD imparts even more negative mobility on them. However, enantiomer selectivity was not observed for this CD. The modeling shows very poor interaction energies with the solutes. This can again be attributed to electrostatic repulsions between the highly negatively charged CD and the

negatively charged AAs. Additionally, the HDMCM-β-CD does not have the secondary hydroxyl groups with which to help achieve the chiral recognition.

The modeling results show that Val has a substantially more energetically favorable value of <e> than does Glu. At first glance this might suggest that Val should elute much later than Glu, given its superior inclusion in the CD. However, the free mobility of each the AAs still has to be taken into account, as Equation 5.1 shows (see page 119). The free mobility (μ_f) of Glu is much higher because it is –2 charged while Val is only –1 charged. The poor inclusion of the AAs with this CD means they spend most of their time migrating as the free species, which causes the μ_f to dictate the order of their elution.

From the electropherogram in Figure 5.13 it can be seen that the 16-me-γ-CD yields the poorest separation of all the CDs. Experiments showed that the mobility of the AAs in a separation with no CD was almost identical to the mobility with 16-me-γ-CD present, indicating they have almost no affinity for it. Like the other methylated species HDMCM-β-CD, it suffers from not having secondary hydroxyl groups with which to interact with the polar ends of the AA. This is reflected somewhat in the modeling data since the calculated interaction energies are poorer than those seen with β-CD or γ-CD.

The modeling, however, still shows that there should be better inclusion of the AAs with the 16-me-γ-CD than with HDMCM-β-CD and on par with the inclusion experienced with CM-β-CD, but this was not observed in the experimental separations. This perplexing issue precipitated further computational exploration of the structure of the 16-me-γ-CD. Additional low energy conformations were searched for using higher

numbers of minimization iterations, and in a solvent environment. It was found that after further minimization the methyl groups on the rim of the cavity took on positions more inward toward the opening of the CD, as depicted in 'Conformer B' in Figure 5.14. This configuration was found to be even lower in energy (1.6 kcal/mol lower) than the one shown in 'Conformer A', which was the structure used in the modeling experiments. The non-polar methyl groups were found to be more stabilized by congregating together rather than facing outward to the polar aqueous environment. This was supported by data that showed significant van der Waals stabilization in this structure due to intramolecular interactions. It is believed that since the methylated CD does not have the secondary hydroxyl groups with which to maintain its structural integrity, the cavity is more collapsed in nature. Given the large size of the CD and the absence of secondary –OH hydrogen bonding, the shape distortions that large CDs experience (see chapter 1) are observed in these CDs as well.

While the more inaccessible opening to the CD explains the lack of inclusion of the AAs, it is believed to also be possibly the result of CD-CD interactions. Under certain conditions, it has been noted that these kind of CD interactions can inhibit inclusion.[200] It is plausible that in an aqueous environment, the inter-CD van der Waals interactions of two CDs will be significant between the lipophilic C2 and C3 methylated portions of two or more 16-me-γ-CD molecules. MolCAD representations supported this idea. The electron density surface of the CD was generated, and the lipophilic potential was mapped on the surface. It was evident the highly hydrophobic portions of the CDs can match each other providing stabilization, as depicted in Figure 5.15. Any such interactions occurring in the separation environment would have a substantial effect on

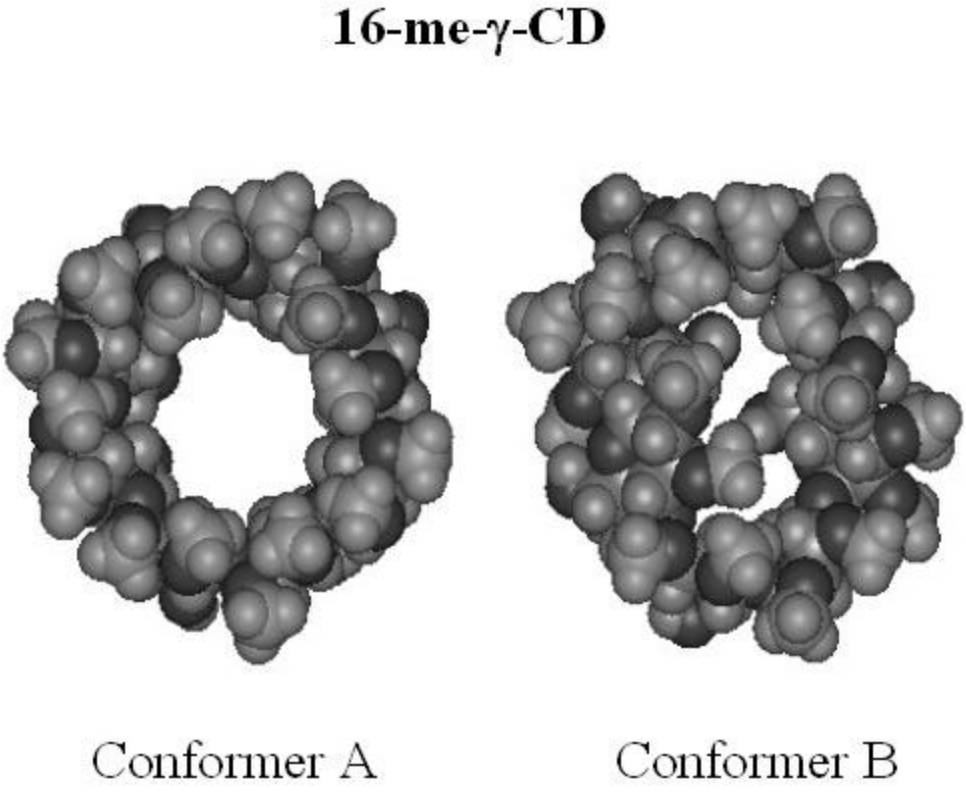

Figure 5.14. Conformer B is a more energetically favorable structure for 16-me-γ-CD than Conformer A which was used in the modeling experiments.

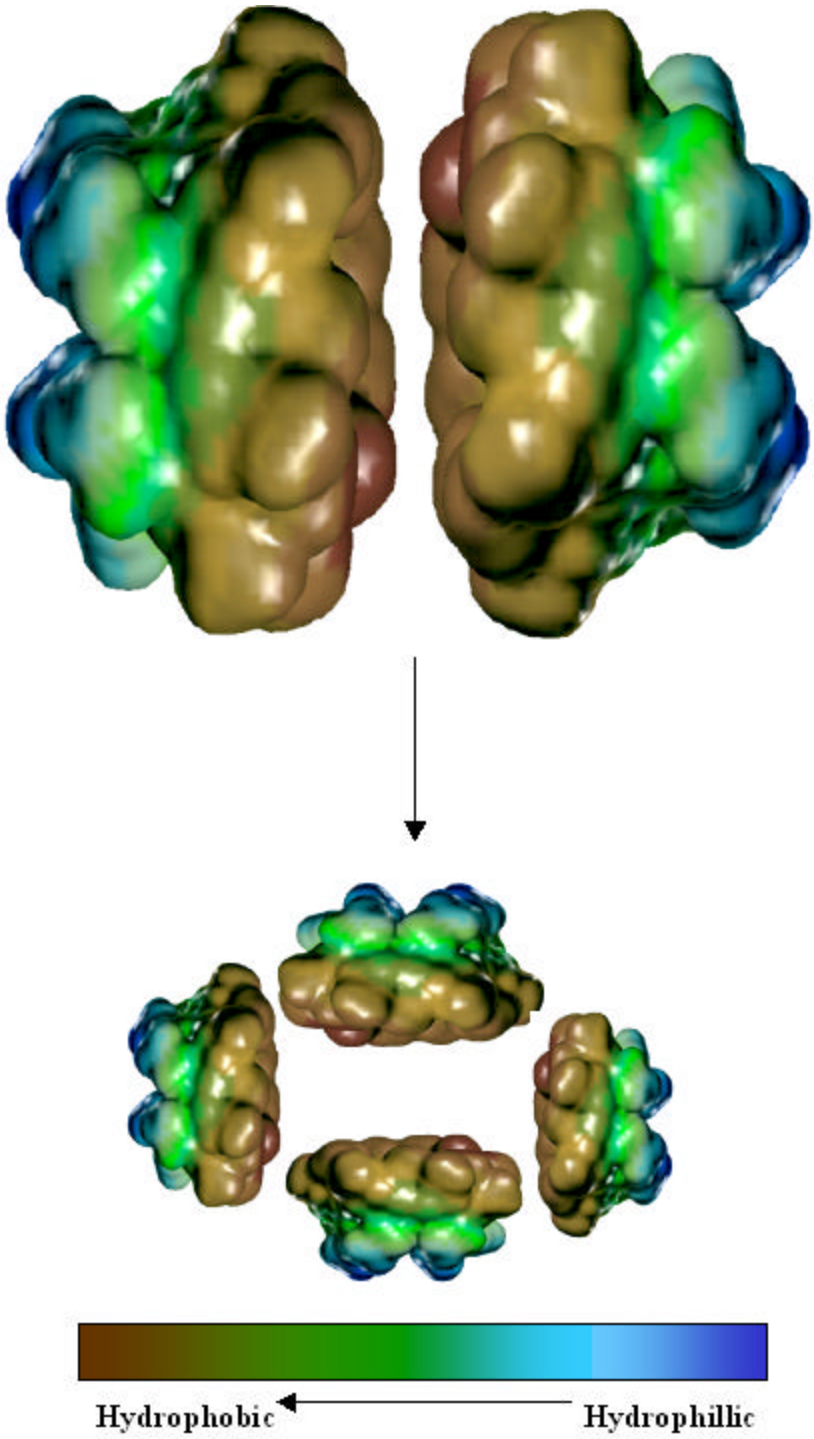

Figure 5.15. The hydrophobic portions (brown) of the methylated CDs (HDMCM-β-CD in this example) can orient themselves toward each other, which can substantially lower the partitioning of analytes into them.

the partitioning of the analyte into them. Additionally the hydrophilic portion of the CD on the opposite side prefer to orient themselves toward the aqueous environment. This suggests the possibility that these types of CDs could act similarly to micelles, aggregating into small clumps to maximize stability. This concept is supported by the findings from the separation experiments which indicate that the methylated CDs (HDMCM-β-CD and 16-me-γ-CD) experienced little to no interaction with the analytes.

Conclusion

The separation experiments have shown that of the 5 CDs employed to attempt enantioselectivity with the AAs, only β-CD was able to achieve this task. Its large elution window and availability of secondary hydroxyl groups on the rim of the cavity enable it to be successful. The methylated CDs were found to be poor, not only at chiral recognition, but with complexing analytes as well. The modeling results revealed that the truncated nature of the cavities and the CD-CD interactions due to the methyl groups keep these species from being able to interact sufficiently with the solutes.

The modeling portion of this work was successful at revealing the nature of the various CDs' interactions with the solutes, and the interaction calculation energies were consistent with observations from the experimental separations. While these modeling techniques (and others) are excellent tools for studying such systems, they cannot currently predict how to best resolve enantiomers chromatographically. This is best achieved using giant graphical molecular databases, such as CHIRBASE[203] which is complete with data from the enantiomeric separations by gas, liquid, supercritical fluid, and other chromatographies. CHIRULE is another database used for column selection, developed by Stauffer and Dessy.[204] Through the use of databases such as these

combined with molecular modeling support, separation scientists today have the tools at their disposal to help understand the fundamental mechanisms of molecular recognition and make superior decisions about how to best achieve resolution.

In 1965, the founder of Intel Gordon Moore predicted that computing power would double every 18 months. "Moore's Law" proven to remarkably resilient, even nearly 40 years since its declaration. Today, the common desktop computers have the processing power of the supercomputers of just a few years ago. New developments in microchip technology promise to breach barriers and continue to keep us advancing at this pace.

With the advent of computer assisted modeling, molecular modeling has unquestionably entered into a new and fascinating era, and the potential of this "quantum leap" in modeling is only beginning to be realized. The incredible advancement in understanding and abilities that computer modeling gives will undoubtedly be central in much of the groundbreaking researching of today and the near future as it matures as a tool and a science.

LIST OF REFERENCES

1. J. M. Lehn, J. L. Atwood, J. E. D. Davies, D. MacNicol, F. Fogtle, (Eds.), *Comprehensive Supramolecular Chemistry*, Pergamon, Oxford, **1996**.

2. Rebek, J., Jr. *Angew. Chem. Int. Ed. Engl.* **1990**, 29, 245-255.

3. Vögtle, F., *Suparmolecular Chemistry*; John Wiley & Sons: New York, **1991**.

4. Amabilino, D. B.; Stoddart, J. F. *Chem. Rev.* **1995**, 95, 2715-2828.

5. Fyfe, M. C. T.; Stoddart, J. F. *Acc. Chem. Res.* **1997**, 30, 393-401.

6. Harada, A.; Li, J.; Kamachi, M. *Nature* **1992**, 356, 325-327.

7. Harada, A.; Li, K.; Kamachi, M. *Nature* **1994**, 370, 126-128.

8. Harada, A. Kamachi, J., *Nature*, **1992**, 356, 325.

9. Wenz, G., Wolf, F., Wagner, M., Kubik, S., *New J. Chem.*, **1993**, 17, 729.

10. Burgemeister, W., Winkler-Oswatitsch, R., *Top. Curr. Chem.*, **1977**, 69, 91.

11. Izatt, R. M., Bradshow, J. S., Nielsen, S. A., Lamb, J. D., Christensen, J. J., Sen, D., *Chem. Rev.*, **1985**, 85, 271.

12. Pedersen, C. J., *J. Inclus. Phenom*, **1988**, 6, 337.

13. Pedersen, C. J., *J. Am. Chem. Soc.*, **1967**, 89, 2495, 7017.

14. Pedersen, C. J., Frensdorff, H. K., *Angew. Chem., Int. Ed. Engl*., 1972, 11, 16.

15. Cram, D. J., Chem. Eng. News, **1984**, 33.

16. Semlyen, J. A., (Ed.), *Large Ring Molecules*,., John Wiley & Sons, New York, **1996**.

17. Pedersen, C. J., *J. Org. Chem.*, **1971**, 26, 1690.

18. Goldberg, I., *Acta Crystallogr. Sect. B*, **1975**, 31, 754.

19. Vogtle, F., Weber, E., *Top. Curr. Chem*., **1981**, 98, 1.

20. Vogtle, F., Sieger, H, Muller, W. M., Weber, E., (Eds.), *Host Guest Complex Chemistry Macrocycles*, Springer, Berlin, **1985**.

21. Gokel, G. W., Korzeniowski, S. H., *Macrocycle Polyether Syntheses*, Springer, Berlin, **1982**.

22. Bradshaw, J. S., Krakowiak, K. E., Izatt, R. M., *Aza-crown Macrocycles*, Wiley-Interscience, New York, **1993**.

23. Baeyer, A., *Ber*, **1872**, 5, 25, 280, 1094.

24. Zinke, A., Ziegler, E., *Ber*., **1941**, B74, 1729.

25. Gutsche, C. D., Kung, T. C., Hsu, M. L., *Abstracts of 11th Midwest Regional Meeting of the AmericanChemical Society*, Carbondale, IL, **1975**, 517.

26. Andreetti, G. D., Ungaro, R., Pochini, A., *J. Chem. Soc. Chem. Commun*., **1979**, 1005.

27. Bocchi, V., Foina, D., Pochini, A. Ungaro, R., Andreetti, G. D., Tetrahedron, **1982**, 38, 373.

28. Gutsche, C. D., *Calixarenes* in 'Monographs in Supramolecular Chemistry, Stoddart, J. F., (Ed.), Royal Society of Chemistry, Cambridge, **1989**.

29. Cornforth, J. W., D'Arcy Hart, P., Nicholls, G. A., Rees, R. J., Stock, J. A., *Br. J. Pharmacol*, **1955**, 10, 73.

30. Cornforth, J. W., Morgan, E. D., Potts, K. T., Rees, R. J., *Tetrahedron*, **1973**, 29, 1659.

31. Olmstead, M. M., Sigel, G., Hope, H., Xu, X, Power, P. P., *J. Am. Chem. Soc.*, **1985**, 107, 8087.

32. Furphy, B. M., Harrowfield, J. M., Ogden, M. I., Skelton, B. W., White, A. H., Wilner, F. R., *J. Chem. Soc.*, Dalton Trans., **1989**, 2217.

33. Atwood, J. L., Bott, S. G., Jones, C., Raston, C. L., *J. Chem. Soc., Chem. Commun.*, **1992**, 1349.

34. Gardiner, M. G., Lawrence, S. M., Raston, C. L., Skelton, B. W., White, A. H., *J. Chem. Soc., Chem. Commun*., **1996**, 2491.

35. Shinkai, S., Mori, S., Arimura, O., *J. Chem. Soc.*, **1988**, 110, 7214.

36. Shinka, S., Manabe, O., Kondo, Y., *Jpn. Kokai Tokkyo Koho*, **1987**, 62, 136, 242.

37. Caciuffo, R., Francescangeli, O., Melone, S., Prager, M., Ugozzoli, F., Andreetti, G. D., *Physica B.* (Amsterdam), **1992**, 180, 691.

38. Brouwer, E. B., Enright, G. D., Ripmeester, *J. A., Supramol. Chem*., **1996**, 7, 7.

39. Brouwer, E. B., Enright, G. D., Ripmeester, *J. A., Supramol. Chem*., **1996**, 7, 143.

40. Williams, R. M., Verhoeven, J. W., *Recl. Trav. Chim. Pays-Bas*, **1992**, 111, 531.

41. Gutsche, C. D., Alam, I., *Tetrahedron*, **1988**, 44, 4689.

42. Molenveld, P., Kapsabelis, S., Engbersen, J. F., Reinhoudt, D. N., *J. Am. Chem. Soc.*, **1997**, 119, 2948.

43. Saito, Y., Ohta, H., Terasaki, H., Katoh, Y., Nagashima, H., Jinno, H., Itoh, K., *J. High Resolut. Chromatogr.*, **1996**, 19, 475.

44. Easton, C. J., Lincoln, S. F., *Modified Cyclodextrins*, Imperial College Press, London, **1999**.

45. A. Villiers, *Compt. Rend*., **1981**, 112, 536.

46. F. Schardinger, Z. *Untersuch. Nahr. u. Genussm.*, **1903**, 6, 865.

47. H. Pringsheim, *Chemistry of the Saccharides*, McGraw-HIll, New York, **1932**, p. 280.

48. H. Pringsheim, in "*A Comprehensive Survey of Starch Chemistry*," R. P. Walton, Chemical Catalog Co., New York, **1928**, p. 35.

49. K. Freudenberg, H. Boppel, and M. Meyer-Delius, *Naturwissenschaften*, **1938**, 26, 123.

50. K. Freundenberg and M. Meyer-Delius, *Ber. Dtsch. Chem. Ges*., **1938,** 71, 1596.

51. K. Freudenberg, G. Blomquist, L. Ewald, and K. Soff, *Ber. Dtsch. Chem. Ges.*, **1936**, 69, 1258.

52. K. Freudenberg and F. Cramer, Z. Naturforsch., *Teil B*, **1948**, 3, 464.

53. Khan, A.R.; Forgo, P.; Stine, K.J. D'Souza, V.T. *Chem. Rev.* **1998**, 98, 1977.

54. Wenz, G. *Angew. Chem. Int. Ed. Engl.* **1994**, 33, 803.

55. Szejtli, J.; Osa, T. *Comprehensive Supra Molecular Chemistry: Cyclodextrins, Volume 3*, Pergamon, New York, **1996.**

56. Szejtli, J., *Chem Rev*., **1998**, 98, 1743.

57. Jacob, J.; Gessler, K.; Hoffmann, D.; Sanbe, H.; Koizumi, K.; Smith, S. M.; Takaha, T.; Saenger, W. *Angew. Chem., Int. Ed.*

58. Bender, M. L., Komiyama, M., *Cyclodextrin Chemistry*, Springer-Verlag, Berlin, **1978**.

59. Hallen, D.; Scho¨n, A.; Shehatta, I.; Wadso¨, I. *J. Chem. Soc., Faraday Trans*. **1992**, *88*, 2859-2863.

60. Rekharsky, M. V.; Mayhew, M. P.; Goldberg, R. N.; Ross, P. D.; Yamashoji, Y.; Inoue, Y.; A *J. Phys. Chem*. **1997**, *101*, 87-100.

61. Matsui, Y.; Mochida, K. *Bull. Chem. Soc. Jpn*. **1979**, *52*, 2808-2814.

62. Barone, G.; Castronuovo, G.; Del Vecchio, P.; Elia, V.; Muscetta, M. *J. Chem. Soc., Faraday Trans. 1* **1986**, *82*, 2089-2101.

63. Fujiwara, H.; Arakawa, H.; Murata, S.; Sasaki, Y.; *Bull. Chem.Soc. Jpn*. **1987**, *60*, 3891-3894.

64. Saenger, W. *Angew. Chem., Int. Ed. Engl*. **1980**, *19*, 344-362.

65. Sanemasa I.; Osajima, T.; Deguchi, T. *Bull. Chem. Soc. Jpn*. **1990**, *63*, 2814-2818.

66. Harrison, J. C.; Eftink, M. R. *Biopolymers* **1982**, *21*, 1153-1166.

67. Tabushi, I.; Kiyosuke, Y.; Sugimoto, T.; Yamamura, K. *J. Am.Chem. Soc.* **1978**, *100*, 916-919.

68. Saenger, W., in J. L. Atwood, J. E. D. Davies, and D. D. MacNicol (Eds), Inclusion Compounds, Academic Press, London, **1984**, Vol. 2, p. 231, and references cited therein.

69. Bergeron, R. J., in J. L. Atwood, J. E. D. Davies, and D. D. MacNicol (Eds), Inclusion Compounds, Academic Press, London, **1984**, Vol. 3, p. 391.

70. Cai, H., Nguyen, T. V., Vigh, G. *Anal. Chem.* **1998**, 70, 580.

71. Chankvetadze, B., Endresz, G., Bergenthal, D., Blaschke, G. *J. Chromatogr. A* **1995**, 717, 245.

72. Chankvetadze, B., Endresz, G., Blaschke, G. *J. Chromatogr. A.*, **1995**, 704, 234.

73. Lurie, I. S., Chan, K. C., Spratley, T. K., Casale, J. F., Issaq, H. J. *J. Chromatogr. B-Biomed. Appl*. **1995**, 669, 3.

74. Ren, X. Q., Dong, Y. Y., Lui, J. Y., Huang, A. J., Liu, H. W., Sun, Y. L., Sun, Z. P. *Chromatographia* **1999**, 50, 363.

75. Skanchy, D. J., Wilson, R., Poh, T., Xie, G. H., Demarest, C. W., Stobaugh, J. F. *Electrophoresis* **1997**, 18, 985.

76. Whitaker, K. W., Copper, C. L., Sepaniak, M. J. *J. of Microcolumn Sep*. **1996**, 8, 461.

77. Hinze, W., Dai, F., Frankkewich, R. P., Thimmaiah, K. N., Szejtli, J. in *Compr. Supramol. Chem*. Szejtli, J., Osa, T., Eds. Elsevier, NY **1996**, p.578.

78. Tiselius, A., *The Moving BoundaryMethod of Studying the Electrophoresis of Proteins (Thesis)*, Nova Acta Regiae Societatis Scientiarum Upsaliensis, **1930**, IV, 7, 4.

79. Hjerten, S., *Chromatogr. Rev*.,**1967**, 9, 122.

80. J.W. Jorgenson and K.D. Lukacs, "Zone Electrophoresis in Open-Tubular Glass Capillaries," *Anal. Chem.*, **1981**, 53**,** 1298.

81. R.L. St. Claire, "Capillary Electrophoresis," *Anal. Chem.*, **1996**, 569R.

82. C.A. Monnig and R.T. Kennedy, "Capillary Electrophoresis," *Anal. Chem.*, **1994**, 280R.

83. P. Grossman and J. Colburn, (Eds.), *Capillary Electrophoresis: Theory and Practice*, Academic Press, **1992,** New York.

84. P.G. Righetti, (Ed.), *Capillary Electrophoresis in Analytical Biotechnology*, CRC Press, **1996**, Boca Raton, FL.

85. J.P. Landers, (Ed.), *Handbook of Capillary Electrophoresis*, CRC Press, Boca Raton, FL.

86. P. Camilleri, (Ed.), *Capillary Electrophoresis Theory and Practice*, CRC Press, **1998**, Boca Raton, FL.

87. Terabe, S., Ozaki, H., Otsuka, K., Ando, T., *J. Chromatogr.*, **1985**; 332, 211.

88. Tanaka, N., Tanigawa, T. , Hosoya, K., Kimata, K., Araki, T., Terabe, S., *Chem. Lett*., **1992**, 959.

89. Kuhn, R., Stoecklin, F., Erni, F., *Chromatographia*, **1992**, 33, 32.

90. Armstrong, D. W., Rundlett, K., Reid, G. L. I., *Anal. Chem.*, **1994**, 66, 1690.

91. Terabe, S., Isemura, T., *J. Chromatogr.,* **1990**, 515, 667.

92. Terabe, S., Isemura, T., *Anal. Chem.*, **1990**, 62, 650.

93. Shamsi, S. A., Warner, I. M., *Electrophoresis*, **1997**, 18, 853.

94. Terabe, S., Otsuka, K., Ichikawa, K. Tsuchiya, A., Ando, T., *Anal. Chem.*, **1984**, 56, 111.

95. Terabe, S., Otsuka, K., Ando, T., *Anal. Chem.*, **1985**, 57, 834.

96. Watari, H., Ogawa, K., Abe, M., Monta, T., Takahashi, I., *Anal. Sci*., **1991**, 7, 245.

97. Watari, H., *Chem. Lett*., **1991**, 391.

98. Terabe, S., Matsubara, N., Ishihama, Y., Okada, Y., *J. Chromatogr.*, **1992**, 608, 23.

99. Zhang, Y., Zhang, R., Hjerten, S., Electrophoresis, **1995**, 16, 1519.

100. Hong, M., Weekley, B. S., Grieb, S. J., Foley, J. P., *Anal. Chem.*, **1998**, 70, 1394.

101. D. E. Burton, M. J. Sepaniak, and M. P. Maskarinec, *J. Chromatogr. Sci.*, **1986**, 24, 347.

102. Nguyen, A. L., Luong, J. H. T., *Anal. Chem.*, **1997**, 69, 1726.

103. Copper, C. L., and Sepaniak, M. J. *Anal. Chem.* **1994**, 66, 147.

104. Marina, M.L.; Benito, I.; Diez-Masa, J.C.; Gonzales, M. J., *Chromatographia*, **1996**, 42, 269.

105. Luong, J. H. T., Guo, Y., *J. Chromatogr., A*, **1998**, 811, 225.

106. S. Terabe, Y. Miyashita, Y. Ishihama and O. Shibata, *J. Chromatogr.*, **1993**, 636, 47.

107. Sepaniak, M.J.; Copper, C.L.; Whitaker, K.W.; Anigbogu, V.C. *Anal. Chem*, **1995**, 67, 2037.

108. Gassman, E., Kuo, J. E., Zare, R. N., *Science*, **1985**, 230, 813.

109. Dobashi, A., Ono, T., Hara, S., Yamaguchi, J., *Anal. Chem*., **1989**, 61, 1984.

110. Dobashi, A., Ono, T., Hara, S., Yamaguchi, J., *J. Chromatogr.*, **1989**, 480, 413.

111. Fanali, S., *J. Chromatogr.*, **1989**, 474, 411.

112. Snopek, J., Soini, H., Novotny, M., Smolkova-Keulemansova, E., Jelinek, I., *J. Chromatogr., A.*, **1991**, 559, 215.

113. Penn, S. G., Godall, D. M., Loran, J. S., *J. Chromatogr., A.*, **1993**, 636, 149

114. Schmitt, T., Engelhardt, H., *Chromatographia*, **1993**, 37, 475.

115. Tait, R. J., Thompson, D. O., Stella, V. J., Stobaugh, J. F., *Anal. Chem.*, **1994**, 66, 4013.

116. Vincent, J. B., Sokolowski, A. D., Nguyen, T. V., Vigh, G., *Anal. Chem.*, **1997**, 69, 4226.

117. Cai, H., Vigh, G., *J. Microcolumn Sep.*, **1998**, 10, 293.

118. Peter T. Cummings, Phillip R. Westmoreland, and Brice Carnahan (Eds.), *First International Conference on Foundations of Molecular Modeling and Simulation*, American Institute of Chemical Engineers, **2001**, Danvers, MA.

119. Hill, T. L., *J. Chem Phys.*, **1946**, 14, 465.

120. Westheimer, F. H., Mayer, J. E., *J. Chem. Phys.*, **1946**, 14, 733.

121. Barton, D. H. R., *J. Chem. Soc.*, **1948**, 340.

122. Westheimer, F. H., 'Calculation of the Magnitude of Steric Effects' in *Steric Effects in Organic Chemistry*, M. S. Newman, (Ed), Wiley, New York, **1956**, 523-555.

123. Hendrickson, J. B., *J. Am. Chem. Soc.*, **1961**, 83, 4537.

124. Bondi, A., *J. Phys. Chem.*, **1964**, 68, 441.

125. Gasteiger, J., Marsili, M., *Tetrahedron*, **1980**, 36, 3219.

126. Saunders, M., *J. Am. Chem. Soc.*, **1987**, 109, 3150.

127. Ferguson, D. M., Raber, D. J., *J. Am. Chem. Soc.*, **1989**, 111, 4371.

128. Chang, G., Guida, W. C., Still, W. C., *J. Am. Chem. Soc.* **1989**, 111, 4379.

129. Cornea, R. L., Thomas, D. D., *Biochemistry*, **1994**, 33(10), 2912..

130. Gu, Jian-De, Tian, An-Min, Yan, Guo-Sen., *Huaxue Xuebao* **1996**, 54(4), 331.

131. Matsukuma, Kunihiro; Shigeta, Hideaki; Matsunaga, Kazuo; Morita, Keiich; Matsukuma, Toshihiro, *Kenkyu Hokoku - Kumamoto Kogyo Daigaku*, **1996**, 21(1), 53.

132. Vilaseca, Eudald, *Journal of Physical Chemistry*, **1993**, 97(8), 1684.

133. Deng, Qiaolin; Han, Yuzhen; Lai, Luhua; Xu, Xiaojie; Tang, Youqi; Hao, Minghong. *Chinese Chemical Letters*, **1991,** 2(10), 809.

134. Dodziuk, H., Journal of Molecular Structure, **2002**, 614, 33.

135. De Amici, M., De Micheli, C., Kassi, L., Carrea, G., Ottolina, G., Colombo, G., *Tetrahedron*, **2001**, 57(9), 1849.

136. Marques, Helder M., *Chemistry and Biochemistry*, **1999**, 289.

137. Baranyai, Andras, *Journal of Chemical Physics*, **2001**, 115(9), 4156.

138. Skaf, Munir S., *Electron and Ion Transfer in Condensed Media: Theoretical Physics for Reaction Kinetics, Proceedings of the Conference, Trieste*, July 15-19, **1996**, 98.

139. Niikura, Hiromichi; Legare, F.; Hasbani, R.; Ivanov, Misha Yu; Villeneuve, D. M.; Corkum, P. B., *Nature*, **2003**, 421(6925), 826.

140. Teleman O, von der Lieth C. W., *Biopolymers*, **1990**, 30(1-2), 13.

141. Tirado-Rives J, Jorgensen W L., *Biochemistry* ,**1991,** 30(16), 3864.

142. Daggett V; Kollman P A; Kuntz I D**.,** *Biopolymers*, **1991,** 31(3), 285.

143. Saviano M; Aida M; Corongiu G., *Biopolymers*, **1991**, 31(8), 1017.

144. MacKerell A D Jr ., *Methods in Enzymology***, 1991**, 202, 449.

145. Levitt M., *Nature*, ***1981***, 294(5839), 379.

146. Grivtsov A G; Malenkov G G; Abaturov L V**.,** *Molecular Biology*, **1983**, 17(3), 587.

147. Balaji P. V., Qasba P. K., Rao V. S., *International Journal of Biological Macromolecules*, **1996,** 18(1-2), 101.

148. Kirkpatrick, S., Gelatt, C. D., Vecchi, M. P., *Science*, **1983**, 220, 671.

149. Goodman, J. M., *Chemical Applications of Molecular Modeling*, **1998**, The Royal Society of Chemistry, Cambridge.

150. *SYBYL 6.6*; Tripos Inc.: 1699 South Hanley Rd., St. Louis, Missouri, 63144, USA.

151. Connolly, M. L., *Science*, **1983**, 221, 709-713.

152. Connolly, M. L., *J. Appl. Crystallogr*., **1983**, 16, 548.

153. Gopinathan, M. S., Vijayakumar, M., Viaidehi, N., *Phys. Rev. A*., **1989**, 40, 6834.

154. Cardoso, M., Salcedo, R., *Computers & Chemical Engineering*, **1996,** 20, 1065.

155. Lipkowitz, K. B., et.al., *J. Am. Chem. Soc*., **1988**, 110, 3446.

156. Powell, M. J. D., *Mathematical Programming*, **1977**, 12, 241.

157. K. Jinno, (Ed.), *Chromatographic Separations Based on Molecular Recognition*, Wiley-VCH, Inc., **1997**, Toronto.

158. Culha, M., Fox, S., Sepaniak, M., *Anal. Chem.*, **2000**, 72, 88.

159. *SigmaPlot 5.0*; SPSS Inc.: Chicago IL, **1999**.

160. Christensen, I. T., Jørgensen, F. S., *J. of Comp. Aided Molec. Design*, **1997**, 11, 385.

161. Weber, T. A., Stillinger, F. H., *J. Chem. Phys*., **1987**, 87, 3252.

162. Melton, L. D., Slessor, K. N., *Carbohydr. Res*., **1971**, 18, 29.

163. Brown, S. E., Coates, J. H., Coghlan, D. R., Easton, C. J., van Eyk, S. J., Janowski, W., Lepore, A., Lincoln, S. F., Luo, Y., May, B. L., Schiesser, D. S., Wang, P., Williams, M. L., *Aust. J. Chem*. **1993**, 46, 953.

164. Fujita, K., Tahara, T., Imoto, T., Koga, T., *J. Am. Chem. Soc.*, **1986**, 108, 2030.

165. Fujita, K., Tahara, T., Yamamura, H., Imoto, T., Koga, T., Fujioka, T., Mihashi, K, *J. Org. Chem*., **1990**, 55, 877.

166. Chen, W. H., Yuan, D. Q., Fujita, K., *Tetrahedron Lett*., **1997**, 38, 4599.

167. Kraus, T., Budesinsky, M.; Zavada, J., *Carbohydrate Research*, **1997**, 304, 81.

168. Takeo, K., Mitoh, H.; Uemura, K., *Carbohydrate Research*, **1989**, 187, 303.

169. Zhang, P., Ling, C.C.; Coleman, A.W., "Formation of Amphiphilic Cyclodextrins via Hydrophobic Esterification at the Secondary Hydroxyl Face", *Tetrahedron Letters*, **1991**, 32 (24), 2769.

170. Fugedi, P., *Carbohydrate Research*, **1989,** 192, 366.

171. Culha, M., *The Use of Native and Modified Cyclodextrins for Method Development in Capillary Electrophoresis and Chemical Sensor Applications, Thesis.* The University of Tennessee, **2002**.

172. Coleman, A. W., Nicolis, I., Keller, N., Dalbiez, J. B. *J. of Inclusion Phenomena and Molecular Recognition in Chemistry*, **1992**, 13(2), 139.

173. Souter, R. W., *Chromatographic Separations of Stereoisomers*, CRC Press, Boca Raton, FL, **1985**.

174. Zeif, M., Crane, L., (Eds.), *Chromatographic Chiral Separations*, Marcel DEkker, New York, **1987**.

175. Konig, W. A., *The Practice of Enantiomer Separations by Capillary Gas Chromatography*, Huthig, Heidelberg, **1987**.

176. Allenmark, S. G., *Chromatographic Enantioseparation Methods and Application*, Ellis Horwood, Chichester, **1988**.

177. Stevenson, D., Wilson, I. D., (Eds.), *Chiral Separations*, Plenum Press, New York, **1988**.

178. Lough, W., J., (Ed.), *Chiral Liquid Chromatography*, Blackie, London, **1989**.

179. Stevenson, D., Wilson, I. D., (Ed.), *Recent Advances in Chiral Separations*, Plenum Press, New York, **1990**.

180. Ahuja, S., (Ed.), *Chiral Separations by Liquid Chromatography (ACS Symposium Series, No. 471)*, American Chemical Society, Washington, DC, **1991**.

181. Subramanian, G., (Ed.), *Chiral Separations by Liquid Chromatography*, VCH, Weinheim, **1994**.

182. Wistuba, D., Diebold, H., Schurig, V., *J. Microcol. Sep*., **1995**, 7, 17.

183. Kuhn, R., Hofstetter-Kuhn, S., *Chromatographia*, **1992**, 34, 505.

184. Verleysen, K., Sandra, P., *J. Microcol. Sep*., **1999**, 11, 37.

185. Kang, J., Yang, J., Ou, Q., *J. Chromatogr. A.*, **1998**, 825, 81.

186. Vespalec, R., Billiet, H., Frank, J., Bocek, P., *Electrophoresis*, **1996**, 17, 1214.

187. Schaeper, J., Sepaniak, M., *Electrophoresis*, **2000**, 21, 1421.

188. Zhu, W., Vigh, G. *Anal. Chem.*, **2000**, 72, 310.

189. C. L. Copper, J. B. Davis, R. O. Cole, and M. J. Sepaniak, *Electrophoresis*, **1994**, 15, 785.

190. S.S. Sun, M.J. Sepaniak, J. Wang, and C.D. Gutsche, *Anal. Chem.*, **1997**, 69, 344.

191. Kohler, J. E. H., Hohla, M., Richters, M., Konig, W. A., *Agnew Chem., Int. Ed. Engl.*, **1992**, 31, 319.

192. de Vries, Koen, Coussens, B., Meier, R. J., *J. High Resolut. Chromatogr*., **1992**, 15, 499.

193. Lipkowitz, K. B., Green, KI., Yang, J. A., Pearl, G., Peterson, M. A., *Chirality*, **1993**, 5, 51.

194. Kobor, F., Angermund, K., Schomburg, G., *J. High Resolut. Chromotogr*., **1993**, 16, 299.

195. Bradshaw, J. S., Izatt, R. M., Christensen, J. J., Krakowiak, K. E., Tarbet, B. J., Bruening, R. L., Lifson, S., *J. Inclus. Phenom. Mol. Recog*., **1989**, 7, 127.

196. Armstrong, R. D., Ward, T. J., Pattabiraman, N., Benz, C., Armstrong, D. W., *J. Chromatogr.*, **1987**, 414, 192.

197. Armstrong, R. D., Hinze, W. L., (Eds.), *Ordered Media in Chemical Separations (ACS Symposium Series, No. 342),* American Chemical Society, Washington, DC, **1987**.

198. Armstrong, D. W., Ward, T. J., Armstrong, R. D., Beesley, T. E., *Science*, **1986**, 232, 1132.

199. Devault, G, Sepaniak, M., *J. Microcol. Sep*., **2000**, 12, 485.

200. Culha, M., Fox, S., Betts, T., Green, T, Sepaniak, M., *J. Microcol. Sep*., in press.

201. Schaeper, James, *Reproducibility and Optimization in Capillary Electrophoresis-Thesis,* The University of Tennessee, **2002**.

202. Yoshinaga, M., Tanaka, M., *J. Chromatogr. A.*, **1994**, 679, 359.

203. Roussel, C., Piras, P., *Pure Appl. Chem.,* **1993**, 65, 235.

204. Stauffer, S. T., Dessy, R. E., *J. Chromatogr.* Sci., **1994**, 32, 228.

205. Weiner, S. J., Kollman, P. A., Case, D. A., Sing, U. C., Ghio, C., Alagona, G., Profeta, S., Weinter, P., *J. Am. Chem. Soc.* **1894**, 106, 765.

206. Cornell, W. D., et al., *J. Am. Chem. Soc.*, **1995**, 117, 5179.

207. Brooks III, C. L., Karplus, M., *J. Mol. Biol*., **1989**, 208, 159.

208. Karplus, M., Petsko, G. A., *Nature*, **1990**, 347, 631.

209. Lifson, S., Hagler, A. T., Dauber, P., *J. Am. Chem. Soc.*, **1979**, 101, 5111.

210. Vinter, J. G., Davis, A., Saunders, M. R., *J. Comp.-Aided. Mol. Des*., **1987**, 1, 31.

211. Mayo, S. L., Olafson, B. D., J. Phys. Chem., **1990**, 94, 8897.

212. Momany, F. A., McGuire, R. F., Burgess, A. W., Scheraga, H. A., *J. Phys. Chem.,* **1975**, 22, 2361.

213. van Gunsteren, W. F., Berendsen, H. J. C., *Angew. Chem., Int. Ed. Engl*., **1990**, 29, 992.

214. Allinger, N. L., *J. Am. Chem. Soc.*, **1977**, 99, 8127.

215. Allinger, N. L., Yuh, Y. H., Lii, J. H., *J. Am. Chem. Soc.*, **1989**, 111, 8551.

216. Allinger, N. L., Chen, K., Lii, J. H., *J. Comp. Chem*., **1996**, 17, 642.

217. Halgren, T. A., *J. Comp. Chem.*, **1996**, 17, 490.

218. Viswanadhan, V. N., Ghose, A. K., Revankar, G. R., Robins, R. K., *J. Chem. Inf. Comput. Sci.,* **1989**, 29, 163.

219. Jorgensen, W. L., Tirado-Rives, J., *J. Am. Chem. Soc.*, **1988**, 110, 1657.

220. Allured, V. S., Kelly, C. M., Landis, C. R., *J. Am. Chem. Soc.*, **1991**, 113, 1.

221. Clark, M., Cramer III, R. D., Van Opdenbosch, N., *J. Comp., Chem*., **1989**, 10, 982.

222. White, D. N. J., Bovill, M. J., *J., Chem. Soc. Perkin Trans. 2*, **1977**, 1610.

223. Rappe, A. K., Casewit, C. J., Colwell, K. S., Goddard III, W. A., Skiff, W. M., *J. Am. Chem. Soc.*, **1992**, 114, 10024.

Appendix

A.1. LIST OF FORCE FIELDS

(Information From Goodman Text) [149]

AMBER: 'Assisted Model Building with Energy Refinement'. The most popular force field for modeling proteins and nucleic acids. AMBER was developed by the Kollman research group at University of California at San Francisco.[205,206]

CHARMm: "Chemistry at Harvard Macromolecular Mechanics'. This is both the name of the force field and the name of the program which manipulates it. They were designed by Karplus to model macromolecular structures, and proteins in particular.[207,208]

CFF93: This force field was designed by Hagler for accurate definitions of both small and large molecules, and is designated a "Class II' force field by it's creators because it contains parameters for anharmonicity and coupling between different distortions. This approach leads to higher accuracy at the expense of greater complexity, and a very large number of parameters are required for the force field. In addition, seven scaling parameters are introduced. The force field has it's roots in the earlier consistent force field, CFF.[209]

COSMIC: 'COmputation and Structure Manipulation In Chemistry'.[210] COSMIC is the name of both a force field and a molecular mechanics package designed to manipulate it, and was designed to be a general purpose force field.

DREIDING: A simple generic force field for predicting the structures and dynamics of organic, biological and main-group inorganic molecules.[211]

ECEPP: 'Empirical Conformational Energy Program for Peptides'. Developed by Scheraga.[212]

GROMOS: 'Groningen Molecular Simulation'. A general molecular mechanics force field.[213]

KOLLMAN: Developed specifically to simulate nucleic acids and proteins. This later evolved into the Amber force field.[205]

MM2: Developed by Allinger and coworkes at the University of Georgia, it is designed to work with small molecules (500 atoms or less).[214] This force field is very popular and is a benchmark by which other force fields are sometimes judged.

MM3: This force field corrects some of the weaknesses of MM2, particularly concentrating on vibrational frequencies, which MM2 does not reproduce very well. While similar to MM2 in many respects, new parameters were added, which increased the complexity and accuracy for systems for which the new force field was designed.[215]

MM4: A further increase in complexity and accuracy over MM3, concentrating on vibrational frequencies and rotational barriers, which are particularly difficult to calculate precisely.[216]

MMFF94: Merck Molecular Force Field.[217,218] It was designed based on high level *ab initio* calculations to work well for both small molecules and large macromolecules.

OLPS: 'Optimized Potentials for Liquid Simulations'. Designed to model proteins in solution.[219]

SHAPES: An empirical force field designed particularly for transition metal complexes.[220]

Tripos: The force field from Tripos Associates used in the Sybyl software.[150, 221] It was developed mainly for treating small organic molecules and biomolecules. Its design was based on COSMIC, and White's force field.[222]

UFF: 'Universal Force Field'. The parameters for this force field are based only on the elements, and not on groups of atoms as is usual.[223]

A2. TRIPOS FORCE FIELD ENERGY TERMS

$$E_{Tripos} = \Sigma E_{bonds} + \Sigma E_{angles} + \Sigma E_{torsion} + \Sigma E_{tors} + \Sigma E_{vdw} + \ldots$$
$$\ldots(+ \Sigma E_{ele} + \Sigma E_{dist\_c} + \Sigma E_{ang\_c} + \Sigma E_{tors\_c} + \Sigma E_{range\_c} + \Sigma E_{multi} + \Sigma E_{field\_fit})$$

Main terms:

E_{bonds} : energy of a bond stretched or compressed from its natural bond length.

$E_{bonds} = \Sigma_{\text{all bonds}} 0.5 * k_{b,i} * (d_i - d_i^0)^2$

where:

d_i : the length of the i-th bond (Å)

d_i^0 : the equilibrium length of the i-th bond (Å)

$k_{b,i}$: the bond stretching force constant (kcal/(mole)(Å)^2)

E_{angles} : energy of bending bond angles from their natural values.

$E_{angles} = \Sigma_{\text{all angles}} 0.5 * k_{\theta,i} * (\theta_i - \theta_i^0)^2$

where:

θ_i : the angle between two adjacent bonds (degrees)

θ_i^0 : the equilibrium value for the i-th angle

$k_{\theta,i}$: the angle bending force constant (kcal/(mole)(degrees)^2)

$E_{torsion}$: energy of bending planar atoms out of the plane.

$E_{\mathbf{torsion}} = \Sigma_{\text{all trigonal atoms}} 0.5 * k_{torsion,i} * d_i^2$

where:

d_i : the distance between the center atom and the plane of its substituents (Å)

$k_{torsion,i}$: the out of plane bending constant (kcal/(mole)(degrees)^2)

E_{tors} : torsional energy due to twisting about bonds.

$E_{tors} = \Sigma_{\text{all torsions}} 0.5 * V_{\Omega,i} * [1 + S_i * \cos (|n_i| * \Omega_i]$

where:

$V_{\Omega,i}$: the torsional barrier (kcal/mole)

S_i : +1 for staggered minimum energy and -1 for eclipsed minimum energy

$|n_i|$: the periodicity

Ω_i : the torsion angle

E_{vdw} : energy due to van der Waals non-bonded interactions.

$E_{vdw} = S_{\text{all non-bonded atom pairs}} E_{ij} * \{ [1 / a_{ij}^{12}] - [2 / a_{ij}^{6}] \}$
where:
E_{ij} : the van der Waals constant (kcal/mole) = $(E_i * E_j)^{0.5}$
a_{ij} : equals $r_{ij} / (R_i + R_i)$
r_{ij} : the distance between atoms i and j (Å)
R_i : the van der Waals radius of the i-th atom (Å)

Optional terms (E_{misc}):

E_{ele} : energy due to electrostatic interactions.

$E_{ele} = 332.17 * S_{\text{all non-bonded atom pairs}} Q_i*Q_j / (D_{ij}*r_{ij})$
where:
D_{ij} : the value of the dielectric function for atoms i and j
Q_i : the net atomic charge at the i-th atom
r_{ij} : the distance between atoms i and j (Å)
332.17 : a unit conversion factor

E_{dist_c} : energy associated with distance constraints.
$E_{dist\_c} = 0.5 * k_d * (d - d^0)^2$
where:
d : the distance between two specified atoms (Å)
d^0 : the requested distance between the two atoms (Å)
k_d : the force constant (kcal/(mole)(Å)^2)

E_{ang_c} : energy associated with angle constrains.
$E_{ang\_c} = 0.5 * k_\theta * (\theta - \theta^0)^2$
where:
θ : the angle between three specified atoms (degrees)
θ^0 : the requested angle between the three atoms (degrees)
k_θ : the force constant (kcal/(mole)(degrees)^2)

E_{tors_c} : energy associated with torsion angle constraints.
$E_{tors\_c} = 0.5 * k_\Omega * (\Omega - \Omega^0)^2$
where:
Ω : the angle between four specified atoms (degrees)
Ω^0 : the requested angle between the foru atoms (degrees)
k_θ : the force constant (kcal/(mole)(degrees)^2)

E_{range_c} : energy associated with range constraints.

$E_{range\_c} = 0$ for $d^{low} < d < d^{high}$

$E_{range\_c} = 0.5 * k_r * (d - d^{low})^2$ for $d^{low} < d < d^{high}$

$E_{range\_c} = 0.5 * k_r * (d^{high} - d)^2$ for $d^{low} < d < d^{high}$

where:

d^{low} : the minimum distance between two specified atoms (Å)

d^{high} : the maximum distance between two specified atoms (Å)

k_r : the force constant (kcal/(mole)(Å)^2)

E_{multi} : energy associated with multifitting.

$E_{multi} = S_{\text{all reference pairs}} k_{s,i} * d_i^2$

where:

$k_{s,i}$: the spring constant (kcal/(mole)(Å)^2

d_i : the distance between the atom and the reference point (Å)

E_{field_fit} : energy associated with fitting fields.

The magnitude of any field fit energy penalty is calculated as the sum of the squared differences in field values over all intersections of a three-dimensional lattice embedded in Cartesian space. Two field values, steric and electrostatic, are calculated at each lattice intersection, using the TRIPOS force field, as the sum of interactions between an artificial probe atom at that intersection and each of the atoms in the target or template molecule.

VITA

Shannon Fox was born in Atlanta, Georgia and resided in Powder Springs until 1986. He and his family then moved to Pisgah Forest, NC, where he attended Brevard High School. In 1990 he enrolled at the University of North Carolina – Asheville, and immediately declared his major in chemistry. He graduated from UNC – Asheville in 1995 with a Bachelor of Science degree, with honors. In 1996, he participated in a Science and Engineering Research Semester at Argonne National Laboratory, where he worked with Dr. Hsein-Hau Wang, investigating superconducting organic crystals using Raman spectroscopy. In the fall of 1996, he was admitted into the graduate chemistry program at the University of Tennessee – Knoxville. He worked in the research group of Dr. Michael Sepaniak, conducting research in capillary electrophoresis, molecular mechanics modeling, and surface enhanced Raman spectroscopy. He completed is doctoral requirements in July, 2003 for his Ph.D. in Chemistry. In August, 2003 he began employment with Battelle at a laboratory near Baltimore, MD.